EFFECT OF POLYMER TOPOLOGY ON NON-COVALENTLY BONDED POLYESTERS

by

Göknil Süsler

B.S., Chemistry, Boğaziçi University, 2016

Submitted to the Institute for Graduate Studies in
Science and Engineering in partial fulfillment of
the requirements for the degree of
Master of Science

Graduate Program in Chemistry

Boğaziçi University

2019

Dedicated to my family

ACKNOWLEDGEMENTS

Firstly, I would like to thank my supervisor Assoc. Prof. A. Ersin Acar for accepting me his research group. It is a pleasure for me to express my sincerest gratitude to him for his endless support, guidance, encouragement and wise advices throughout my master studies.

I would like to thank to my thesis committee members Prof. Duygu Avcı Semiz and Prof. Uğur Ünal for giving their valuable time and reviewing my thesis.

I would also thank to all the members of Acar Lab aka Acarhane. During my thesis I worked with amazing people. I would like to thank Banu, Fatma, Gülizar, Kübra, Sedef, Seda and Şule for their help, support and friendship. Especially, Ayşenur, Ayşe Zeyneb, Halenur, Işıl for all their support, help and all the good times we had. They made all the difficult times easier and enjoyable. I am grateful for the times we had fun and laughed so much. It was a great chance to work in a research group full of such supportive people. And biggest thanks to Refia for sharing this experience with me and all the fun we had throughout the all master years. Once again, I would like to thank all the people I work with in lab for their endless support.

In addition, I would like to thank my friends Özlem, Tuğçe, Esin, Fatma and Esra. I would like to thank my best friend Melis for being always there for me for almost 10 years.

Finally, my biggest appreciations go to my family. This thesis would not have been accomplished without them. I would like to thank my brother Lütfi for being a life mentor and a friend to me. Especially, I would like to thank my mother Mürvet Süsler. I feel so lucky to have such supportive mother in my life. I owe them a lot. Lastly, I would like to thank my father. I know he is watching me over the clouds. I appreciate all the good people in my life for their unrequited love and support.

ABSTRACT

EFFECT OF POLYMER TOPOLOGY ON NON-COVALENTLY BONDED POLYESTERS

Synthetic polymers have a crucial role in our daily lives. The irreversible nature of covalent bonding in conventional synthetic polymers makes them non-recyclable and prevents re-processing of the materials. Throughout the years with the development in technology, the demand for more advanced materials such as, reversible, recycable, and re-processable materials has increased. Supramolecular chemistry has emerged to solve this need for reversibility in polymer materials. Supramolecular polymers are more tunable and dynamic due to their non-covalent and reversible nature. Non-covalent interactions include metal-ligand coordinations, host-guest, $\pi - \pi$ stacking, ionic interactions and hydrogen bonding.

Ionic hydrogen bonding has the known characteristics of hydrogen bonding such as directionality, strength and versatility. For instance, a carboxylic acid and an amine give rise to ionic hydrogen bonding by acid-base complexation reaction. Thus, carboxyl-terminated polyesters, in principle, may coordinate with amines to produce supramolecular materials.

In this study, the carboxyl-terminated polyesters and amines having different functionalities were mixed/reacted in a melt reactor to form acid-base coordinates. The thermal and mechanical properties of the amine treated polyesters were investigated through DSC and rheometric measurements, respectively.

ÖZET

KOVALENT OLMAYAN BAĞLARALA BAĞLANMIŞ POLİESTERLERDE POLİMER TOPOLOJİSİNİN ETKİLERİ

Sentetik polimerler günlük yaşamımızda önemli bir role sahiptir. Sentetik polimerlerdeki kovalent bağların tersinmez özelliği geleneksel polimerler geri-döndürülemez yapmakta ve tekrar işlenmesini olanaksız hale getirmektedir. Yıllar içinde teknolojide yaşanan ilerleme sonucunda geri-dönüştürülebilir, tersinir ve tekrar işlenebilen daha gelişmiş materyallere ihtiyaç duyulmuştur. Supramoleküler kimya bu ihtiyacı karşılamada önemli bir görev üstlenmiştir. Supramoleküler polimerler kovalent olmayan tersinir bağlarından dolayı özelliklerini kontrol etmede ve değiştirmede geleneksel polimerlerle karşılaştırıldığında önemli bir üstünlüğe sahiptir. Kovalent olmayan bağlar, metal-ligand koordinasyonu, konak-konuk, $\pi - \pi$, ionic etkileşimler ve hidrojen bağı gibi etkileşimleri içermektedir.

İyonik hidrojen bağı, normal hidrojen bağının direksiyonelliğine, kuvvetine ve çok yönlülüğüne sahiptir. Örnek vermek gerekirse, bir karboksilik asit ile bir amin asit-baz kompleks reaksiyonu ile aralarında iyonik hidrojen bağı oluşturabilir. Buna bağlı olarak, asit-uç gruplu bir polyesterler aminlerle prensipte iyonik hidrojen bağı ile supramoleküler bir materyal oluşturabilir.

Bu çalışmada, endüstride kullanılan asit-uç gruplu poliesterler ve farklı fonsiyonaliteye sahip aminler asit-baz koordinasyonu oluşturması için eriyik hal şartlarında reaksiyona sokuldu/karıştırıldı. elde edilecek polimer kompleksinin ana poliesterin T_g ve mekanik özellikleri üzerindeki etkisi incelenmiştir. Oluşan polimer kompleksleri DSC ve reoloji teknikleriyle karakterize edilmiştir.

TABLE OF CONTENTS

LIST OF FIGURES

LIST OF TABLES

LIST OF ACRONYMS/ABBREVIATIONS

2MI	2-Methylimidazole
A	Shear area
CEG	Carboxyl-end groups
CHDA	1,4- Cyclohexanedicarboxylic acid
CHDM	1,4- Cyclohexanedimethanol
$CDCl_3$	Deuterated Chloroform
DABCO	1,4-Diazabicyclo[2.2.2]octane
DOPA	3,4-dihydroxyphenylalanine
DSC	Differential Scanning Calorimetry
F	Shear force
G	Shear modulus
G^*	Complex modulus
H	Hydrogen
HMBC	Heteronuclear multiple-bond correlation spectroscopy
HMDA	Hexamethylenediamine
IHB	Ionic hydrogen bond
M_n	Number average molecular weight
M_w	Weight average molecular weight
MWD	Molecular weight distribution

NMR	Nuclear Magnetic Resonance
NX3P	2,4,6-Tris (dimethylaminomethyl) phenol
PCCD	Poly (1,4-cyclohexylidenecyclohexane- 1,4-dicarboxylate)
PDMS	Polydimethylsiloxane
PEI	Poly (ethylene imine)
PET	Poly (ethylene terephthalate)
SAOS	Small amplitude oscillatory shear
t	Time
TAB	Tetrabutylammonium Bromide
tanδ	Loss factor
T_g	Glass transition temperature
T_m	Crystalline melting temperature
UPy	Ureidopyrimidinone
v	Velocity
σ	Shear stress
σ_0	Maximum stress
γ	Shear strain
γ_0	Maximum strain
$\dot{\gamma}$	Shear rate
η	Viscosity

η_0	Zero-shear viscosity
$\lvert\eta^*\rvert$	Complex viscosity
τ	Relaxation time
ω	Angular frequency

1. INTRODUCTION

Synthetic polymers have become an essential part of our daily life since they were introduced for the first time by Leo Hendrik Baekeland, more than a century ago. In 1920, the pioneering work of Hermann Staudinger, which earned him a Nobel Prize in 1953, revealed that the macromolecular nature of molecules gave the polymers their unique properties in the solid state and in solution. The term 'polymers', which he also called macromolecules, was first described as to be multiple covalently bound monomer [1]. The macroscopic properties of polymers are directly acquired from the molecular structure of the monomers. The irreversible nature of covalent bonds between monomers causes an unwanted alteration of material's properties upon external stimuli and leads to non-recyclable materials [2].

In its modern sense, supramolecular chemistry was introduced in 1978 by Jean Marie Lehn, who won the Nobel Prize for his work in 1987. He defined it as the ''chemistry of molecular assemblies and of the intermolecular bond'' [3]. Contrarily to conventional polymers, supramolecular polymers are defined as materials whose constituents, which can be small molecules or polymers, are held together with dynamic covalent bonds such as Diels-Alder, disulfide bonds, urea bonds, and imine bonds or reversible non-covalent connections including host-guest interactions, metal-ligand coordination, π–π stacking, ionic interactions, and hydrogen bonds. These dynamic bonds exhibit association-dissociation upon exposure to an external stimulus such as heat, light or chemicals, enabling the as-formed materials to be reprocessed and recycled [2][4][5]. Spider silk is an example of this type of design in nature. It's densely hydrogen-bonded structure supply spider silk with high tensile strength and great extensibility making it exceptionally tough and extensible [6].

Nowadays, advanced materials with unique properties are synthesized by utilizing non-covalent interactions on the main-chain or side-chains of the polymer backbone [7][8]. The building blocks for supramolecular materials are various and usually contain only small molecules, a polymer and a small molecule, or only polymers, regardless of the non-covalent interaction type. Each particular supramolecular interaction has its own distinctive bond strength and characteristics, which give rise to different architectural and dynamic

parameters, such as chain dynamics, performance lifetime, mechanics, the degree of polymerization, and conformation [9]. The reversible and tunable nature of supramolecular interactions provide these polymers with dynamic features such as the ability to change crosslinking degree and length, structure, and composition, which potentially leads to properties like, the ability to self-repair and self-heal, stimuli-responsiveness and improved processing [10]. The non-covalent interactions and their application areas are depicted in Figure 1.1.

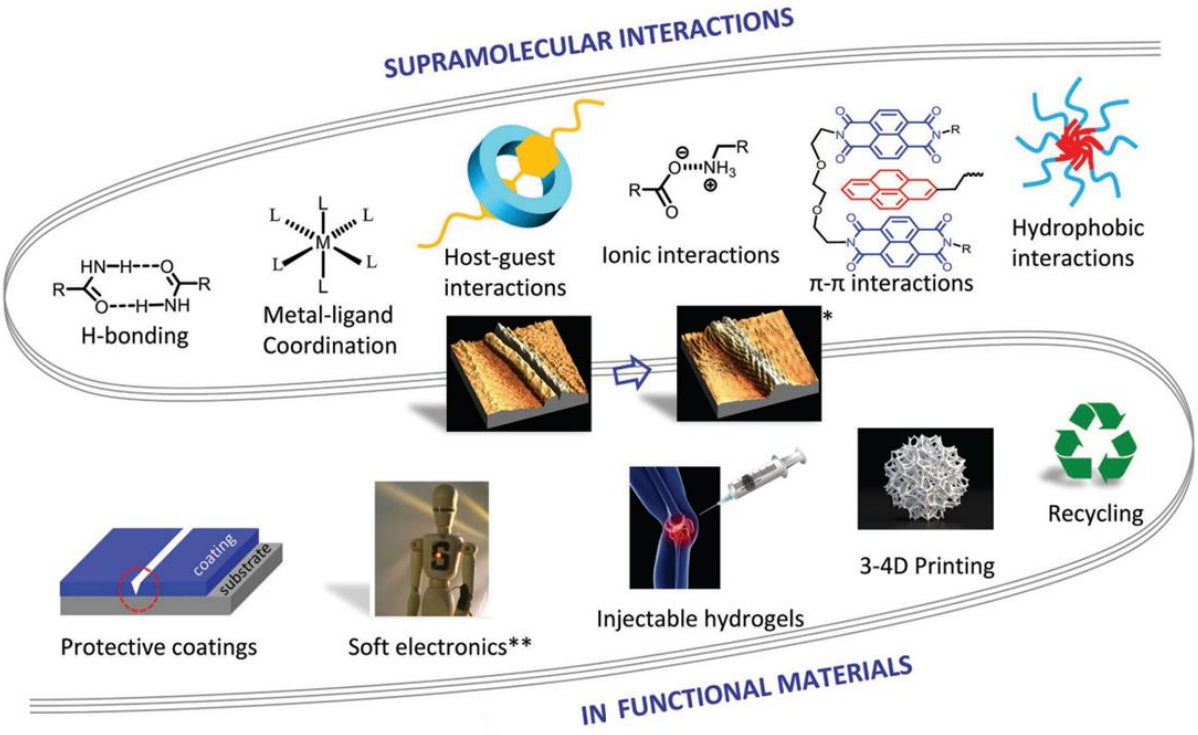

Figure 1.1. Supramolecular interactions and their application areas [11].

1.1. Supramolecular Interactions

The strength of non-covalent interactions adopted in the synthesis of supramolecular polymeric materials are summarized in Fig 1.2 and can fall into three major classes: i) weak interactions (0–20 kcal/mol in bond strength), such as π – π stacking interactions, hydrophobic interactions, van der Waals forces, and hydrogen bonds; ii) medium interactions (20–60 kcal/mol in bond strength), such as (weak) metal coordination

complexes and multiple hydrogen bonds; and iii) strong interactions (>60 kcal/mol in bond strength), such as host-guest interactions, (robust) metal coordination or chelate complexation and ionic interactions. The particular strength of these interactions has a high dependence on external influences such as temperature, solvent, etc., thus we cannot put most of the non-covalent interactions in a single category [12][13].

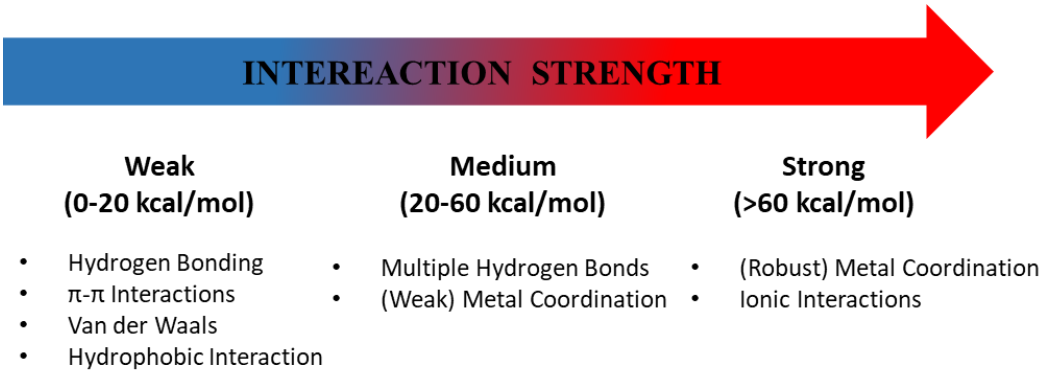

Figure 1.2. Supramolecular interaction strengths [12].

1.1.1. Metal-Ligand Coordination Interactions

The metal-ligand coordination has been widely utilized by a large number of researchers due to its kinetical volatility, directionality, high bond energy, and thermodynamic stability [14]. The monomeric unit includes an organic ligand, mostly terpyridines or other heterocyclic compounds, and a metal ion. Fe, Cu, Co, Ni, Zn, Cd cations are mostly used. Metal-ligand coordination strength differs from weak to closely covalent with changing ligands, metal ions, and counter ions [15]. Also, depending on the coordination number, the supramolecular polymers can be linear, star-shaped, hyperbranched or dendritic as shown in Figure 1.3 [16]. Furthermore, by selecting different metal-ligand pairs and tuning their binding strength one can adjust the properties of the material, such as the geometric shapes, kinetic and thermodynamic stabilities, and functional properties [17]. Owing to the presence of metal ions, the application area mainly covers electromagnetism and photoelectricity [16].

A well-known example of metal-ligand complexation in biological systems, which was an inspiration for synthetic polymers, is the byssal threads secreted by mussels. It has

strong adhesion to substrate surface underwater in consequence of coordination between imidazole-containing histidines and 3,4-dihydroxyphenylalanine (DOPA) and metal ions like Fe(III) and Zn(II) can bind [11]. By mimicking mussels, researchers synthesized DOPA-modified polyallylamine hydrogels that showed high strength and self-healing, and the degree of crosslinking was pH-controllable [18].

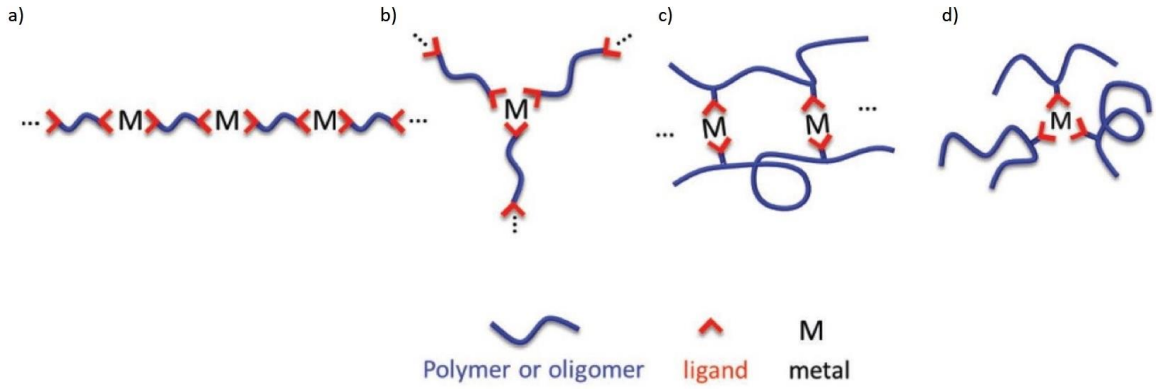

Figure 1.3. Metal-coordination types in supramolecular polymers a) Linear, b) star-shaped, c) Hyper-branched d) Dendritic [11].

Terpyridines are important ligands for metal-ligand complexes. Rowan *et al.* assembled a series of supramolecules that comprise ditopic monomers based on pentaethylene glycol core and poly(tetrahydrofuran) telechelic cores which appended at the ends with 4-oxy-2,6 bis(1` -methylbenzimidazolyl)pyridine derivatives as shown in Figure 1.4. Complexation with metal ions (Fe(II), Co(II), Zn(II) and Cd(II)) resulted in self-assembled linear metallosupramolecular polymers which showed improvements in mechanical properties compared to uncomplexed monomers. Polyethylene glycol cores showed an inclination to form macrocyclic species where slight improvement in mechanical properties was observed. Poly(tetrahydrofuran) cores showed phase-separation with soft polyether segments and hard ionic segments whose mechanical properties could be tuned by changing metal ions [19].

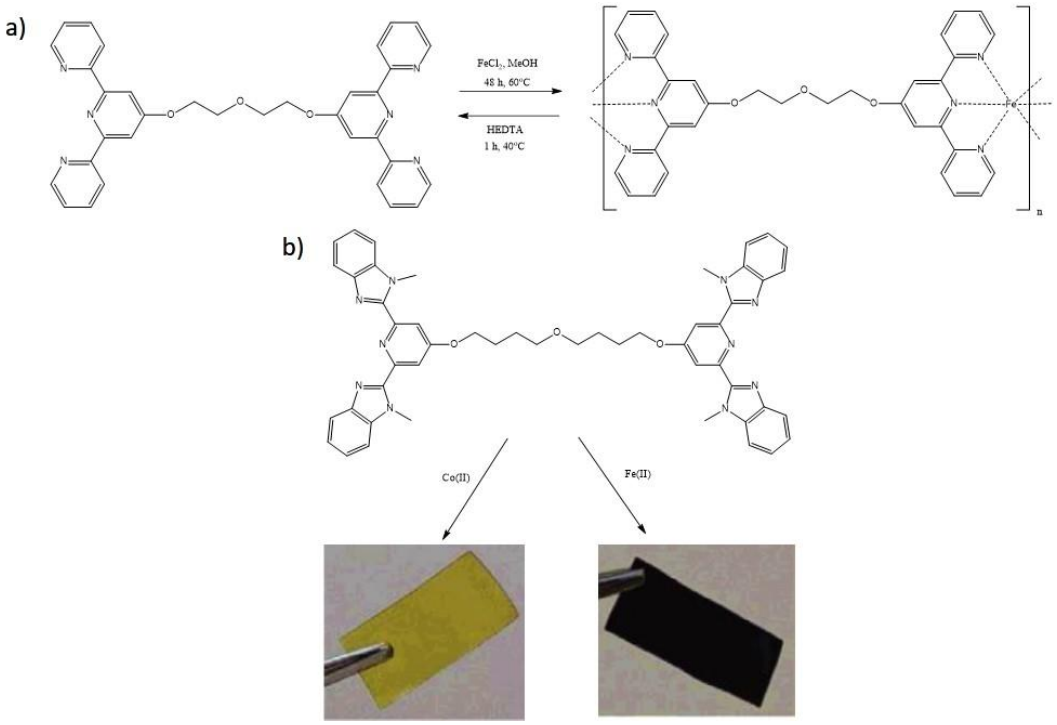

Figure 1.4. Metallosupramolecules formed by complexation between 4-oxy-2,6 bis(1`-methylbenzimidazolyl)pyridine derivatives and metal ions [19].

A more recent example is cross-linking of carboxyl-modified polysiloxanes with Al(III) ions according to the work of Lei *et al.* and were shown in Figure 1.5. Complexation of Al(III)-carboxylate resulted in an elastic network with self-healing and thermally reprocessing capability. They emphasized that the chain length of polysiloxanes, carboxylic acid density, and Al(III) feed were important features to control the properties of the cross-linked network [20].

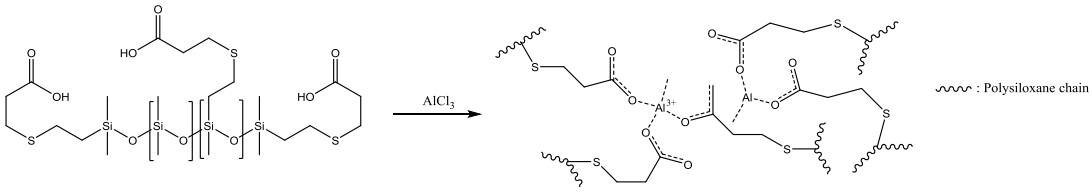

Figure 1.5. The supramolecule formed by complexation between carboxylates and Al(III) [20].

1.1.2. π-π Interactions

In particular, π–π interaction has been observed with compounds containing aromatic moieties. It is a result of intermolecular overlapping of π–orbitals in the system [21]. Naturally, this interaction plays a crucial role in securing biological structures such as, DNA, RNA, protein folding and mediating molecular recognition phenomena [22]. The strength of intermolecular interaction depends strongly on the number of π-electrons and as expected becomes stronger with the increasing number of the aromatic rings. Generally, π-π stacking is combined with other non-covalent interactions like metal-ligand or hydrogen bonding because it is not as strong or directional as these interactions [16].

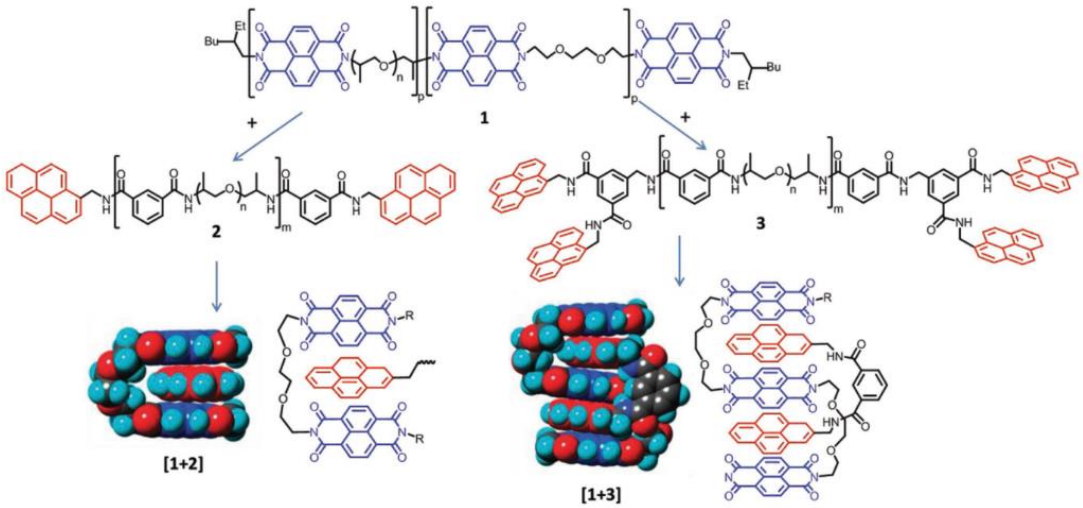

Figure 1.6. The chemical structures of (1) naphthalene-diimide bearing chain folding sections, (2) polyamide bearing pyrenyl groups at the ends, (3) polyamide bearing bis-pyrenyl groups at the ends. [1+2] and [1+3] are polymers containing two and four face-to-face π–π stacking interactions [23].

π–π Interactions were used mostly in the development of self-healing polymer materials. Burattini *et al.* were the first to use this interaction as a way to achieve a self-healing polymer. He combined π-electron deficient naphthalene-diimide units incorporated to polyimides and π-electron rich pyrenyl group end-capped polyamide chains. They adopted a chain-folded conformation due to π–π stacking interactions between naphthalene-diimide and pyrene units, thus a supramolecular network is formed as shown in Figure 1.6 [24]. Self-

healing of polymeric materials was achieved *via* thermal treatment. At elevated temperatures π–π interactions is interrupted, and mobility, which is necessary for closing the cracks, is attained. While cooling, the secondary interactions are reformed and polymer with original properties was re-obtained [25]. The T_g of the material can be fine-tuned by changing the spacer and the composition of the blend. They also used (tweezer-type) bis-pyrenyl end-capped polyimides instead of (non-tweezer-type) monopyrenyl groups and as expected, had obtained a network with enhanced mechanical properties [23]. Moreover, materials with perylene end-terminated polyamides showed lower self-healing temperature and better mechanical properties compared to pyrenyl end-terminated polymers [26].

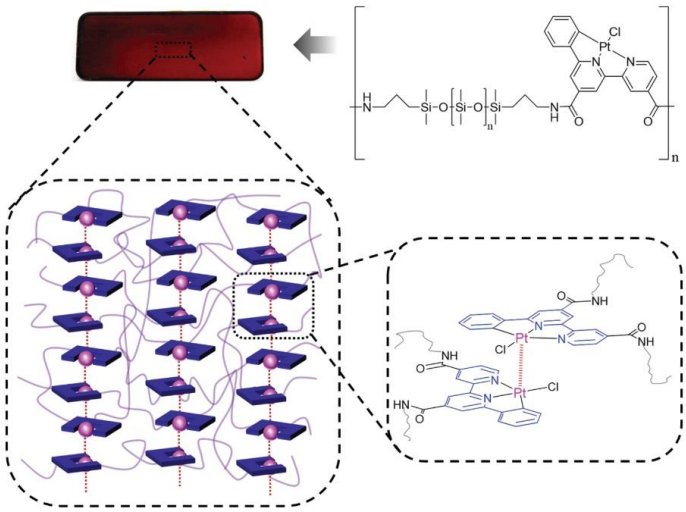

Figure 1.7. The proposed network between PDMS and Platinum [27].

In a different study, Mei *et al.* used cyclometalated platinum(II) complex Pt(6-phenyl-2,2′-bipyridyl)Cl incorporated PDMS to observe the combined effect of π–π interactions with metal-ligand interactions. Resulting in a polymer network with high mechanical strength and stretchability, also full recovery of mechanical properties at room temperature within 12 h or at 50^{o} C within 2 h was achieved [27].

1.1.3. Hydrogen Bonding Interactions

Considering all the non-covalent interactions, hydrogen bonding is the most studied due to its directionality, strength, and versatility [28]. The hydrogen bond arises between a proton donor and a proton acceptor. Proton donors are groups containing hydrogen atom bonded to an electronegative atom; thus, hydrogen atom bears a partial positive charge and they form a dipole. Proton acceptors are dipoles containing electron-withdrawing atoms. The partial positively charged hydrogen can interact with these electron-withdrawing atoms and form hydrogen bonds [29].

Hydrogen bond ensures the structures of water, DNA, protein folding and is crucial for the development of life on earth. Its strength and reversibility depend on temperature, solvent, and pH. Even though it is considered weak compared to other non-covalent interactions like metal-ligand and ionic interactions or 10 times weaker than the covalent bonds, with the incorporation of multiple hydrogen bonds to the system, the bonding strength can be increased. The strength of hydrogen bonding can be fine-tuned by changing proton acidity and the number of hydrogen bonds. H-bonding alters polymers' viscoelastic properties, phase separation and the degree of crystallinity [28].

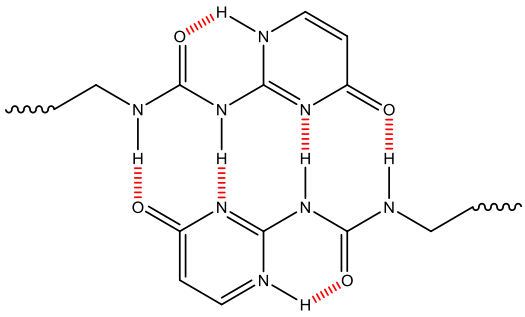

Figure 1.8. Hydrogen bonding between 2-ureido-4[1H]-pyrimidinone (UPy) groups at the chain ends [30].

As an example, the introduction of the ureidopyrimidinone (UPy) group which is a quadruple H-bonding unit with a very high association constant pave the way for different end-functionalized supramolecular polymers (Figure 1.8) [30]. Low molecular weight polymers show low viscosity at elevated temperatures but mechanical strength at room

temperature is not good enough for engineering polymers. To overcome this difficulty, Houston *et al.* reported a glycol modified poly(ethylene terephthalate) (PETG) prepolymer which end-functionalized with UPy moieties by using different linkers. UPy-UPy association-dissociation is temperature dependent, so they obtained improved melt viscosity at a suitable temperature range for non-degradative processing and also did not sacrifice the mechanical properties at room temperature. The tensile strength of the obtained polymer was 3 times and T_g was 28°C higher than the prepolymer used [31].

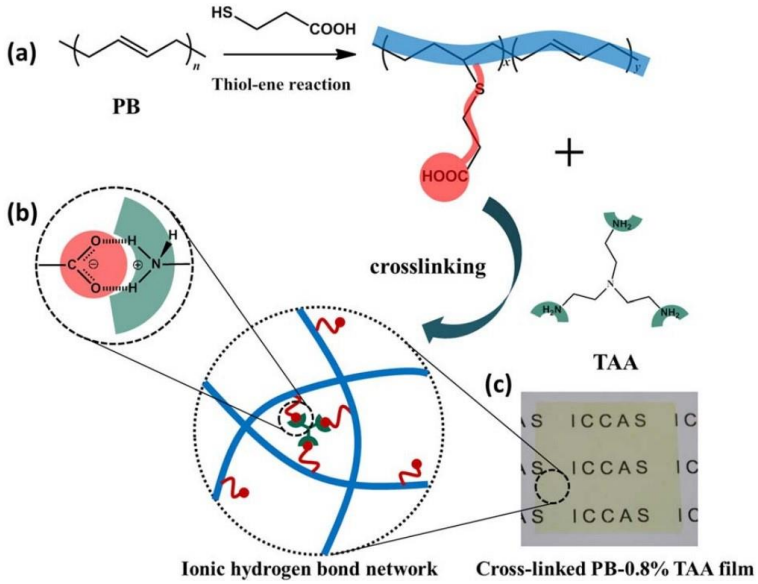

Figure 1.9. (a) Polybutadiene functionalization using Thiol-ene reaction. (b) Illustration of ionic hydrogen bonding between carboxylic acid on polybutadiene and tris(2-aminoethyl) amine. (c) The image of the film made by this crosslinked polymer [6].

Ionic hydrogen bonds (IHBs) have higher bond energy and are less-directional compared to neutral hydrogen bonds. It forms with a potential proton transfer between organic cations and anions which is well observed in biological systems like cell membranes [32][33]. Recently, IHB has been widely utilized to assemble supramolecular polymers, owing to its high stability and accessibility. Wang *et al.* reported a new elastomer by using polybutadiene functionalized with carboxylic acid side groups and tris(2-aminoethyl) amine as non-covalent cross-linker as shown in Figure 1.9. The ionic hydrogen bonds induced an important increase in toughness, stretchability, and a good self-recovery. Most importantly,

it enabled the recycling and reprocessing of elastomer by thermoreversible ionic hydrogen bonds [6].

1.1.4. Ionic Interactions

Ionic interactions are based on the attraction between two oppositely charged species. Ionic interaction strength strongly depends upon the magnitude of the charges, temperature, and dielectric constant [22]. It follows Coulomb's law, decreases with increasing distance between the charges, however proportional to the density of charges. Therefore, the binding strength of ionic interactions would be stronger with the involvement of multivalent ions, such as dipole, quadrupole, etc [29].

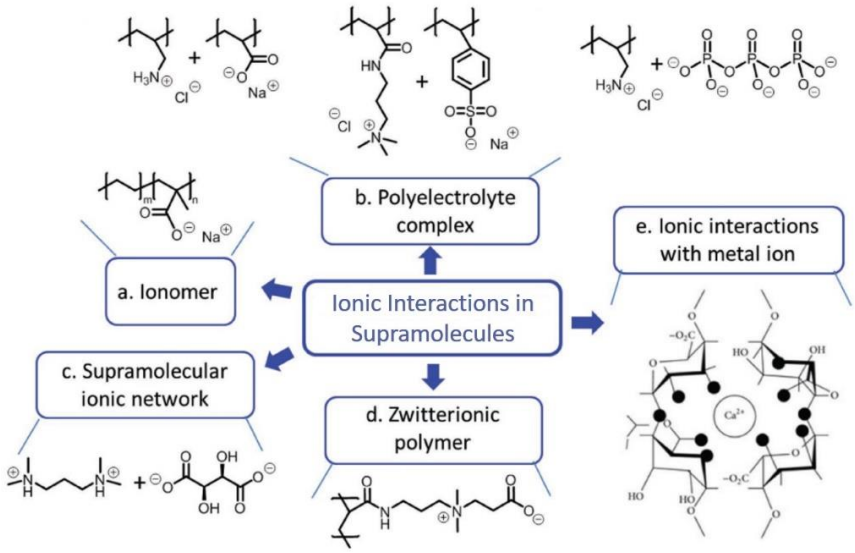

Figure 1.10. (a) Ionomers contain <10% ionic parts (b) Polyelectrolytes must contain an ionic unit on the monomers (c) Supramolecular ionic networks form between multianionic and multicationic molecules (d) Zwitterionic polymers have equal number of anionic and cationic groups on polymer (e) Ionic interaction with metal ion when there is negatively charged groups on the polymer [11].

In comparison to other physical interactions, ionic interactions have some distinct advantages such as, they are stronger, asymmetric and non-directional. They are prone to form ionic multiplets or clusters depending on the chemical and steric environment. Lastly, they can be fine-tuned by using different anion and cation pairs. Accordingly, only ionic

interaction strength is comparable to covalent bonding (100 to 350 kJ/mol) [34]. The ionic interactions in supramolecular polymers vary depending on the positions on the chain and the % amount in the polymer and shown in Figure 1.10.

The introduction of new anions and cations from ionic liquids chemistry has broadened the applications of ionic interactions in supramolecular polymers. Ten years ago, Grinstaff *et al.* reported a supramolecular ionic network by mixing an alkyl phosphonium dication which is an ionic liquid and polyacrylate/poly(acrylic acid). Interaction between phosphonium dication (P^{2+}) and polyacrylate results in network formation as shown in Figure 1.11.

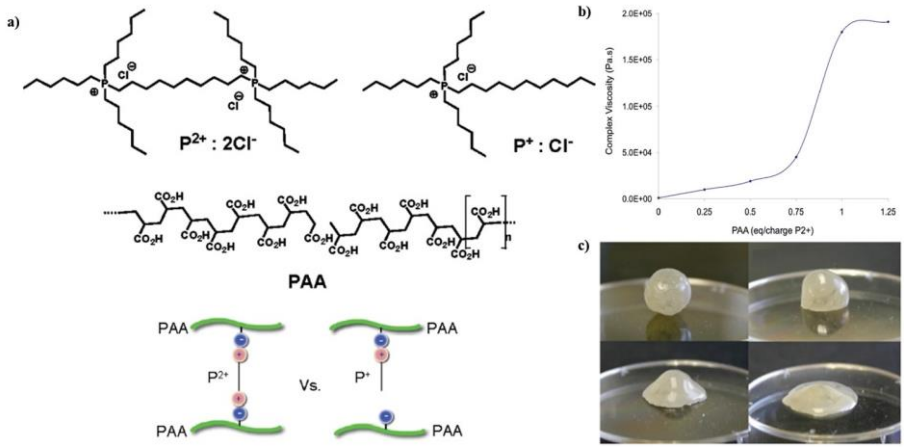

Figure 1.11. (a) The chemical structures of alkyl phosphonium dication/monocation and poly (acrylic acid) (top) and illustration of supramolecular network between ionic liquid and PAA (bottom) (b) viscosity curve of network (c) The photographs of supramolecule's shape stability upon several days [35].

The geminal phosphonium dication is symmetrical and has two positive charges so it cannot participate in hydrogen bonding. The product showed viscoelastic liquid properties and also showed a significant increase in viscosity with the increasing amount of P^{2+}. However, the use of monocationic phosphonium (P^{+}) instead of (P^{2+}) did not result in any network formation due to lack of ionic interactions [35].

In another study, Aboudzadeh *et al.* reported supramolecular polymers prepared from citrate anion and ionic liquids based on imidazolium, pyrrolidinium, and pyridinium. The

final products were non-crystalline soft solids and show viscoelastic properties. The elastic modulus and network-liquid transition temperature order for final products were 1-benzylimidazolium > meyhtlpyrrolidinium > 1-methylizidazolium > pyridinium. The final products also showed thermal reversibility [36].

1.2. Basics of Rheology

Rheology is defined as the study of the deformation and flow behavior of matter and its structural changes under the applied stress or strain [37]. The response of materials to an applied force depends on the different states of matter [38]. Idealviscous liquids will flow, that is they deform irreversibly. The deformation energy cannot be recovered simply by removing the applied stress because it is dissipated within the liquid in the form of heat. They follow Newton's law of viscosity. Idealelastic solids will deform elastically, meaning they deform reversibly. When the applied stress is removed, the deformation energy is fully recovered. They follow Hooke's law of elasticity [37]. However, most materials we encounter are in between these two extreme behaviors. They follow neither Newton's law nor Hooke's law [39]. These materials are called viscoelastic, which have a combination of a viscous and elastic portion [40].

1.2.1. Terminology

The parallel-plate model in Fig 1.12 is used to introduce some essential rheological concepts.

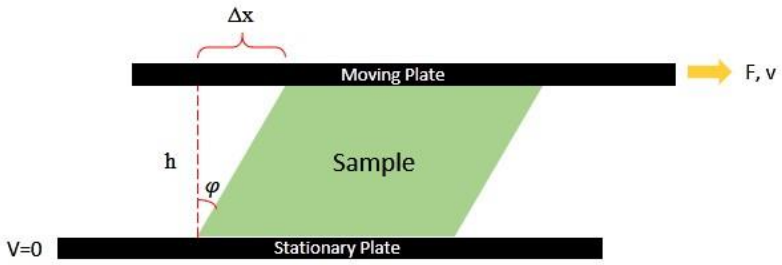

Figure 1.12. Illustration of parallel-plate model [40].

When a force is applied parallel to the material placed between the two plates, the material responds. Upper plate with area A moved by force F and resulting velocity v while the bottom plate is stationary (v=0). The material is sheared between the plates with h being the gap distance. The shear stress σ [Pa] is the shear force F [N] applied on the material divided by the shear area A [m^2] [40].

$$\sigma = \frac{F}{A} \tag{1.1}$$

The materials response to applied stress is called deformation that is a change in shape or dimension. In order to make the required calculations, the relative deformation is expressed as shear strain (γ). Strain is defined as relative displacement in length meaning, the ratio of deflection (Δx) of material to the gap between plates (h).

$$\gamma = \frac{\Delta x}{h} \tag{1.2}$$

The shear rate ($\dot{\gamma}$) [s^{-1}] is defined by the derivative of the time-dependent strain with respect to time. It can be viewed as the movement rate of adjacent layers of material [41].

$$\dot{\gamma} = \frac{d\gamma}{dt} = \frac{v}{h} \tag{1.3}$$

1.2.2. Mechanical Models

A material is categorized as elastic, viscous or viscoelastic according to its response when a force is exerted on it. In order to explain the viscoelastic behavior of materials, several mechanical models were proposed. Ideal solids are explained by Hooke's law of elasticity by using a spring model while viscous fluids are explained by Newton's law of viscosity by using a dashpot model. Viscoelastic materials, however, are explained by using two models; Maxwell model which a spring and a dashpot combined in a serial manner, and Kelvin-Voight model which a spring and a dashpot is connected in a parallel manner [42].

1.2.2.1. Hooke's law: Ideal Elastic Deformation. The mechanical response of elastic ideal solids is described by Hooke's law for simple shear in equation (Eq) (1.4), and their behavior is illustrated on the basis of a spring model in Figure 1.13a [43].

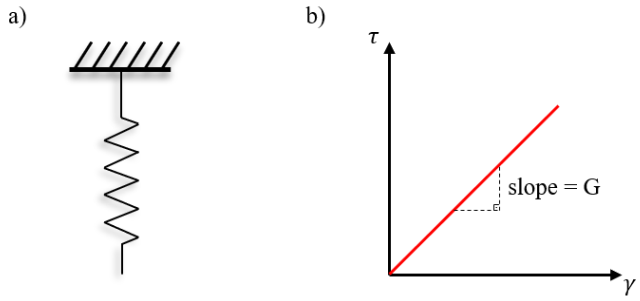

Figure 1.13. (a) The illustration of a spring model (b) The slope of stress-strain curve for Hooke's Law [40].

Application of a load to a spring yields an instantaneous deformation proportional to the applied force. The material stores all the energy gained during deformation and when the load is removed returns to its original shape using the stored energy without any residual deformation. Therefore, the elastic deformation is instantaneous and recoverable [29][41].

$$\sigma = G.\gamma \tag{1.4}$$

Hooke's law states that the shear stress varies linearly with the shear strain or the relative deformation. The proportionality between stress and strain is called the shear modulus, G, which is a material constant and describes deformation behavior of ideal elastic solids [29].

1.2.2.2. Newton's Law: Ideal Viscous Flow. The mechanical response of ideal viscous fluid when a force exerted on it is described by Newton's law in Eq (1.5) and their behavior is illustrated using a dashpot model which is a piston-cylinder arrangement, filled with a viscous fluid in Fig 1.14a.

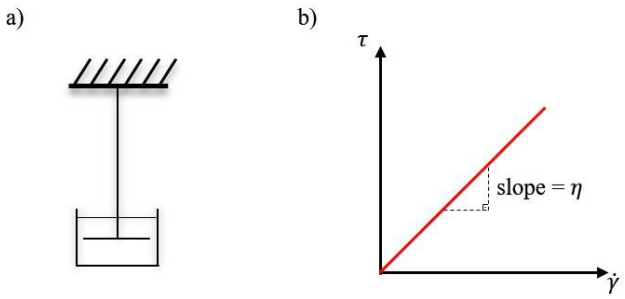

Figure 1.14. (a) The illustration of a dash-pot model (b) The slope of stress-strain curve for Newton's Law [40].

An application of a constant load and deformation velocity (by pushing the piston) leads to an increasing strain of the dashpot continuously. After the removal of the load the dashpot does not return to its original position, in other words, the ideal fluid remains in the deformed state without a shape recovery [37]. Ideal fluids do not store the deformation energy, it is completely dissipated within the fluid as heat. Therefore, the viscous deformation is unrecoverable [41].

$$\sigma = \eta . \dot{\gamma} \tag{1.5}$$

Based on Newton's law, the shear stress is always proportional to the shear rate at a constant temperature and is independent of strain itself [44]. The slope, η, is called viscosity. The viscosity is a measure of the resistance to the flow of a fluid and is a constant which is unique to the material [29].

1.2.2.3. Maxwell's Model. Maxwell model is the combination of a spring and a dashpot in series as in Fig 1.15a. The spring represents the elastic behavior and the dashpot represents the viscous behavior of the material. Maxwell model describes viscoelastic liquid behavior. In this model under a load, viscous deformation is time-dependent but elastic deformation is instantaneous. After removal of the load viscoelastic liquids remains partly deformed due to its dominating viscous portion [29].

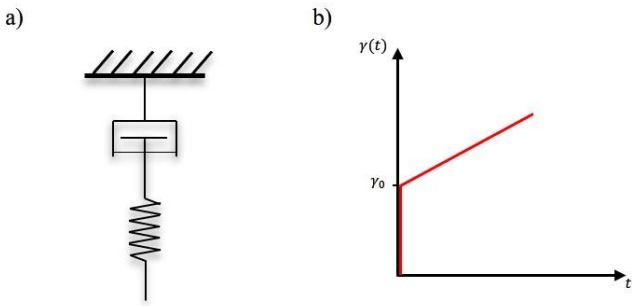

Figure 1.15. (a) The illustration of spring and dash-pot connected in a serial manner (b) The slope of stress-strain curve for Maxwell model [40].

As the spring and dashpot combined in series, they would suffer the same amount of shear stress:

$$\sigma = \sigma_v = \sigma_e \tag{1.6}$$

and the deformation is the sum of each element's shear strain:

$$\gamma = \gamma_v + \gamma_e \tag{1.7}$$

Combining with Eq (1.3) differential of deformation with respect to time yields a shear rate of:

$$\dot{\gamma} = \dot{\gamma}_v + \dot{\gamma}_e \tag{1.8}$$

By using Hooke's law, Eq (1.4) shear rate of elastic part is

$$\dot{\gamma} = \frac{\dot{\sigma}_e}{G} \tag{1.9}$$

By using Newton's law, Eq (1.5) shear rate of viscous part is

$$\dot{\gamma} = \frac{\sigma_v}{\eta} \tag{1.10}$$

The sum of shear rates yields the equation of Maxwell:

$$\dot{\gamma} = \dot{\gamma}_v + \dot{\gamma}_e = \frac{\sigma_v}{\eta} + \frac{\dot{\sigma}_e}{G} = \frac{\sigma}{\eta} + \frac{\sigma}{G} \tag{1.11}$$

A characteristic relaxation time of the Maxwell element, τ, is defined as,

$$\tau = \frac{\eta}{G} \tag{1.12}$$

The Eq (1.11) can be written as,

$$\dot{\gamma} = \frac{\dot{\sigma}}{G} + \frac{\sigma}{G\tau} \tag{1.13}$$

When a constant strain is applied, by using this model, the change in stress with respect to time is computed. This model simulates the stress relaxation behavior of viscoelastic materials [40].

1.2.2.4. Kelvin-Voight Model. Kelvin-Voigt model is based on the parallel connection of a spring and a dashpot. The illustration of Kelvin-Voigt model is shown in Figure 1.16a and spring represents the elastic part while the dashpot represents the viscous part the same as in the Maxwell model. Kelvin-Voigt model describes the viscoelastic solid behavior which is a material behaves like solid with a small pronounced viscous part [45].

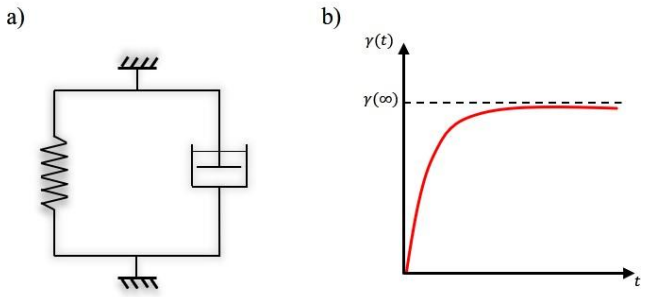

Figure 1.16. (a) The illustration of a parallel connected spring and a dash-pot (b) The slope of stress-strain curve for Kelvin-Voight model [43].

When sudden stress is applied to a viscoelastic solid, the spring element eventually attains a steady-state strain, but the dashpot element delays the increment of the strain. They show a time-delayed but complete relaxation.

Unlike the Maxwell model, in the Voigt model, the spring and the dashpot have the same amount of shear strain and shear rate, instead of shear stress.

$$\gamma = \gamma_e = \gamma_v \;\; and \;\; \dot{\gamma} = \dot{\gamma}_e = \dot{\gamma}_v \tag{1.14}$$

The total stress is the sum of the stress on the elastic component and stress on the viscous component:

$$\sigma = \sigma_e + \sigma_v \tag{1.15}$$

By using Hooke's law, Eq (1.4) shear stress of elastic part is

$$\sigma_e = \frac{G}{\gamma_e} \tag{1.16}$$

By using Newton's law, Eq (1.5) shear stress of viscous part is

$$\sigma_v = \frac{\eta}{\dot{\gamma}_v} \tag{1.17}$$

The summation of shear stress on the both elements give us the differential equation of Kelvin-Voigt:

$$\sigma = \sigma_e + \sigma_v = \eta \,.\dot{\gamma}_v + G \,.\gamma_e = \eta \,.\dot{\gamma} + G \,.\gamma \tag{1.18}$$

$$\sigma = G\gamma + \eta\dot{\gamma} \tag{1.19}$$

Accordingly, this model is used in creep behavior of viscoelastic material [42].

1.2.3. Small Amplitude Oscillatory Shear (SAOS)

When the material is subjected to a very small strain or a very small shear rate, modulus and viscosity are assumed to be independent of the strain and shear rate. This region of test conditions is called the linear region.

Small amplitude oscillatory shear (SAOS) is generally the go-to test for exploration of the linear viscoelasticity and relaxation time. A small sinusoidal deformation is applied to the material during SAOS measurement. This sinusoidal deformation may be written as a function of time:

$$\gamma(t) = \gamma_0 . \sin(\omega t) \tag{1.20}$$

where γ_0 is the maximum strain amplitude imposed on the material, ω is the angular frequency and t is time. Since the shear rate is the differential of shear strain with respect to time:

$$\dot{\gamma} = \gamma_0 . \omega . \cos(\omega t) \tag{1.21}$$

For linear viscoelastic systems, the corresponding stress will also alternate sinusoidally except for the presence of a phase difference.

$$\sigma(t) = \sigma_0 . \sin(\omega t + \delta) \tag{1.22}$$

where σ_0 is the maximum stress imposed on the material, and the δ is the phase shift between shear strain and shear stress [43].

As illustrated in Figure 1.17, the stress and strain are in phase in the case of ideal elastic solids and therefore δ=0 whilst there is a phase difference for ideal viscous liquids and is equal to $\delta = 90°$ and for viscoelastic materials, $0° < \delta < 90°$ [42].

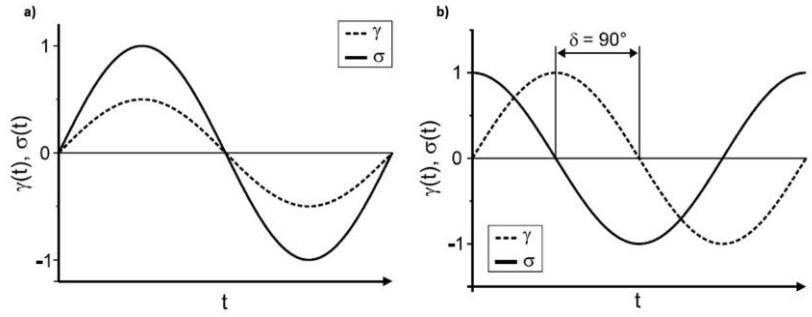

Figure 1.17. The phase difference for (a) elastic solids (b) viscous liquids [42].

By expanding Eq (1.22):

$$\sigma = [\sigma_0 \cos(\delta)] \sin(\omega t) + [\sigma_0 \sin(\delta)] \cos(\omega t) \tag{1.23}$$

when we divide each sides of the Eq (1.23) by maximum strain, we get shear modulus:

$$G = G' \sin(\omega t) + G'' \cos(\omega t) \tag{1.24}$$

Where $G' = \frac{\sigma_0}{\gamma_0} \cos(\delta)\ and\ G'' = \frac{\sigma_0}{\gamma_0} \sin(\delta)$ are storage and loss modulus, respectively. The storage modulus or elastic modulus is a degree of the stored energy in the material during elastic deformation and corresponds to the elastic component of the material. On the other hand, the loss modulus or viscous modulus is a degree of the energy dissipated as heat during the shear process and corresponds to the viscous component of the material. They give us information about the viscoelastic nature of the material. For instance, at low frequencies viscoelastic solids would have $G' > G''$ condition. After crossover point of storage and loss modulus ($G' = G''$) at a critical frequency $\left(\omega_c = {}^{1}/_{\tau}\right)$, they would have $G' < G''$ conditions and at higher frequencies the viscoelastic solids would behave more liquid-like [46]. The ratio between G'' and G' is the loss factor, which is tangent of the phase angle,

$$tan\delta = \frac{G''}{G'} \tag{1.25}$$

The loss factor is a comparison of the dissipated energy to stored energy during the sinusoidal deformation cycle.

For a given frequency, ω, amplitude stress, σ_0, divided by the strain, γ_0, gives complex modulus, G^*.

$$|G^*(\omega)| = \frac{\sigma_0}{\gamma_0} \tag{1.26}$$

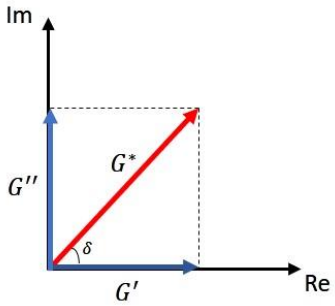

Figure 1.18. The complex modulus described as a combination of storage and loss modulus [40].

As shown in Figure 1.18, the complex modulus can be described as a combination of storage and loss modulus,

$$G^*(i\omega) = G'(\omega) + iG''(\omega) \tag{1.27}$$

And the complex viscosity is [43],

$$|\eta^*| = \frac{|G^*|}{\omega} \tag{1.28}$$

2. AIM OF THE STUDY

This study aims to synthesize polyesters containing ionic hydrogen bondings at their end groups by using various amines and carboxylic acid terminated polyesters in a melt reactor to examine the effect of non-covalent interactions on T_g and rheological properties. Due to the non-covalent nature of the ionic hydrogen bonding, the resulting polymeric network was expected to have some reversibility. By using polyesters and amines with various structures and different number of functionalities, the effect of polymer topology and functionality on the resulting polymeric networks was examined.

3. EXPERIMENTAL

Five amines with different functionalities were reacted with four polyesters with different functionalities. Reactions were carried out in glass melt reactors and silicon oil was used for heat transfer to reactor. The silicone oil was heated *via* ESM4450 48 x 48 1/16 DIN Universal Input PID Process Controller with Smart I/O Module System. Heidolph overhead stirrer was used. The rate of the stirrer was 50 rpm.

3.1. Materials

1,4-Cyclohexane dicarboxylic acid (CHDA) with ~70% trans content was obtained from Acros Organics. 1,4-Cyclohexane dimethanol (CHDM), 2,4,6-tris (dimethylaminomethyl)phenol, 2-methylimidazole, poly (ethylene imine), 1,4-diazabicyclo [2.2.2]octane, tetrabutylammonium bromide were obtained from Aldrich.

3.2. Synthesis of Poly (1,4-cyclohexylidenecyclohexane-1,4-dicarboxylate) (PCCD)

1,4-Cyclohexanedicarboxylic acid (CHDA) and 1,4-Cyclohexanedimethanol (CHDM) were reacted in different ratios in a melt reactor as shown in Figure 3.1 and Table 3.1. 0.01 mol-% ratio of Dibutyltin(IV) oxide, $[(C_4H_9)_2SnO]$, was used as catalyst. The reaction was run under a nitrogen atmosphere. The reaction temperature was gradually increased from 220^0 C to 250^0 C and the torque was recorded throughout the reaction. 5 mbar vacuum was applied in the last 90 min of the reaction. The distilled water was collected to favour the equilibrium towards products. The reaction was terminated after 6 hours.

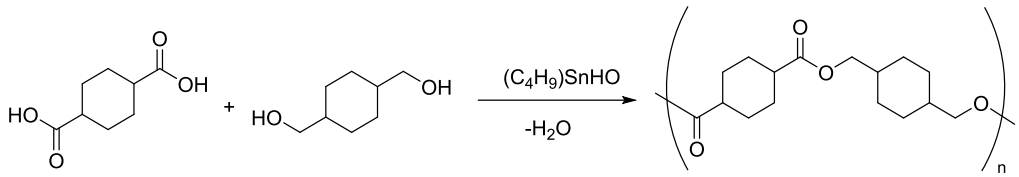

Figure 3.1. Synthesis of PCCD.

Table 3.1. Mole ratios of monomers in PCCD synthesis.

Sample Name	CHDA:CHDM (mole ratio)	CHDA		CHDM	
		mole	weight (g)	Mole	weight (g)
PCCD_1	1,02 : 1,00	0,08	13,7744	0,0580	8,3642
PCCD_2	1,00 : 1,005	0,1182	20,3532	0,1188	17,1259
PCCD_3	1,00 : 1,005	0,1288	22,1738	0,1294	18,6646
PCCD_4	1,005 : 1,00	0,1305	22,4316	0,1298	18,7192
PCCD_5	1,00 : 1,00	0,0876	15,0946	0,0876	12,6426

3.3. Synthesis of Non-Covalently Bonded Polyesters

Polyesters which were used in this study summarized in Table 3.2. PE-1, PE-2, and PE-4 are commercially available semi-aromatic polyesters while PE-3 was a fully aliphatic PCCD polyester which was synthesized in this study. PE-1, PE-3 and PE-4 are linear polyesters with having functionality of two. PE-2 is a polyester having four functionalities and hyperbranching toward to the end of the polymer chains.

Table 3.2. Functionality and end-groups of polyesters.

Polyester	**Functionality**	**End Group**
PE-1	2	-COOH
PE-2	>2	-COOH
PE-3	2	-COOH
PE-4	2	-OH

3.3.1. Synthesis of Non-Covalently Bonded Polyesters with 2-Methyl Imidazole

PE-1 and PE-2 were mixed with different ratios of 2-methyl imidazole (2MI) in a melt reactor. Mole ratios of synthesized polymers are depicted in Table 3.3. The reaction was conducted under nitrogen atmosphere and reaction temperature was kept between 100-115^0 C and torque was recorded. The reaction was finished 1 hour after complete melting of the components. By-product formation was not observed.

Table 3.3. Mole ratios of polyesters and 2MI.

Sample Name	Polyester	PE:2MI (mole ratio)	PE		2MI	
			mole (mmol)	weight (g)	mole (mmol)	weight (g)
2MI-1_0.25	PE-1	1.00 : 0.25	0.0286	50.0000	0.0143	1.1729
2MI-1_0.50	PE-1	1.00 : 0.50	0.0286	50.0000	0.0286	2.3457
2MI-1_1.00	PE-1	1.00 : 1.00	0.0143	25.0000	0.0286	2.3457
2MI-2_0.25	PE-2	1.00 : 0.25	0.0625	50.0000	0.2500	20.525
2MI-2_0.50	PE-2	1.00 : 0.50	0.0625	50.0000	0.1250	10.2625
2MI-2_1.00	PE-2	1.00 : 1.00	0.0625	50.0000	0.0625	5.1313

3.3.2. Synthesis of Non-Covalently Bonded Polyesters with Hexamethylenediamine

PE-1 and PE-2 were mixed with different ratios of hexamethylenediamine (HMDA) in a melt reactor. Mole ratios of synthesized polymers are depicted in Table 3.4. The reaction was conducted under nitrogen atmosphere and reaction temperature was kept between 100-115^0 C and torque was recorded. The reaction was finished 1 hour after complete melting of the components. By-product formation was not observed.

Table 3.4. Mole ratios of polyesters and HMDA.

Sample Name	Polyester	PE:NX3P (mole ratio)	PE		NX3P	
			mole (mmol)	weight (g)	mole (mmol)	weight (g)
HMDA-1_0.25	PE-1	1.00 : 0.25	0.0286	50.0000	0.0072	0.8308
HMDA-1_0.50	PE-1	1.00 : 0.50	0.0286	50.0000	0.0143	1.6616
HMDA-1_1.00	PE-1	1.00 : 1.00	0.0286	50.0000	0.0286	3.3233
HMDA-2_0.25	PE-2	1.00 : 0.25	0.0639	51.1515	0.0159	1.8576
HMDA-2_0.50	PE-2	1.00 : 0.50	0.0625	50.0000	0.0625	7.2625
HMDA-2_1.00	PE-2	1.00 : 1.00	0.0625	50.0000	0.1250	14.5250

3.3.3. Synthesis of Non-Covalently Bonded Polyesters with 2,4,6-Tris (dimethyl-aminomethyl) phenol

PE-1 and PE-2 were mixed with different ratios of 2,4,6-tris (dimethylaminomethyl) phenol (NX3P) in a melt reactor. Mole ratios of synthesized polymers are depicted in Table 3.5. The reaction was conducted under nitrogen atmosphere and reaction temperature was kept between 100-115^0 C and torque was recorded. The reaction was finished 1 hour after complete melting of the components. By-product formation was not observed.

Table 3.5. Mole ratios of polyesters and NX3P.

Sample Name	Polyester	PE:NX3P (mole ratio)	PE		NX3P	
			mole (mmol)	weight (g)	mole (mmol)	weight (g)
NX3P-1_0.25	PE-1	1.00 : 0.25	0.0286	50.0000	0.0107	2.8421
NX3P-1_0.50	PE-1	1.00 : 0.50	0.0286	50.0000	0.0214	5.6793
NX3P-1_1.00	PE-1	1.00 : 1.00	0.0337	59.1013	0.0506	13.4442
NX3P-2_0.25	PE-2	1.00 : 0.25	0.0625	50.0000	0.0117	3.1100
NX3P-2_0.50	PE-2	1.00 : 0.50	0.0625	50.0000	0.0234	6.2200
NX3P-2_1.00	PE-2	1.00 : 1.00	0.0625	50.0000	0.0468	12.4400

3.3.4. Synthesis of Non-Covalently Bonded Polyesters with Tetrabutylammonium Bromide

PE-1 and PE-2 were mixed with different ratios of tetrabutylammonium bromide (TAB) in a melt reactor as shown in Table 3.6. The reaction was conducted under nitrogen atmosphere and reaction temperature was kept between 100-115^0 C and torque was recorded. The reaction was finished 1 hour after complete melting of the components. By-product formation was not observed.

Table 3.6. Mole ratios of polyesters and TAB.

Sample Name	Polyester	PE:TAB (mole ratio)	PE		TAB	
			mole (mmol)	weight (g)	mole (mmol)	weight (g)
TAB-1_0.25	PE-1	1.00 : 0,25	0.0286	50.0000	0.0142	4.6051
TAB-1_0.50	PE-1	1.00 : 0.50	0.0286	50.0000	0.0286	9.2103
TAB-2_0.25	PE-2	1.00 : 0.25	0.0375	30.0000	0.0375	12.0885
TAB-2_0.50	PE-2	1.00 : 0.50	0.0187	15.0000	0.0374	12.0800

3.3.5. Synthesis of Non-Covalently Bonded Polyesters with 1,4-Diaza bicycle [2.2.2]octane

PE-1 and PE-2 were mixed with different ratios of 1,4-Diazabicyclo[2.2.2]octane (DABCO) in a melt reactor. Mole ratios of synthesized polymers were depicted in Table 3.7. The reaction was conducted under nitrogen atmosphere and reaction temperature was kept between 100-115^0 C and torque was recorded. The reaction was finished 1 hour after complete melting of the components. By-product formation was not observed.

Table 3.7. Mole ratios of polyesters and DABCO.

Sample Name	Polyester	PE:DABCO (mole ratio)	PE		DABCO	
			mole (mmol)	weight (g)	mole (mmol)	weight (g)
DABCO-1_0.25	PE-1	1.00 : 0.25	0.0286	50.0000	0.0071	0.8022
DABCO-1_0.50	PE-1	1.00 : 0.50	0.0286	50.0000	0.0143	1.6044
DABCO-1_1.00	PE-1	1.00 : 1.00	0.0286	50.0000	0.0286	3.2048
DABCO-2_0.25	PE-2	1.00 : 0.25	0.0375	30.0000	0.0047	0.5258
DABCO-2_0.50	PE-2	1.00 : 0.50	0.0375	30.0000	0.0093	1.0500
DABCO-2_1.00	PE-2	1.00 : 1.00	0.0375	30.0000	0.0187	2.1000
DABCO-3_1.00	PE-3	1.00 : 1.00	0.0065	15.0000	0.0065	0.7392
DABCO-4_1.00	PE-4	1.00 : 1.00	0.0267	30.0000	0.0267	3.0045

3.3.6. Synthesis of Non-Covalently Bonded Polyesters with Poly (ethylene imine)

The four polyesters were reacted with different ratios of branched poly (ethylene imine) (PEI) in a melt reactor. Mole ratios of synthesized polymers are depicted in Table 3.8. The reaction was conducted under nitrogen atmosphere and reaction temperature was kept between 100-115^0 C and torque was recorded. The reaction was finished 1 hour after complete melting of the components. By-product formation was not observed.

Table 3.8. Mole ratios of polyesters and PEI.

Sample Name	Polyester	PE:PEI (mole ratio)	PE		PEI	
			mole (mmol)	weight (g)	mole (mmol)	weight (g)
PEI-1_0.25	PE-1	1.00 : 0.25	0.0300	52.5833	0.0075	0.3155
PEI-1_0.50	PE-1	1.00 : 0.50	0.0299	52.3250	0.0149	0.6279
PEI-1_1.00	PE-1	1.00 : 1.00	0.0183	32.0000	0.0183	0.7680
PEI-2_0.25	PE-2	1.00 : 0.25	0.0718	57.4400	0.0179	0.7539
PEI-2_0.50	PE-2	1.00 : 0.50	0.0625	50.0000	0.0316	1.3125
PEI-2_1.00	PE-2	1.00 : 1.00	0.0200	16.0000	0.0200	0.8400
PEI-3_1.00	PE-3	1.00 : 1.00	0.0043	10.0000	0.0043	0.1845
PEI-4_1.00	PE-4	1.00 : 1.00	0.0267	30.0000	0.0267	1.1214

3.4. Characterization

3.4.1. DSC Analysis

Exstar SII DSC 7020 instrument was used for thermal analysis.

Table 3.9. DSC run method

Initial T (ºC)	**Final T (ºC)**	**Rate (ºC /min)**	**Hold time (min)**
0	200	10	1
200	0	10	2
0	200	10	1

3.4.2. Rheology Analysis

Anton Paar MCR302 rheometer with 20 mm parallel plate was used. Viscosity tests were conducted at 90^0 C with shear rate ranging from 0,001 s^{-1} to 1000 s^{-1}. Temperature ramp tests were operated at a constant strain of 1% and a constant angular frequency of 10 rad/s with temperature ranging from 20^0 C to 200^0 C.

3.4.3. ^{1}H-NMR Analysis

Varian Gemini 400 MHz spectrometer was used in $CDCl_3$ for ^{1}H-NMR analysis.

4. RESULTS AND DISCUSSION

The work carried out will be presented in the following order where four essential subjects will be covered:

(i) In the first part of this work, the synthesis of PCCD polyesters using different ratios of cycloaliphatic monomers is discussed. The aim to synthesize PCCD polyesters was to further mix/react them with amines and thus to compare the results with semi-aromatic commercial polyesters.

(ii) In the second part, the synthesis of non-covalently bonded polyesters was targeted. The polyesters were reacted with different ratios of 2MI, NX3P, HMDA, TAB, DABCO and PEI to see their effect on the T_g and the mechanical properties of the polyesters. An increase was generally expected in T_g of carboxyl-terminated polyesters due to ionic hydrogen bonding with the amines.

(iii) Then, the thermal behaviour of the non-covalently bound polyesters by DSC measurements will be presented.

(iv) Finally, the rheological studies on the polyesters will be presented.

4.1. Synthesis of Poly (1,4-cyclohexylidenecyclohexane-1,4-dicarboxylate) (PCCD)

Alcohol and acid-terminated PCCD polymers with various molecular weights and glass transition temperatures were synthesized using different ratios of cyclohexane dimethanol (CHDM) and cyclohexane dicarboxylic acid (CHDA) (Table 4.1).

Table 4.1. The properties of synthesized PCCD.

Sample Name	Acid Value	M_n	M_w	T_g (◦C)
PCCD_1	19.21	8590	14022	42.7
PCCD_2	17.41	4632	7521	39.4
PCCD_3	23.39	4975	9586	39.3
PCCD_4	21.337	4552	7848	38,8
PCCD_5	12.89	7003	12806	39.6

In the synthesis of the PCCD polyesters several subjects had to be taken into account:

(i) It is important to note that both the diol and the diacid have *cis-trans* isomerism; therefore, we can see the *cis* and *trans* signals of both monomer repeat units in the resulting PCCD (Figure 4.1). The control over *cis-tans* ratio is critical to have a tailor made PCCD. *Trans* conformation leads to better packing of chains since its more symmetrical and stretched. So PCCD's with higher *trans* ratio have higher T_g's and are more crystalline. Process conditions and the catalyst used have a direct effect on the *cis/trans* ratio of the repeat units.

(ii) Another important parameter is the monomer ratio. Considering that the CHDM monomer is not a volatile diol, the excess alcohol cannot be removed from the reaction medium therefore, stoichiometric ratio is important in tuning the M_w of PCCD.

(iii) High catalyst loading is found to lead discoloration for some catalyst [47]. Therefore, for a transparent and colourless polymer the catalyst loading had to be optimized.

The PCCD polyesters were synthesized considering these factors so that the targeted polymers with tunable *cis/trans* ratio, T_g and M_w could be obtained in reasonable polymerization times.

The H^1-NMR spectrum of PCCD_3 is shown in Figure 4.1.

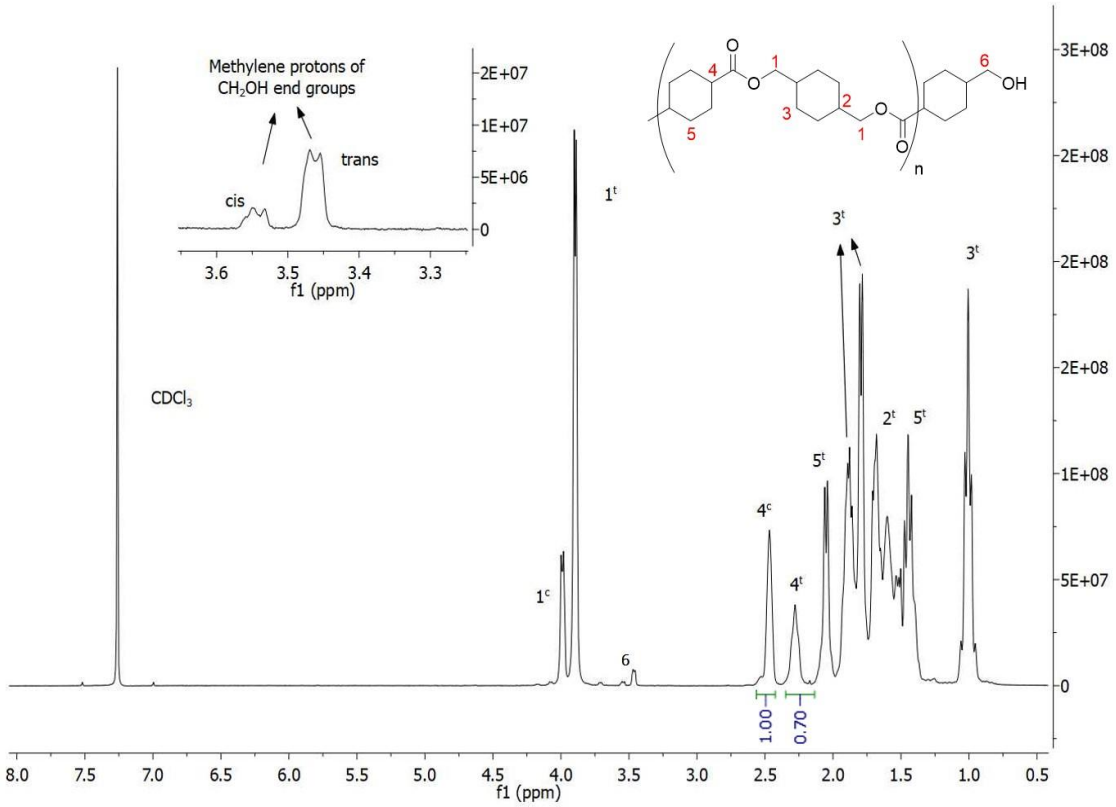

Figure 4.1. H^1-NMR spectrum of PCCD_3.

The *cis-trans* ratio of 1,4-cyclohexylene unit is normally 34-66 mol%. The ratio of 4^c peak ($\delta = 2.47\,ppm$) and 4^t peak ($\delta = 2.28\,ppm$) showed that the *cis-trans* ratio in polymer was 58-42 mol%. The CEG, M_n, M_w and T_g of the synthesized PCCD polymers are shown in Table 4.1.

The PCCD_3 was then used as one of the carboxylic acid terminated polyesters in the synthesis of ionically bonded polyesters due to its higher acid value.

4.2. Synthesis of Non covalently Bonded Polyesters

Various compounds containing different type (1^0 , 2^0 , 3^0) and number of amines were reacted with four different carboxyl-terminated polyesters, of which three were commercially available. Same experimental method was applied for all polyesters and care was taken so that reaction temperature did not exceed 110^0 C to prevent any potential Hofmann elimination (especially for tertiary amines, section 4.2.4). All reactions were terminated after 1 hour of complete melting of the reagents.

4.2.1. Synthesis of Non-Covalently Bonded Polyesters with 2-Methylimidazole (2MI)

2-Methylimidazole is widely used in curing of epoxy-anhydride and epoxy-polyester systems in powder coating applications. The goal to use 2MI in this study was to see if it induces ionic interactions with carboxyl end groups besides its known activity as catalyst. Since 2MI has in average only one amine group that can act as a base and accept a proton from the acid, a network formation was not expected. Instead, any acid-base complexation was expected to result in an end-capping type of interaction. The only possible network formation could come from the sharing of the mono-functional amine by multiple carboxylic acid through partial ionization of the acid end groups. The proton transfer between secondary amine of 2MI and acid groups of polyester is illustrated in Figure 4.2.

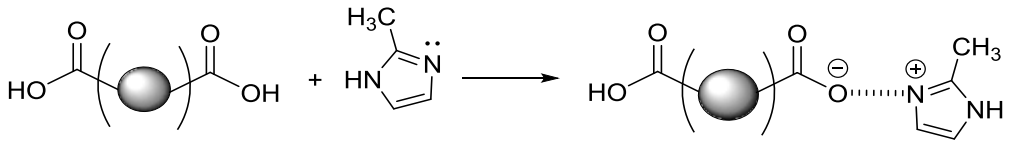

Figure 4.2. Acid-base complexation between carboxyl-terminated polyester and 2MI.

4.2.2. Synthesis of Non-Covalently Bonded Polyesters with Hexamethylenediamine (HMDA)

Hexamethylene diamine is a linear two-functional molecule. It has two secondary amines at the ends of the molecule therefore, in an acid-base complexation with a di-acid polymer, it should lead to a chain extension type of interaction. However, with a multi-

functional (>2) acid terminated polymer, it can form an ionically crosslinked network. The proton transfer between the primary amines of HMDA and acid groups of polyesters is illustrated in Figure 4.3.

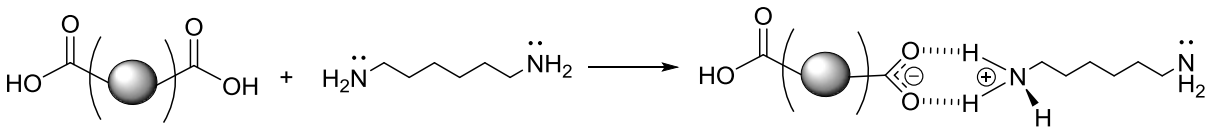

Figure 4.3. Acid-base complexation between carboxyl-terminated polyester and HMDA.

4.2.3. Synthesis of Non-Covalently Bonded Polyesters with 2,4,6-Tris (dimethylaminomethyl) phenol (NX3P)

NX3P is another widely used catalyst for epoxy-anhydride and epoxy-polyester systems. It has three tertiary amine groups therefore, if all amines in NX3P were to accept proton from acid groups of polyester chains, it would be expected to lead to a crosslinked network type of structure. This network formation can in principle be achieved with any carboxyl terminated polyester whose functionality is greater than one. The proton transfer between tertiary amines of NX3P and acid groups of polyester is illustrated in Figure 4.4.

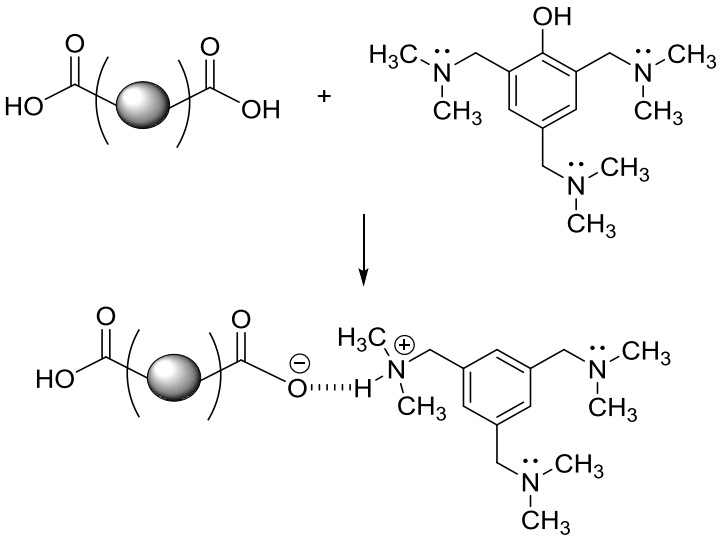

Figure 4.4. Acid-base complexation between carboxyl-terminated polyester and NX3P.

4.2.4. Synthesis of Non-Covalently Bonded Polyesters with Tetrabutylammonium Bromide (TAB)

TAB is a quaternary ammonium salt. It is also used as catalyst in curing of the epoxy resin systems. The goal was to see its effect in polyester resins in higher ratios. Considering that it does not have a lone pair electron on nitrogen atom, it cannot accept a proton from the acid groups. However, quaternary ammonium salts are known to give elimination reaction called Hofmann elimination at moderate temperatures (>110^0 C) especially but not necessarily under basic conditions. In order to have Hofmann elimination reaction, beta hydrogen and antiperiplanar conformation between beta hydrogen and quaternary amine group is required (Figure 4.5a).

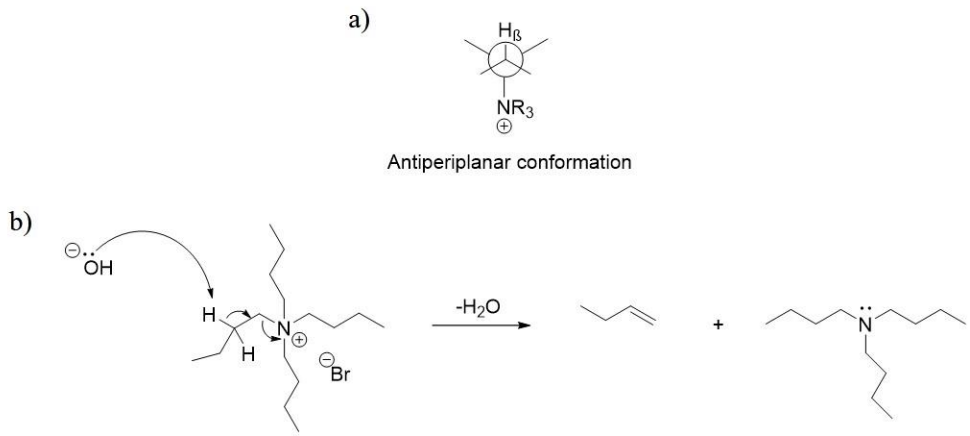

Figure 4.5. (a) Antiperiplanar conformation of quaternary amine and beta hydrogen and (b) Degradation mechanism of quaternary ammonium salts by Hoffmann elimination.

The degradation mechanism of TAB by Hoffmann elimination is illustrated in Figure 4.5b. So, it was assumed that the acid-base complexation between TAB and polyester would not occur, unless a tertiary amine is produced by a Hoffmann elimination. So, it was employed to check, how an ionic organic additive, that is not complexing with the polyester end groups would affect the properties of the polyesters. This can give an idea on the pure ionic effect separate from the complexation. In other words, it was used to resolve the effect of ionic charge on the material properties (for example by inductive effect, secondary interactions with chains, etc.). TAB may be not the perfect candidate to resolve such interactions due to the large alkyl groups that must affect the physical properties, however,

it is one of the most widely used acid/epoxy catalyst in powder coatings. Therefore, it could be useful to check, if there was any ionic benefit or loss by the use of TAB.

Although the detailed results will be presented later, it was interesting to observe that the polyesters reacted with TAB had good extensibility in its melt form as shown in Figure 4.6.

Figure 4.6. The photograph of TAB-1_0.50.

4.2.5. Synthesis of Non-Covalently Bonded Polyesters with 1,4-Diazabicyclo [2.2.2]octane (DABCO)

DABCO is widely used as catalyst and as an acid scavenger in elimination reactions. Dicationic form of DABCO has a very low pKa value (pKa=2.97) [48] therefore, protonation of both amine is only achieved with very strong acids. If DABCO reacts from both sides, it would lead to a chain extension type of interaction similar to HMDA with bifunctional acids, but to a network formation with multi-acids (>2). Although it has beta hydrogens, due to its rigid cage structure it cannot attain antiperiplanar conformation thus, it does not undergo Hoffmann (when quaternized) or Cope (when oxidized) elimination. The potential proton transfer between tertiary amines of DABCO and acid groups of polyesters is illustrated in Figure 4.7.

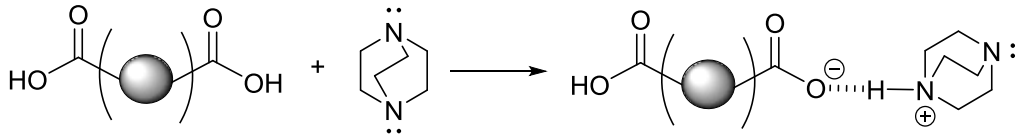

Figure 4.7. Acid-base complexation between carboxyl-terminated polyester and DABCO.

4.2.6. Synthesis of Non-Covalently Bonded Polyesters with Polyethylene Imine (PEI)

In this study a branched PEI was used. It contains primary, secondary and tertiary amine groups. It is widely used in synthesizing various ionic supramolecular polymers and curing reaction of epoxy resins. Since it bears a large number of amine groups, it is expected to lead a strong network formation *via* acid-base complexation with acid groups of polyesters. The proton transfer between amines of PEI and acid group of polyester is illustrated in Figure 4.8 (only one is shown however almost all nitrogens may be subject to protonation as far as the resulting cationic repulsions are minimized).

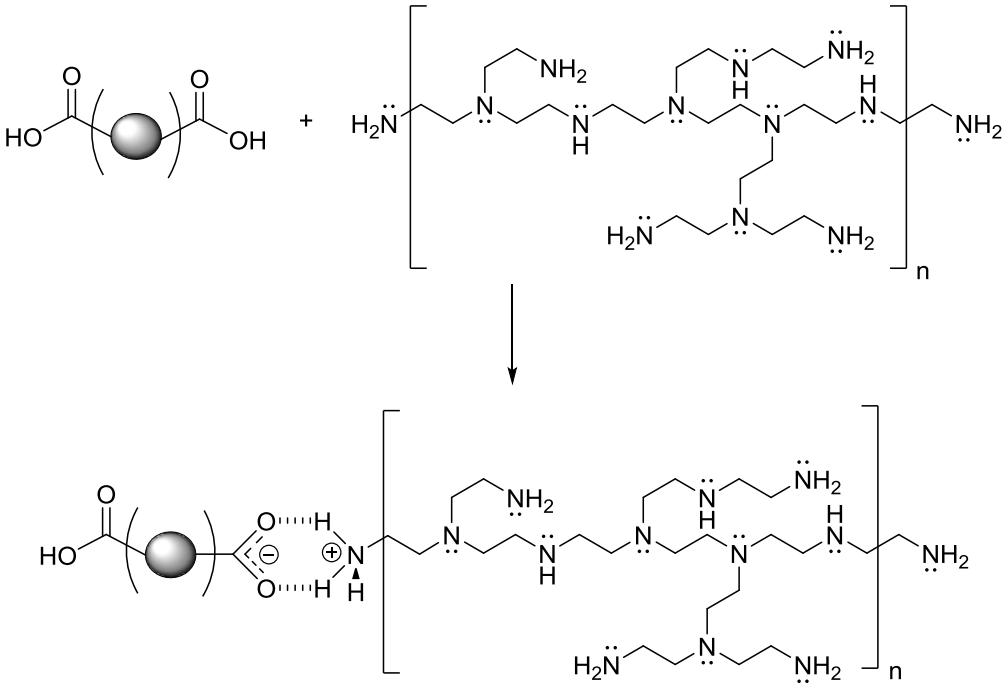

Figure 4.8. Acid-base complexation between carboxyl-terminated polyester and PEI.

4.3. Differential Scanning Calorimeter Results of Non-Covalently Bonded Polyesters

DSC results of four polyesters that are used in this study are depicted in Table 4.2. PE-1, PE-2, and PE-3 were carboxyl-terminated polyesters that is expected to have ionic hydrogen bonding with the amines. PE-4 was an alcohol-terminated polyester which was used as a control sample for comparative studies. Another set of control experiments was done with blank polyesters, where the latters were processed under the same conditions used in the melt reactor to check whether or not there was a change in polyesters themselves at the reaction/processing conditions. Such change could potentially affect the T_g of the heat-processed polyesters and could (Table 4.2) potentially act as a noise in the T_g measurements. PE1-control showed no T_g increase at the reaction conditions, but PE-2-control showed a slight increase in T_g.

Table 4.2. Glass transition temperatures of polyesters.

Sample Name	T_g (◦C)
PE-1	53.3
PE-2	43.7
PE-3	39.3
PE-4	57.6
PE-1control	53.4
PE-2control	47.2

The DSC results of the synthesized polymers are shown in Table 4.3. According to the results, among the five amine complexing agents PEI and DABCO seemed to be the ones with the most promising results where significant T_g increases were observed, indicating good complexations with the acid terminated polyesters.

Complexation of 2MI and PE-1: The action of 2MI on polyesters seemed very complex and confusing. The addition of 2MI on PE-1 resulted in an increase in T_g of PE-1 at acid/amine mole ratio of 1.00:0.25. When the amount of 2MI was doubled (mol ratio of 1.00:0.50) there was no change in the T_g of PE-1. Finally, when the ratio was increased to 1.00:1.00, the T_g decreased. In general, the end groups of a carboxyl-terminated polyester

form hydrogen bonds among themselves. It is assumed that this results in a higher T_g value for carboxyl-terminated polyesters compared to their analogues with none coordinative end groups. 2MI has only one amine that can act as a base and accept a proton from acid groups therefore, it cannot have a network or linear chain extension type interactions with polyesters. So, when the ratio was increased to 1.00:1.00, 2MI may block most of the, if not all, acid groups and prevent their interactions with each other. This may lead to an increase of the free volume in the polyester, hence causes T_g to drop. The reason for the decrease in T_g at 1.00:1.00 ratio could be this blocking of acid groups by 2MI.

Table 4.3. Glass transition temperatures of all non-covalently bonded polyesters.

Sample Name	T_g (◦C)	Sample Name	T_g (◦C)
2MI-1_0.25	56.2	DABCO-1_0.25	55.3
2MI-1_0.50	52.8	DABCO-1_0.50	60.2
2MI-1-1.00	37.4	DABCO-1_1.00	57.7
2MI-2_0.25	44.1	DABCO-2_0.25	47.4
2MI-2_0.50	36.2	DABCO-2_0.50	46.7
2MI-2_1.00	21.7	DABCO-2_1.00	52.2
NX3P-1_0.25	56.2	DABCO-3_1.00	42.3
NX3P-1_0.50	48.3	DABCO-4_1.00	44.0
NX3P-1_1.00	n/a	PEI-1_0.25	55.0
NX3P-2_0.25	44.5	PEI-1_0.50	57.8
NX3P-2_0.50	46.8	PEI-1_1.00	59.2
NX3P-2_1.00	43.3	PEI-2_0.25	39.6
HMDA-1_0.25	54.4	PEI-2_0.50	41.9
HMDA-1_0.50	54.2	PEI-2_1.00	42.3
HMDA-1_1.00	44.7	PEI-3_1.00	42.8
HMDA-2_0.25	n/a	PEI-4_1.00	54.6
HMDA-2_0.50	36.7	TAB-1_0.25	24.7
HMDA-2_1.00	26.3	TAB-1_0.50	38.0

Complexation of 2MI and PE-2: In the case of PE-2 and 2MI, at acid/amine ratio of 1.00:0.25 the T_g was not affected and was the same with original PE-2 while with increasing ratios of 2MI, T_g dropped gradually. PE-2 has hyperbranching at the very ends of polymer chains. This structure may disfavor the interaction of 2MI with all end groups because of ionic repulsions. In other words, 2MI may not complex with all the acid groups as easily as it could in PE-1, therefore at high loading of 2MI, it can act as a plasticizer. It is known that

the presence of soluble low molecular weight components increases the free volume of a polymeric system and subsequently lowers the glass transition temperature. This effect is described by the Fox equation in Eq (4.1) where w_1 *and* w_2 are weight fractions and $T_{g,1}$ and $T_{g,2}$ are T_g's of polymer-1 and polymer-2, respectively. [48]

$$\frac{1}{T_g} = \frac{w_1}{T_{g,1}} + \frac{w_2}{T_{g,2}} \tag{4.1}$$

Complexation of NX3P and PE-1: NX3P showed an increase in T_g for PE-1, similar to 2MI, at acid/amine mole ratio of 1.00:0.25 but differently from 2MI, T_g started to decrease at 1.00:0.50 ratio and decreased even more drastically at 1.00:1.00 ratio. Since NX3P has three tertiary amines that could accept proton from acids, at low ratio it may lead to an ionic network type interaction but at higher loadings of amine, the plasticizing effect seem more dominant which is reasonable considering that NX3P is liquid at room temperature.

Complexation of NX3P and PE-2: The interaction of PE-2 and NX3P showed no increase in T_g. Actually, when we compare with the blank control of PE-2 there was even a slight decrease.

Complexation of HMDA with PE-1 and PE-2: HMDA did not show any significant increase in T_g with PE-1 at acid/amine mole ratios of 1.00:0.25 and 1.00:0.50. Taken into account the T_g decreases observed with the above amines due to the plasticizing effect of the amines used, one could expect similar action from the HMDA. The fact that T_g did not drop, is most probably pointing out some ionic interactions. However, when the HMDA used was increased and the acid/amine ratio reached 1.00:1.00 there was a decrease in T_g. Given that HMDA is not a rigid molecule, at high loadings HMDA molecules that could not find or bind to any acid ends of polyester may acted again as plasticizer. However, the combination of PE-2 and HMDA showed a drastic decrease at all acid/amine ratios.

Complexation of TAB with PE-1 and PE-2: TAB is a quaternary ammonium salt and since it does not have any lone pair on the nitrogen atom, it cannot act as a base and

accept a proton from acid groups. As expected, it decreased T_g of all polyesters. Moreover, some did not even show any T_g values at temperatures above 0^0 C.

According to the results from Table 4.3, DABCO and PEI were the two amines that gave the most anticipated outcomes. DABCO increased T_g of all carboxyl-terminated polyesters (PE-1, PE-2, and PE-3). This was expected considering that it does not undergo Hofmann elimination and has a rigid structure. PEI gave promising results with PE-1 and PEI-3 whereas PE-2 did not show any increase in T_g. Due to branched structure of PEI, it may restrict the chain motions and also form network structure, consequently leading to an increase in T_g. Furthermore, control experiments with alcohol-terminated polyester (PE-4) showed no increase with both PEI and DABCO, even showed a serious decrease with DABCO. The T_g of PEI is about -62^0 C and it is a very viscous substance at room temperature. Since PEI and alcohol-terminated polyester cannot have any ionic interactions PEI acted as a plasticizing agent lowering the T_g of PE4 to 54^0 C. Compared to PEI, DABCO is a more rigid compound but its effect on T_g of PE-4 was more severe than in PEI.

Considering the DSC results, DABCO and PEI seemed to be the ones with best complexation abilities. The results with HMDA indicate that there is also some complexation but the low T_g values obtained would not serve the purpose of increasing T_g. Therefore, DABCO and PEI were chosen for their further effects on the polyesters.

4.4. Rheological Results of PEI and DABCO Containing Polyesters

Firstly, an amplitude sweep test was done to determine the linear viscoelastic regions of polymers for further rheological tests. After finding linear viscoelastic regions, temperature sweep tests were done to see the behavior of polymers with respect to temperature. Lastly, rotational viscosity tests were done to find zero shear viscosities of polymers to compare their average molar masses.

In the temperature sweep graphs, the points where G'' is beginning to raise were taken as the glass transition temperatures. The crossover points, where $G' = G''$, were taken as the melting points of polymers. They all showed an amorphous polymer behavior where

$G' > G''$ in the low temperature range below the T_g, which is so-called the glassy-state. In this region, polymer chains are almost immobile and they exhibit the consistency of a rigid and brittle solid. Raising the temperature, introduces more mobility, and after the glass transition temperature materials became softer, more elastic. After $G' = G''$, loss modulus starts to dominate and molecules start to have more mobility, they move along each other and the number of disentanglements increase. The polymer is now in a molten state and act as a viscoelastic liquid. A steady drop of both storage and loss modulus after melting, points out a typical amorphous polymer behavior.

Viscosity depends on temperature, shear rate, shear rate history and sometimes pressure in structured materials. For viscosity tests, all samples were measured at the same temperature and shear rate ranges and were allowed to rest for two minutes prior to the measurements to allow relaxation of the molecules after the gap setting, which could cause internal stresses. In the low shear ranges, which is below $\dot{\gamma} = 1$, amorphous polymers exhibit zero-shear viscosity plateau which stems from the superposition of the two processes. The orientation of polymer chains under shear leads to disentanglements. As a result, viscosity decreases. Some of the other polymer chains which were already disentangled recoil due to elastic behavior which leads to an increase in viscosity. These two processes balance each other out and as a consequence in the low shear rate range viscosity does not show any significant change and gives a plateau value which is called the zero-shear viscosity, η_0. The importance of η_0 is it gives us the insight to compare average molecular weight ($\overline{M_w}$) of polymers. The higher the η_0, the higher the $\overline{M_w}$ the polymer has. At higher shear rates, which is above 1, disentanglements overpower the re-entanglements and polymers show shear-thinning behavior and viscosity starts to decrease. This range is called flow range and polymers with a steeper slope here have a narrower molecular weight distribution. High M_w means more entanglements in polymer, increasing in entanglements leads to a decrease in free volume, which eventually results in an increase in T_g. When comparing zero shear viscosities with DSC results, the relation between T_g and M_w can be obtained.

The test results of PE-1 with PEI are shown in Table 4.4.

Table 4.4. Rheological results of PEI-1 series.

Sample Name	T_g (◦C)	T_m(◦C)	η_0(Pa.s)
PEI-1_0.25	57	63	1192
PEI-1_0.50	55	64	3630
PEI-1_1.00	60	71	14348

Complexation of PEI and PE-1: The temperature ramp graphs of PEI-1 series are shown in Figure 4.9. As shown previously in Figure 4.2, all samples were amorphous with $G' > G''$ at low temperatures. After crossover point, they showed a drop of both loss and storage moduli similar to a typical amorphous polymer. The T_g and T_m results from rheometer was slightly higher for all ratios of PEI, but the order was same with DSC which confirmed the DSC results. All the ratios showed increase in T_g, but PEI-1_1.00 had the highest and PEI-1_0.25 had the lowest T_g.

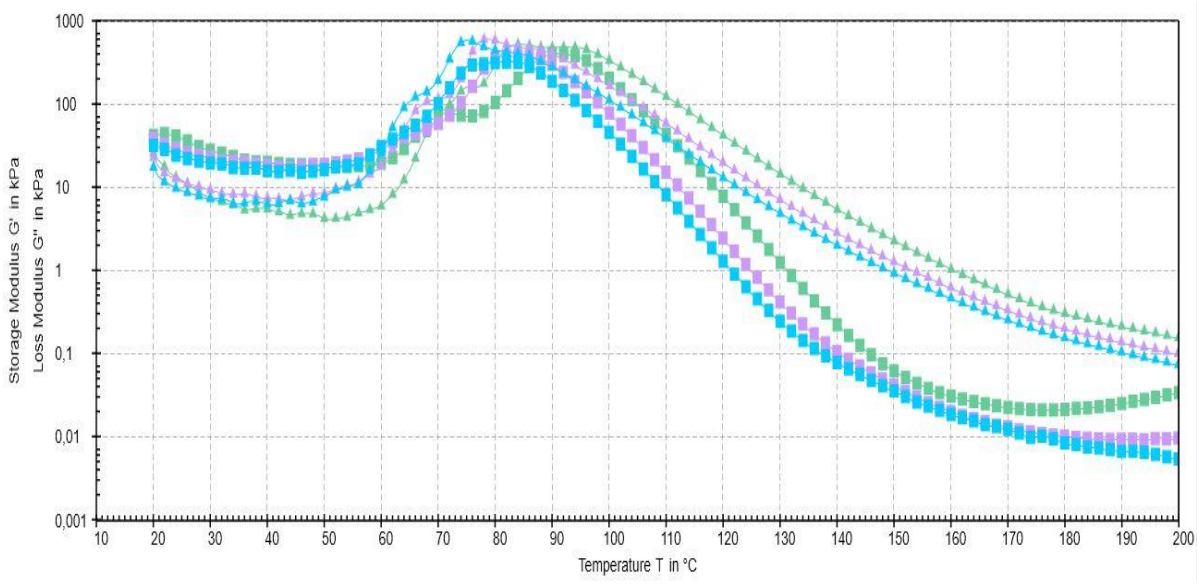

Figure 4.9. The storage modulus of PEI-1_1.00 (green), PEI-1_0.50 (purple), PEI-1_0.25 (blue) represented by square lines and loss modulus represented by triangle lines.

Figure 4.10 below shows the flow curves of the samples in Table 4.4. When $\overline{M_w}$ of the samples were compared, the order from highest to lowest is PEI-1_1.00 > PEI-1_0.50 >

PEI-1_0.25. If the results from the previous DSC measurements is taken into account, this order seems reasonable since the magnitude of glass transition temperatures follows the same order. Also, when molecular weight distributions were analyzed the PEI-1_1.00 has the narrowest MWD because its slope in the flow range is steeper, while PEI-1_0.25 has the broadest MWD. The three polymers showed the same viscosity at high shear rates.

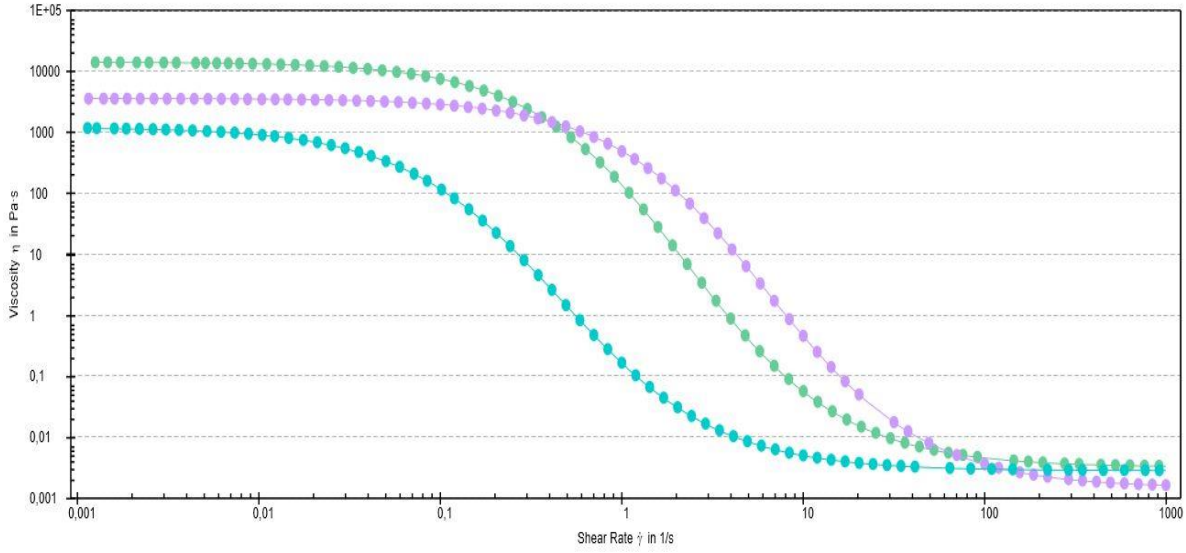

Figure 4.10. The flow curves of PE-1_1.00 (green), PEI-1_0.50 (purple) PEI-1_0.25 (blue).

Figure 4.11 below is the loss factor *versus* temperature graph which shows transitions in the materials. The point where $tan\delta = 1$ shows the glass transition temperature and after reaching a maximum which is the point of melting, the loss factor starts to decrease for most amorphous polymers but for polymers with secondary interactions like ionic interactions there should be a second peak. All three ratios showed a second peak in Figure 4.11 below. This may be the indication of a second relaxation in the non-covalently bonded polyester, which most likely indicates potential ionic interactions between PEI and PE-1.

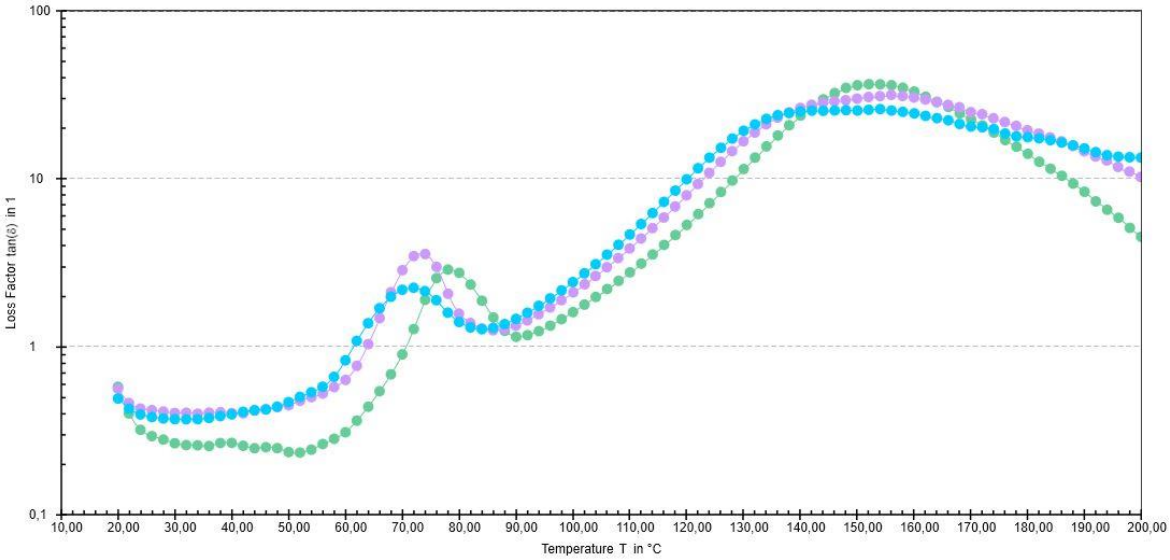

Figure 4.11. The loss factor versus temperature graph of PE-1_1.00 (green), PEI-1_0.50 (purple) PEI-1_0.25 (blue).

Complexation of PEI and PE-2: The viscosity and temperature ramp test results of PE-2 with PEI are shown in the Table 4.5 below.

Table 4.5. Rheological results of PEI-2 series.

Sample Name	T_g (◦C)	T_m(◦C)	η_0(Pa.s)
PEI-2_0.25	39	48	520
PEI-2_0.50	41	51	1532
PEI-2_1.00	31	42	2336

The temperature ramp graphs of PEI-2 series are shown in Figure 4.12. Comparing T_g results from the rheometer with DSC, only PEI-2_1.00 showed almost 10^0 C lower value in rheometer. When compared to PE-2 all samples had a decrease in T_g, it was an exact opposite behavior of PE-1, even though PE-2 has more carboxyl-groups and lower molecular weight. PE-2 has a branched structure at the ends of the chains, hence it may not give any ionic hydrogen bonding due to the steric hinderance and ionic repulsion of both polyester and PEI. Alternatively, they may form a polymer blend, therefore based on the Fox equation

in Eq (4.1), the glass transition of polymers may drop. It is reasonable considering T_g decrease is more evident with increasing ratio of amine.

All samples were amorphous with $G' > G''$ at low temperatures. After crossover point, they showed a drop of both loss and storage moduli similar to a typical amorphous polymer up to 130^0 C. After this value, they all showed different behaviors.

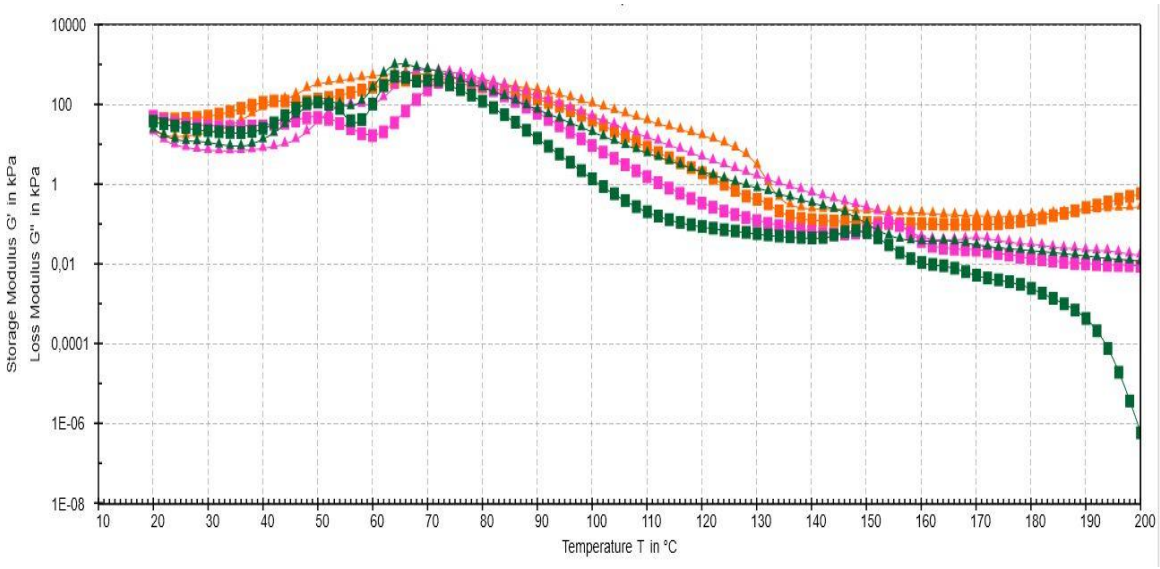

Figure 4.12. The storage modulus of PEI-2_1.00 (orange), PEI-2_0.50 (pink), PEI-2_0.25 (green) represented by square lines and loss modulus represented by triangle lines.

A second crossover point is observed at around 190^0 C for PEI-2_1.00. After this point, material became solid again. As for PEI-2_0.50, there is a point around 155^0 C where G' showed a sudden increase while G'' had been decreasing before a crossover occurs, the material showed viscoelastic liquid behavior again with decreases in both moduli steadily. The same pattern as PEI-2_0.50 is observed for PEI-2_0.25, but while having viscoelastic liquid behavior after a sudden increase in G' at 150 ^{0} C, there is a steep decrease of G' at 190^0 C.

Aminolysis is a well-known reaction in the degradation of polyesters [49]. Ammonia, primary and secondary amines lead to aminolysis of polyesters at elevated temperatures. The reaction mechanism of PET degradation is depicted in Figure 4.13.

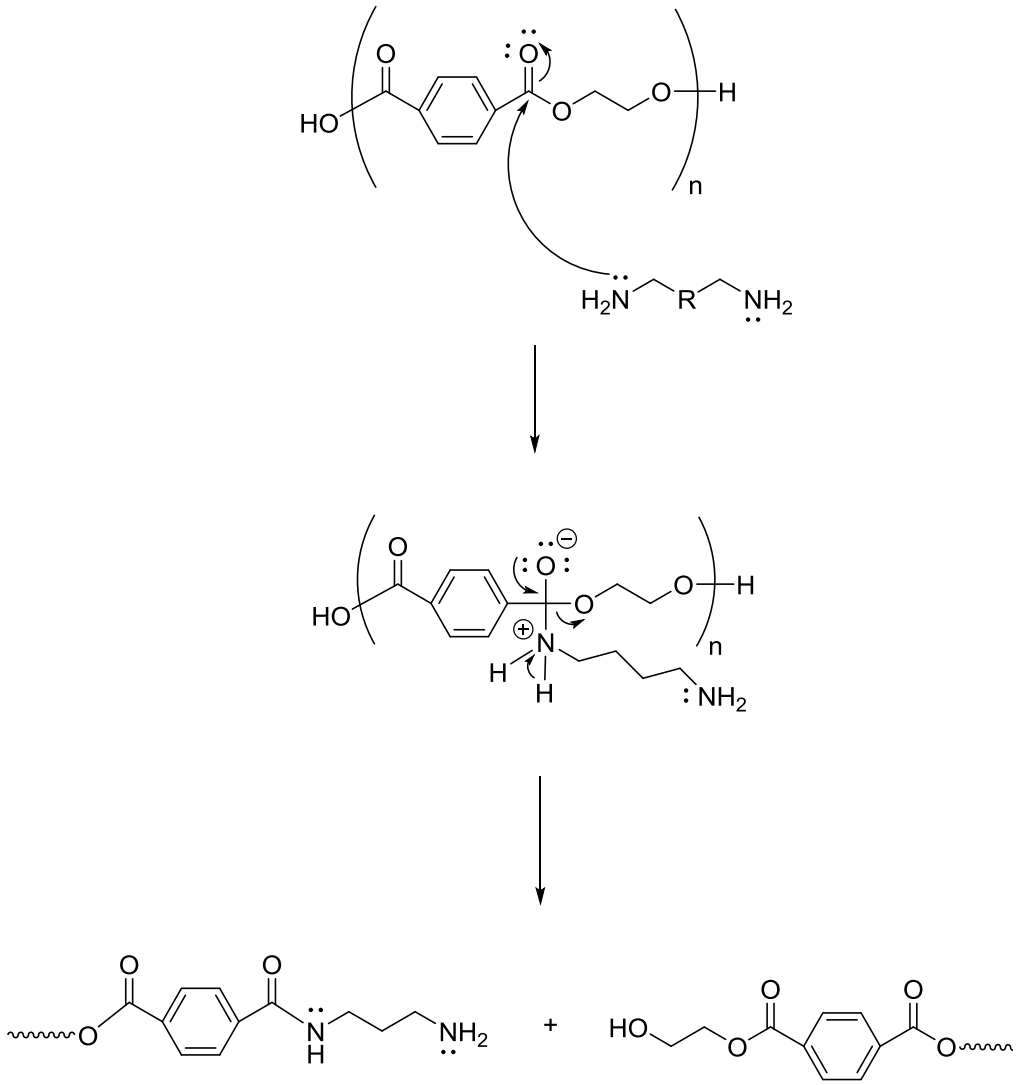

Figure 4.13. The mechanism of PET degradation by amine via Aminolysis [49].

In this study, the main polymer is a polyester, and it was reacted with a polyamine which has primary, secondary and most importantly tertiary amines. The reason for a sudden solidification at 190^0 C may be caused by ester-amide exchange and aminolysis reactions caused by the primary/secondary and tertiary amines, respectively. While chain scission is happening at one side of the PEI (aminolysis), other sides may also react with PE-2 (ester amide exchange reactions) and leading to the formation of a network for PEI-2_1.00. As a result of the network formation, material may become solid again which could be the reason why its G' increased. The relative rate of the chain scission and amide-ester exchange reactions may be governing the rheological behaviour observed.

Since reaction occurs due to the collision of reactants, reaction kinetics strongly depends on the concentration of the reactants and temperature. With increasing temperature, more molecules have sufficient energy to react and since at high temperatures they have more thermal energy, number of collisions increases. PE-2_1.00 has the highest amine concentration among the three samples. This could be the reason why the same pattern was not observed for the lower ratios of amine. The concentration of PEI in PE-2_0.25 may not be sufficient for a network formation thus material did not become solid like PE-2_1.00. Furthermore, at 190^0 C the materials' storage modulus drops rapidly. This may point out that chain scission is dominant compared to network formation at the lower concentration of amines. This could explain why PE-2_0.50 acts like neither PE-2_1.00 nor PE-2_0.25, because at medium concentration chain scission and network formation may balance out each other.

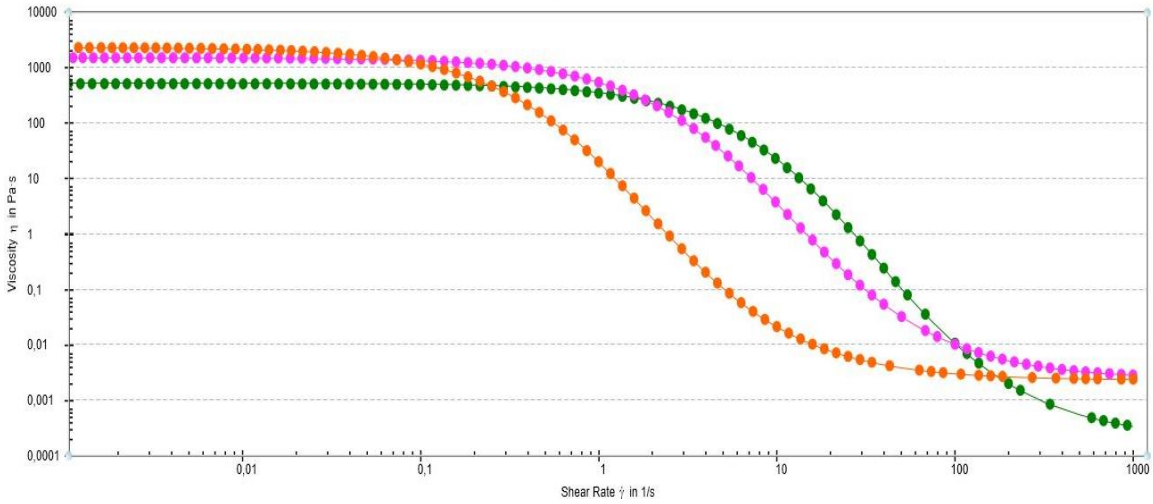

Figure 4.14. The flow curves of PE-2_1.00 (orange), PEI-2_0.50 (pink) PEI-2_0.25 (green).

The flow curve graph of PEI-2 series are shown below in Figure 4.14. The order for $\overline{M_w}$ is PEI-2_1.00 > PEI-2_0.50 > PEI-2_0.25. Considering DSC results presented earlier, the M_w order was rational since the glass transitions followed the same order. Comparing the MWD, PEI-2_0.25 had the narrowest while PEI-2_1.00 had the broadest distribution. When compared to PE-2 from Figure A.3, PEI-2_1.00 was more similar in MWD but had higher η_0. PEI-2_0.50 and PEI-2_0.25 had lower η_0 than PEI-2_1.00, but still higher than

PE-2 and had narrower MWD. There seems to be an increase in $\overline{M_w}$ for all ratios, but since there was no increase in T_g, this could be the result of chain entanglements between hyperbranches of PE-2 and PEI.

The loss factor graphs are shown in Figure 4.15. All three ratios showed second relaxation peaks which their highest point was decreased to a lower temperature with decreasing amine ratio. Also, after about 155^0 C, PEI-2_0.25 showed a very steep increase in loss factor which means its loss modulus started to increase immensely. From temperature sweep graphs, the aminolysis was assumed to happen at 190^0 C, but one can see the chain scission was started around 155^0 C for PEI-2_0.25 and PEI-2_0.50, around 140^0 C for PEI-2_1.00.

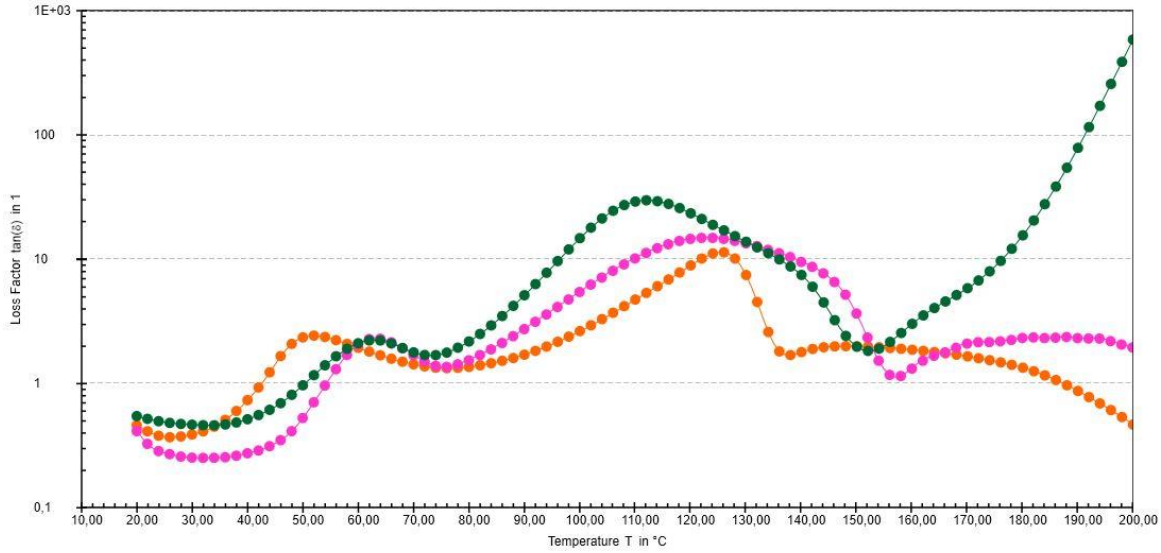

Figure 4.15. The loss factor versus temperature graphs of PEI-2_1.00 (orange), PEI-2_0.50 (pink), PEI-2_0.25 (green).

Complexation of PEI and PE-3: The temperature ramp test results of PE-3 and PE-3 with PEI are shown in the Table 4.6 below.

Table 4.6. Rheological results of PE-3 andd PEI-3_1.00.

Sample Name	T_g (◦C)	T_m(◦C)
PE-3	36	44
PEI-3_1.00	41	58

The temperature ramp graphs of PE-3 and PEI-3_1.00 are shown in Figure 4.16. All samples were amorphous with $G' > G''$ at low temperatures. After crossover point, they showed a drop of both loss and storage moduli similar to a typical amorphous polymer. T_g and T_m results from rheology confirmed the DSC results, where PE-3 has T_g=36^0 C and PEI-3_1.00 has T_g=41^0 C according to rheology. Viscosity of PE-3 was higher in the glassy state, while PEI-3_1.00 has higher viscosity in the molten state since it has higher storage modulus after melting.

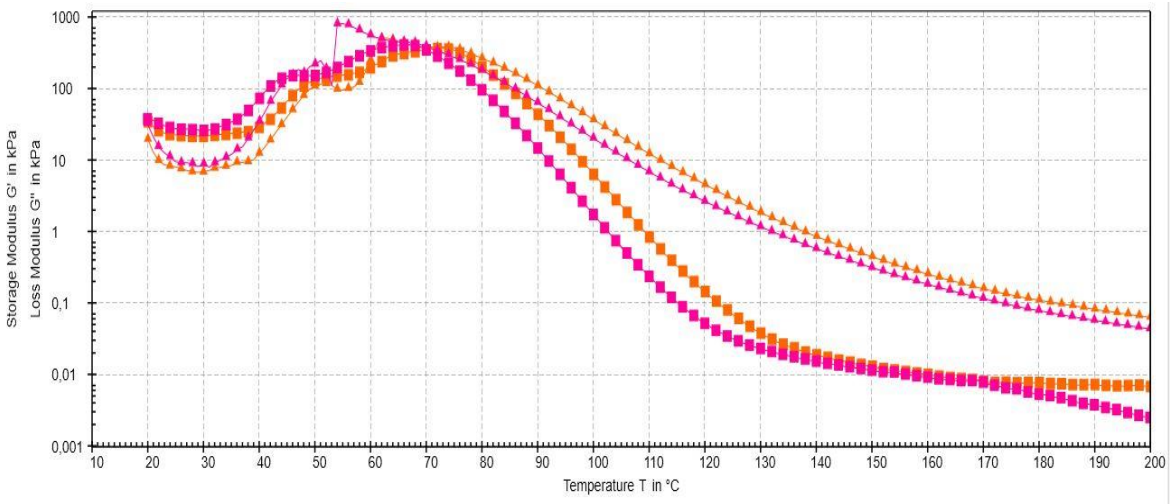

Figure 4.16. The storage modulus of PE-3 (pink), PEI-3_1.00 (orange) represented by square lines and loss modulus represented by triangle lines.

The loss factor graphs are shown in Figure 4.17. PE-3 and PEI-3_1.00 had relaxation peaks but the maximum of the peak was shifted to a higher temperature in PEI-3_1.00. The relaxation in the PE-3 could be caused by the hydrogen bonding between acid groups of polyester. When PEI complex with acid groups, due to the fact that ionic hydrogen bonding is stronger than hydrogen bonding, it may shift the relaxation temperature.

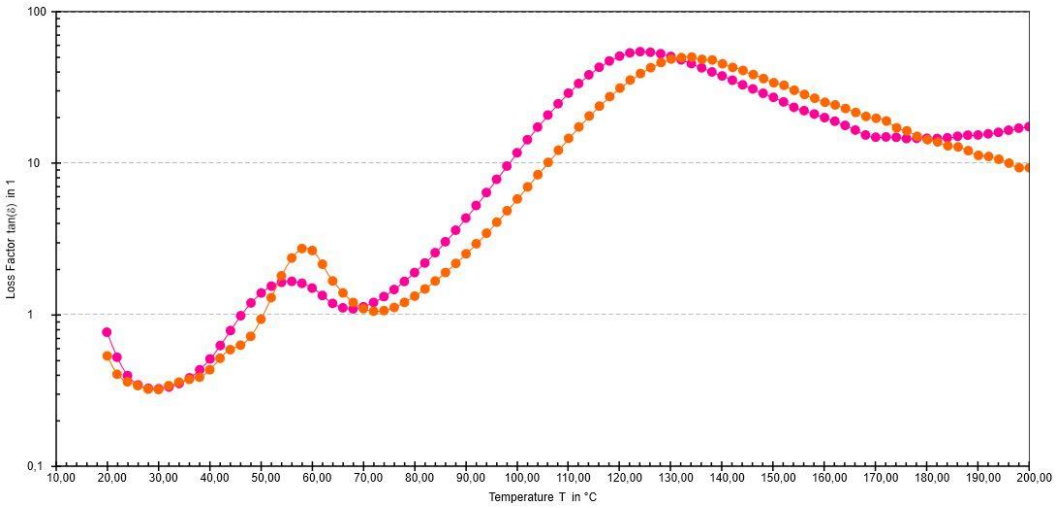

Figure 4.17. The loss factor versus temperature graphs of PE-3 (pink) and PEI-3_1.00 (orange).

Complexation of DABCO and PE-1: The viscosity and temperature ramp test results of PE-1 with DABCO are shown in the Table 4.7.

Table 4.7. Rheological results of DABCO-1 series.

Sample Name	T_g (◦C)	T_m(◦C)	η_0(Pa.s)
DABCO-1_0.25	53	61	4970
DABCO-1_0.50	60	63	2811
DABCO-1_1.00	55	65	670

The temperature ramp graph is shown in Figure 4.18. Rheometer results on the T_g and T_m were in accordance with the DSC results. Considering the T_g values, after a certain increase up to 1:0.50 mole ratio, T_g started to decrease. Given the fact that the protonation of both amines of DABCO requires very strong acids, at high concentrations of DABCO protonation from one side would be favored, since excess DABCO is present, thus DABCO may start to block the acid groups similar to 2MI and prevent hydrogen bonding between acid ends of the chains.

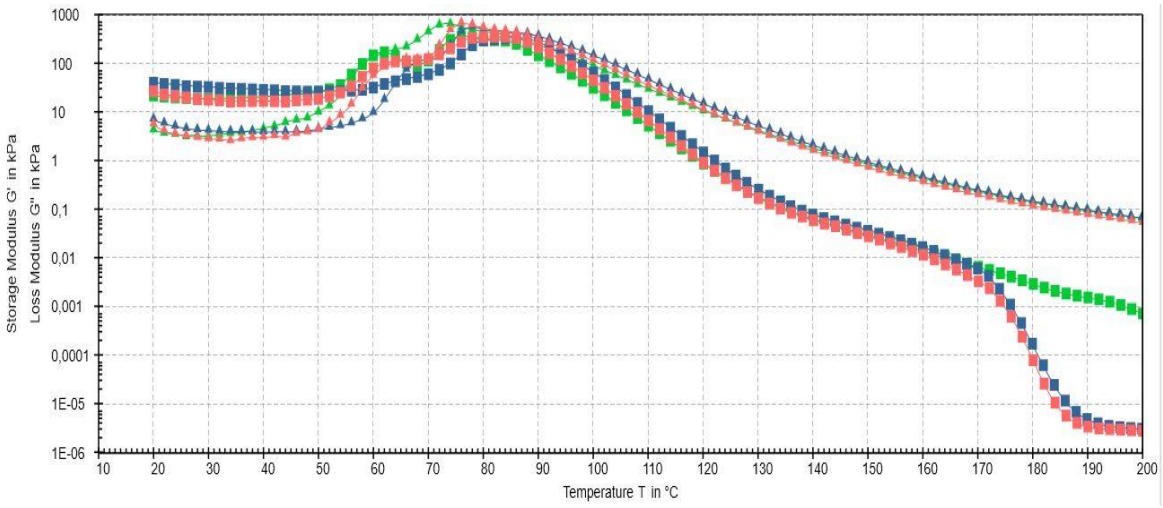

Figure 4.18. The storage modulus of DABCO-1_1.00 (pink), DABCO-1_0.50 (blue), DABCO-1_0.25 (green) represented by square lines and loss modulus represented by triangle lines.

All three polymers showed a typical amorphous behavior, having $G' > G''$ in the low temperature range and having a steady decrease of both storage and loss modulus after melting. However, DABCO-1_1.00 and DABCO-1_0.50 had a sudden decrease in storage modulus after about 165^0 C. DABCO has a melting point of 160^0 C. The reason for this rapid decrease in materials' modulus may be the melting of DABCO around the same temperature range. The DABCO concentration was higher for those two samples compared to DABCO-1_0.25. This may explain the reason for the absence of such a decrease in DABCO-1_0.25, where the DABCO concentration was low.

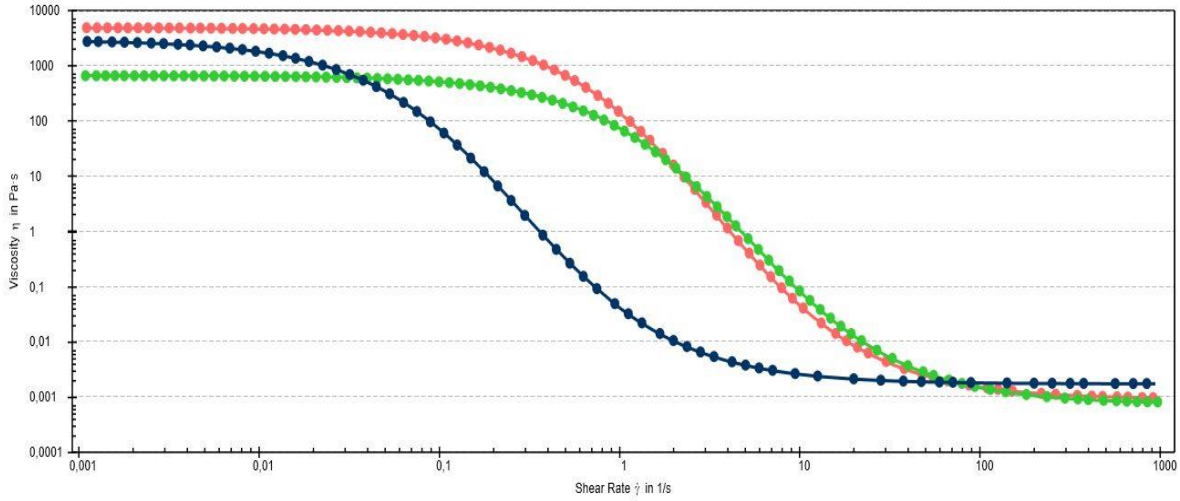

Figure 4.19. The flow curves of DABCO-1_1.00 (pink), DABCO-1_0.50 (blue), DABCO-1_0.25 (green).

The flow curves of DABCO-1 series are shown Figure 4.19. The order for $\overline{M}_w$ is DABCO-1_1.00 > DABCO-1_0.50 > DABCO-1_0.25. Regarding DSC results, DABCO-1_0.50 should have the highest η_0, but in flow curves DABCO-1_1.00 has higher η_0. Comparing the MWD, DABCO-1_0.50 had the broadest MWD, while DABCO-1_1.00 and DABCO-1_0.25 showed similar MWDs.

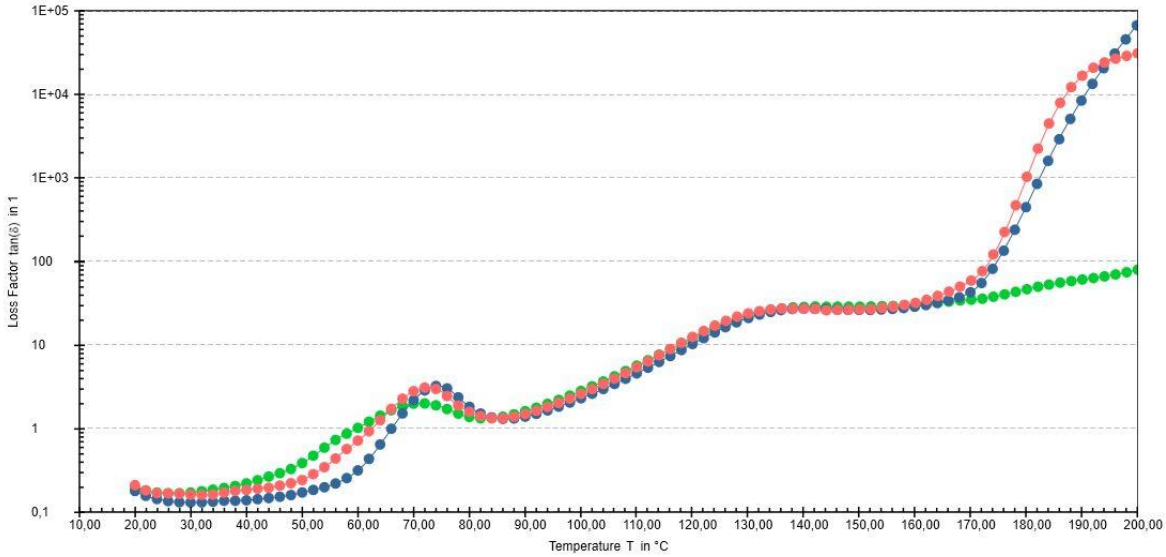

Figure 4.20. The loss factor versus temperature graphs of DABCO-1_1.00 (pink), DABCO-1_0.50 (blue), DABCO-1_0.25 (green).

The loss factor graphs of three polymer are shown below in Figure 4.18 The samples did not show any distinct second relaxation peaks. The DABCO-1_1.00 and DABCO-1_0.50 showed an immense increase after 160^0 C which is reasonable considering T_m of DABCO is 160^0 C.

Complexation of DABCO and PE-2: The viscosity and temperature ramp test results of PE-2 with DABCO are shown in the Table 4.8 below.

Table 4.8. Rheological results of DABCO-2 series.

Sample Name	T_g (◦C)	T_m(◦C)	η_0(Pa.s)
DABCO-2_0.25	46	52	102
DABCO-2_0.50	52	59	469
DABCO-2_1.00	51	69	365

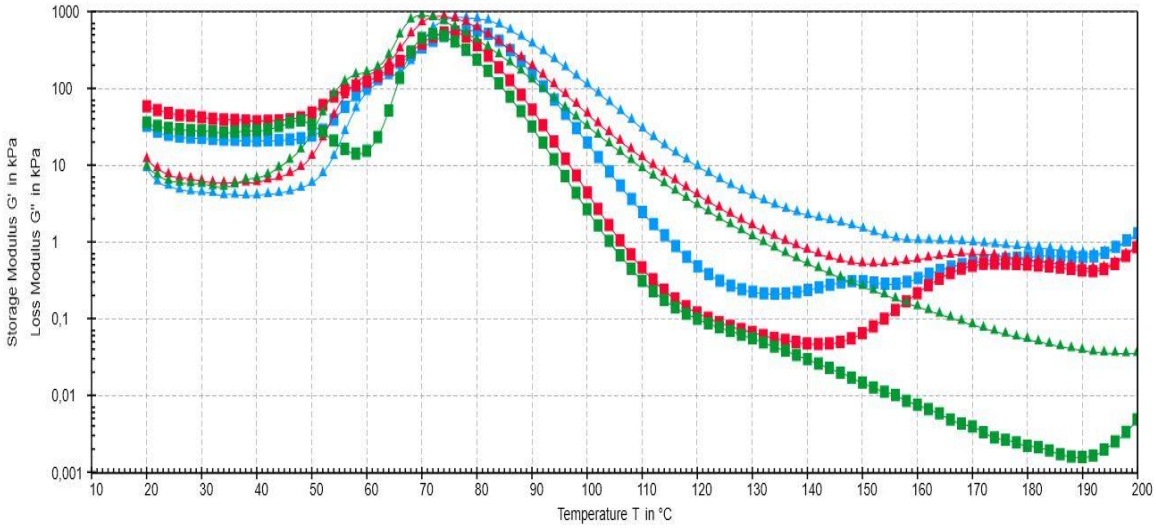

Figure 4.21. The storage modulus of DABCO-2_1.00 (red), DABCO-2_0.50 (blue), DABCO-2_0.25 (green) represented by square lines and loss modulus represented by triangle lines.

The temperature ramp graphs are shown in Figure 4.21. Rheometer results for T_g and T_m were consistent with the results from DSC except for DABCO-2_1.00 which showed a

lower T_g then DABCO-2_0.50 in the rheometer. At mole ratio of 1.00:0.25 DABCO amount was not sufficient to lead an increase in T_g. At the 1.00:0.50 mole ratio T_g reaches its highest value among three ratios and starts to decrease slightly. Similar to PE-1 case, after a certain DABCO concentration PE-2 and DABCO may not have more interactions, thus starts to show a plasticizing effect but the ionic interaction between PE-2 and DABCO is still dominant since T_g is still high compared to original PE-2.

All three samples show an amorphous behavior having a $G' > G''$ at low temperatures. They also showed a decrease in both moduli after melting, but G' of DABCO-2_1.00 and DABCO-2_0.50 started to increase at about 155-160^0 C. This temperature range again correlates to the melting point of DABCO, but instead of a decrease in G', in this situation there was an increase. Keeping in mind that the surface area of a solid is rather smaller because the molecules in solid state are more compact, the reason of this increase in G' may be caused the increase in interaction between PE-2 and DABCO when they both in the molten state. Also, PE-2 has a branched structure so when DABCO gains more mobility after its melting point, it could overcome the steric hinderance more easily. Since the rheometer's temperature limit is 200^0 C material's behavior at higher temperatures could not be examined.

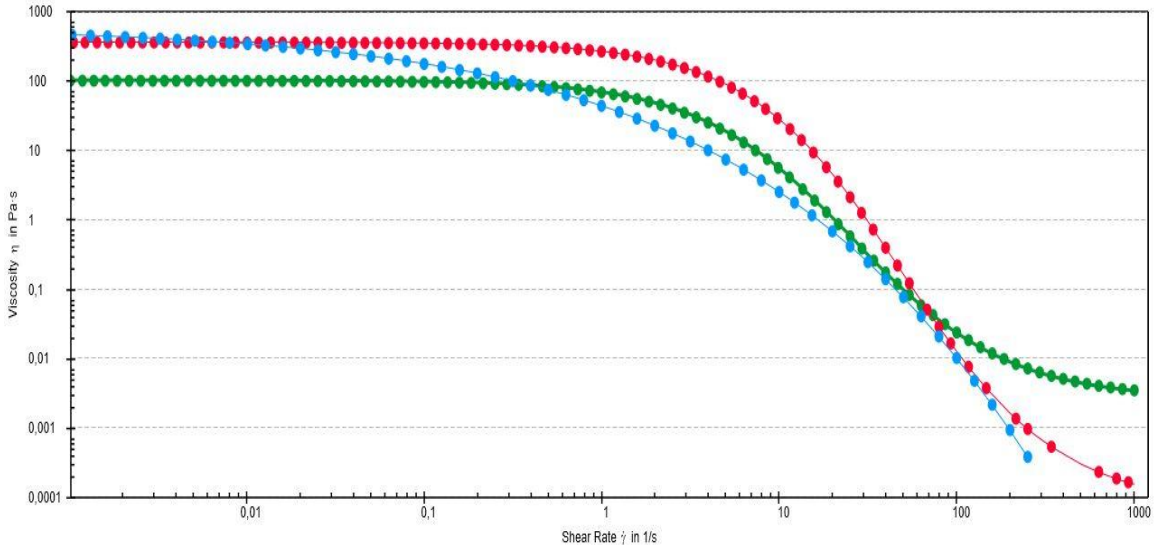

Figure 4.22. The flow curves of DABCO-2_1.00 (red), DABCO-2_0.50 (blue), DABCO-2_0.25 (green).

The flow curve graph of DABCO-2 series are shown below in Figure 4.22. The order for $\bar{M}_w$ is DABCO-1_0.50 > DABCO-1_1.00 > DABCO-1_0.25 which correlates with T_g results from rheology.

The loss factor graphs of three polymer are shown below in Figure 4.23 DABCO-2_1.00 and DABCO-2_0.50 showed distinct second relaxation peaks but DABCO-2_0.25 did not show a second relaxation. Considering T_g results, it is reasonable since DABCO-2_0.25 did not show a remarkable increase.

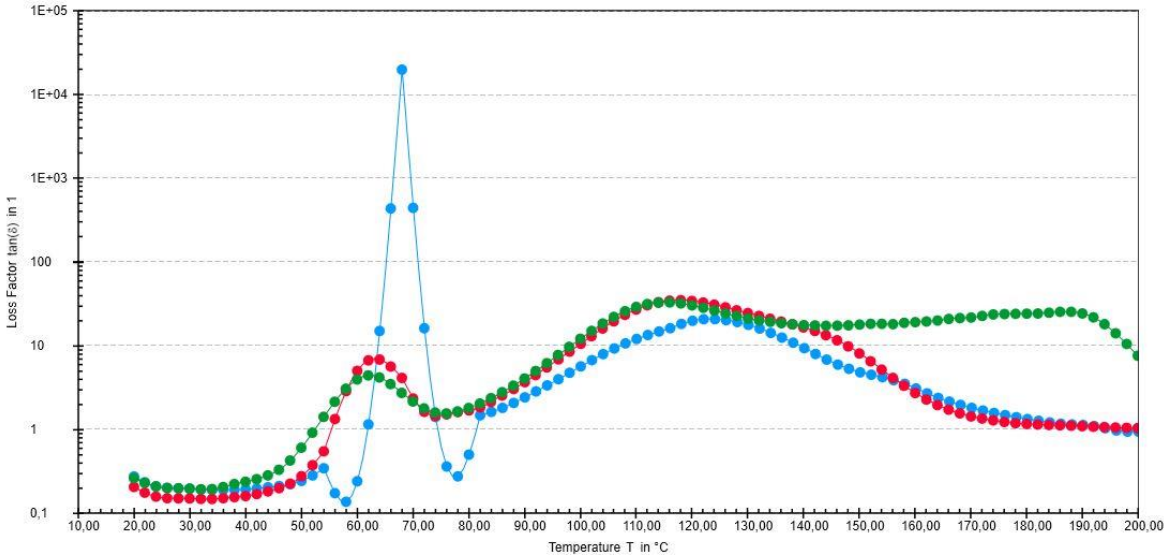

Figure 4.23. The loss factor versus temperature graphs of DABCO-2_1.00 (red), DABCO-2_0.50 (blue), DABCO-2_0.25 (green).

Complexation of DABCO and PE-3: The temperature ramp test results of PE-3 and PE-3 with DABCO are shown in the Table 4.9 below.

Table 4.9. Rheological results of PE-3 and DABCO-3_1.00.

Sample Name	T_g (◦C)	T_m(◦C)
PE-3	32	44
DABCO-3_1.00	40	51

The temperature ramp graphs of PE-3 and DABCO-3_1.00 are shown in Figure 4.24. All samples were amorphous with $G' > G''$ at low temperatures. After crossover point, they showed a drop of both loss and storage moduli similar to a typical amorphous polymer. T_g and T_m results from rheology confirmed the DSC results of DABCO-3_1.00, but PE-3 showed lower T_g in rheology, where PE-3 has T_g =32^0 C and DABCO-3_1.00 has T_g =40^0 C according to rheology. Viscosity of PE-3 was lower than DABCO-3_1.00 in both glassy state and molten state since it has higher storage modulus.

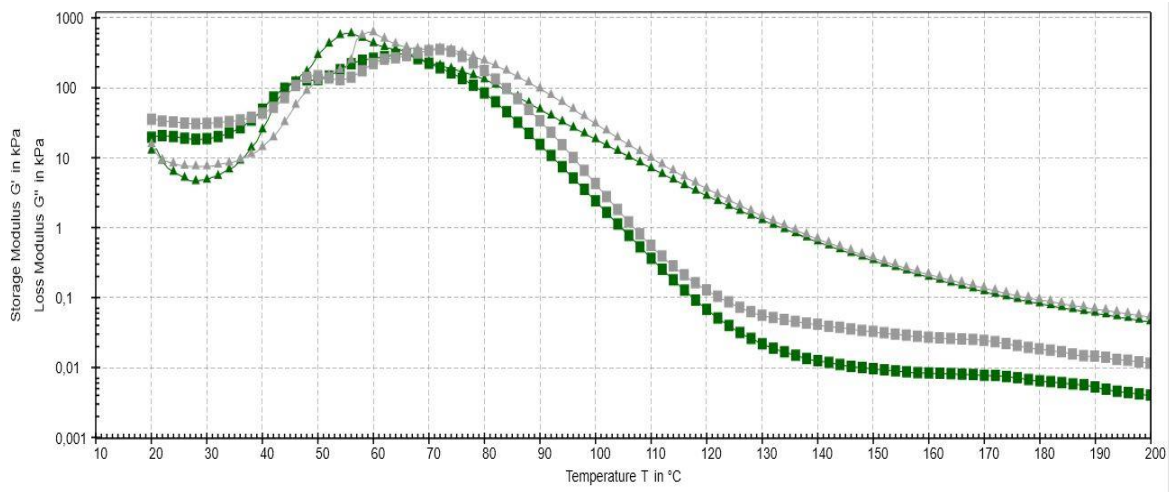

Figure 4.24. The storage modulus of PE-3 (green), DABCO-3_1.00 (grey) represented by square lines and loss modulus represented by triangle lines.

The loss factor graphs are shown in Figure 4.25. PE-3 and PE-3_1.00 had relaxation peaks but the maximum of the peak was shifted to a lower temperature in DABCO-3_1.00. The relaxation in the PE-3 could be caused by the hydrogen bonding between acid groups of polyester. When DABCO complex with acid groups, due to the fact that ionic hydrogen bonding is stronger than hydrogen bonding, it may shift the relaxation temperature.

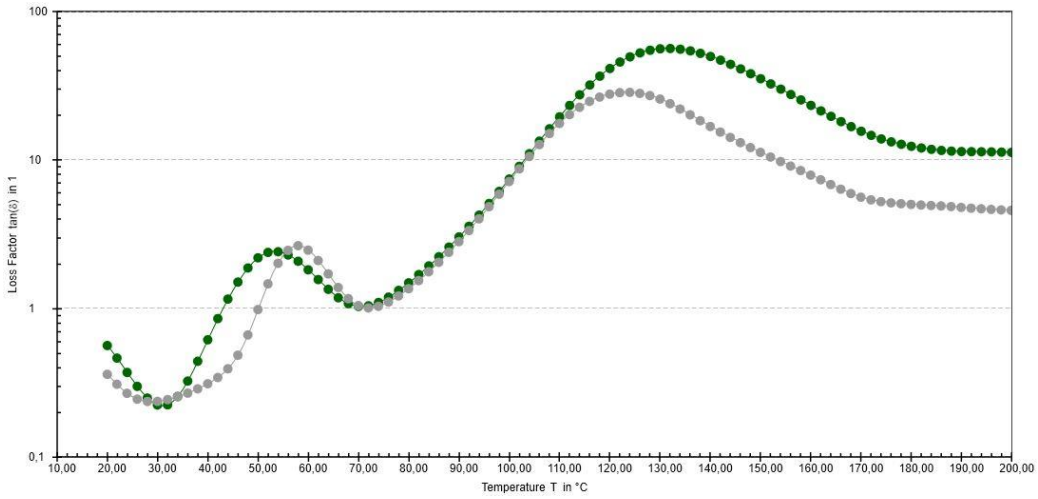

Figure 4.25. The loss factor versus temperature graphs of PE-3 (green) and DABCO-3_1.00 (grey).

4.5. Reversibility Study of DABCO-1_1.00

The reversibility of polymer complex was examined by adding acid to DABCO-1_1.00 complex to protonate DABCO and remove DABCO from PE-1. 0.5 g DABCO-1_1.00 was dissolved in 6 mL chloroform, then 5 drops of 5% HCl solution was added and stirred. Chloroform phase was extracted and evaporated. After drying in the vacuum overnight, the glass transition temperature of the sample was measured. T_g of the DABCO-1_1.00 was 57.7^0 C and PE-1 was 53.3^0 C. After acid treatment T_g of sample had dropped to 52.4^0 C, which is similar to PE-1. This could be the confirmation of reversibility of the interaction between DABCO and PE-1.

Furthermore, the HMBC spectra of DABCO, acid treated DABCO and DABCO-1_1.00 was examined to see DABCO peak shifts. The DABCO and acid treated DABCO HMBC spectra are shown below Figure 4.26 and 4.27, respectively.

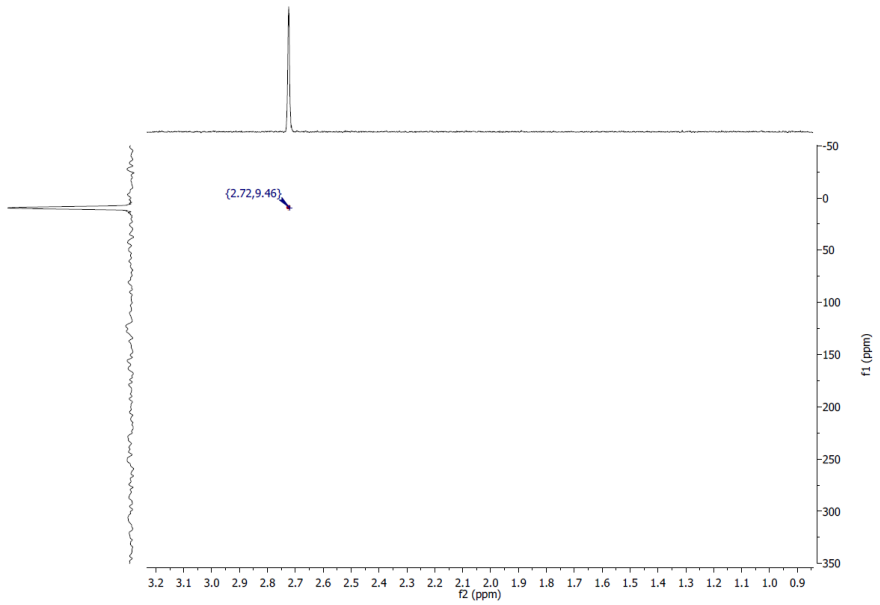

Figure 4.26. The HMBC spectrum of DABCO.

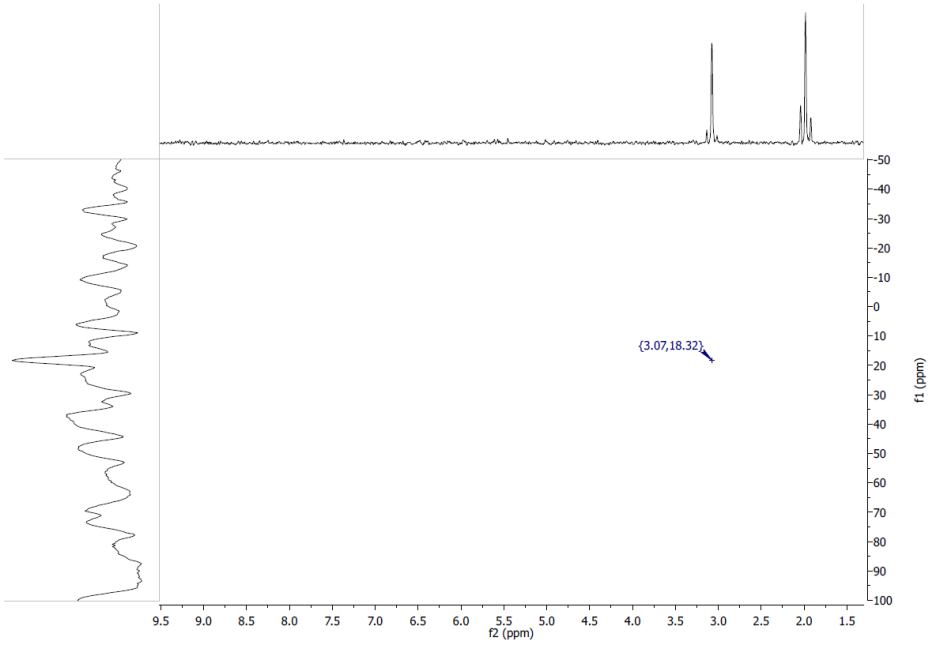

Figure 4.27. The HMBC spectrum of acid treated DABCO.

The chemical shifts of DABCO (H, $\delta = 2.72\ ppm$ and N, $\delta = 9.46\ ppm$) shifted to downfield when protonated (H, $\delta = 3.07\ ppm$ and N, $\delta = 18.32\ ppm$).

The HMBC spectrum of DABCO-1_1.00 is shown in Figure 4.28. As it can be seen, the chemical shifts of DABCO in polymer complex was also shifted to downfield (H, $\delta = 3.03\ ppm$ and N, $\delta = 14.93\ ppm$). This can indicate that DABCO in polymer complex was in its protonated form.

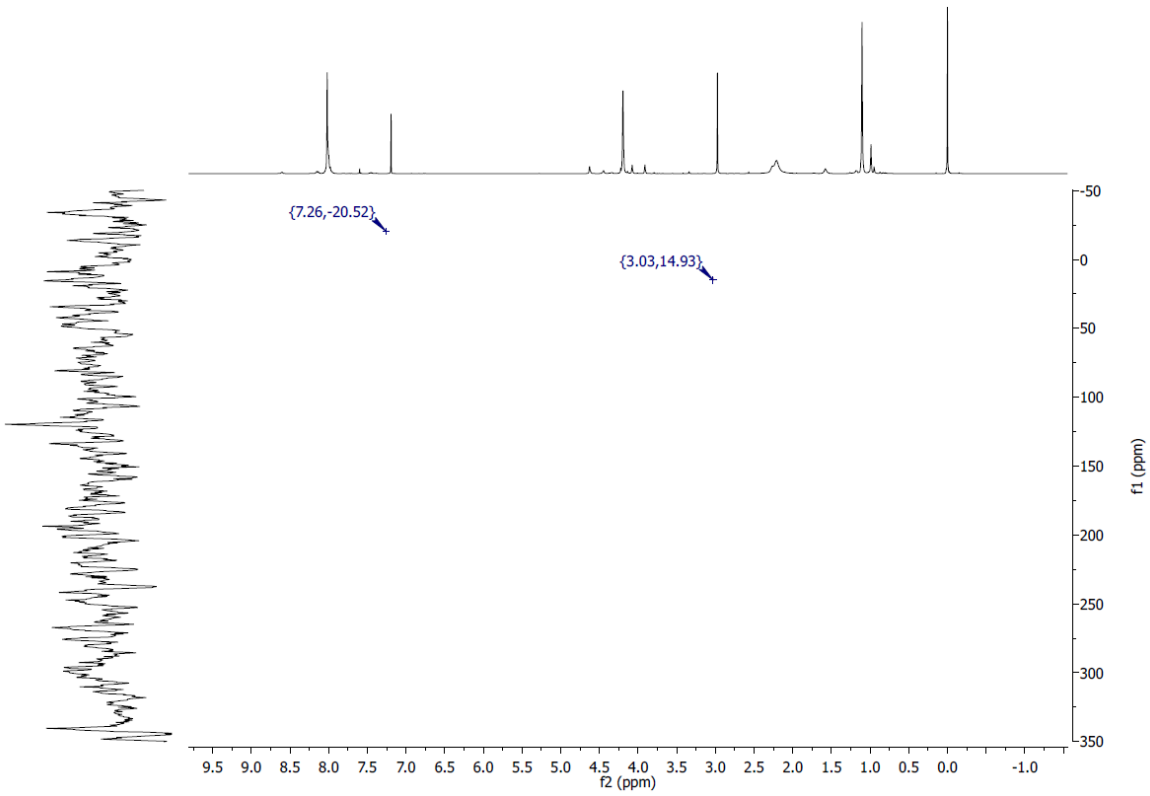

Figure 4.28. The HMBC spectrum of DABCO-1_1.00.

5. CONCLUSION

As a conclusion, it was shown that by formation of ionic hydrogen bondings between amines and acid groups of polyesters, glass transition temperature of original polyesters could be increased. Moreover, the relationship between amine functionalities, acid/amine mole ratio and T_g was examined. However, at high temperatures due to aminolysis some polymers showed chain scission. It was observed that interaction between amines and acids changes the polymers' properties, but there is an ideal acid/amine ratio for every polyesters and amines. Lower and higher values than this optimal range would result in negative effect in the obtained polymer.

6. FUTURE WORK

The acid/amine ratios need to be optimized to have better results with every amines. Using lower M_w polyesters or hyperbranched polyesters the ionic effect should be increased. The ionic hydrogen bonding should be observed with a spectroscopic method more clearly. Rheometer could be used for M_w determination, since GPC is not suitable for observing increase in M_w with ionic interactions.

REFERENCES

1. Hermann, S., "Über Polymerisation" *Berichte Dtsch. Chem. Ges.*, Vol. 53, No. 6, pp. 1073–1085, 1920.

2. Yan, X., F. Wang, B. Zheng, and F. Huang, "Stimuli-Responsive Supramolecular Polymeric Materials" *Chem. Soc. Rev.*, Vol. 41, No. 18, pp. 6042–6065, 2012.

3. Lehn, J., "Supramolecular Chemistry-Scope and Perspectives Molecules, Supermolecules, and Molecular Devices (Nobel Lecture)," *Angewandte Chemie,* vol. 27, no. 1, pp. 89–112, 1988.

4. Peng, Y., Y. Yang, Q. Wu, S. Wang, G. Huang, and J. Wu, "Strong and Tough Self-Healing Elastomers Enabled by Dual Reversible Networks Formed by Ionic Interactions and Dynamic Covalent Bonds," *Polymer*, Vol. 157, pp. 172–179, 2018.

5. Cui, K., *et al.*, "Preparation of Recyclable Polybutadiene Rubber Based on Acid–Base Complexation," *J. Appl. Polym. Sci.*, Vol. 134, No. 36, pp. 6–11, 2017.

6. Wang, D., *et al.*, "Dynamic Crosslinks to Facilitate Recyclable Polybutadiene Elastomer with Excellent Toughness and Stretchability," *J. Polym. Sci. Part A*, Vol. 54, No. 10, pp. 1357–1366, 2016.

7. Shimizu, L. S., "Perspectives on Main-Chain Hydrogen Bonded Supramolecular Polymers", *Polymer International*, Vol. 452, pp. 444–452, 2007.

8. Weck, M., "Side-Chain Functionalized Supramolecular Polymers", *Polymer International*, Vol. 460, pp. 453–460, 2007.

9. Xinrong, L, "*Synthesis, Characterization and Applications of Ionic Supramolecular Assemblies*", PhD Thesis, Boston University , 2014.

10. Bergman, S. D., and F. Wudl, "Mendable Polymers" *J. Mater. Chem.*, Vol. 18, No. 1, pp. 41–62, 2008.

11. Yang, Y., and M. W. Urban, “Self-Healing of Polymers via Supramolecular Chemistry,” *Adv. Mater. Interfaces*, Vol. 5, No. 17, pp. 1–19, 2018.

12. Pollino, J. M., and M. Weck, “Non-Covalent Side-Chain Polymers : Design Principles, Functionalization Strategies, and Perspectives”, *Chemichal Society Reviews*, pp. 193–207, 2005.

13. Sanchez, A., and J. A. Pomposo, “Single-Chain Polymer Nanoparticles via Non-Covalent and Dynamic Covalent Bonds” , *Particle & Particle Systems Characterization*, pp. 11–23, 2014.

14. Yu, D., X. Zhao, C. Zhou, C. Zhang, and S. Zhao, “Room Temperature Self-Healing Methyl Phenyl Silicone Rubbers Based on the Metal–Ligand Cross-Link: Synthesis and Characterization”, *Macromol. Chem. Phys.*, Vol. 218, No. 8, pp. 1–6, 2017.

15. Wang, W., J. Zhang, F. Jiang, X. Wang, and Z. Wang, “Reprocessable Supramolecular Thermoplastic BAB-Type Triblock Copolymer Elastomers with Enhanced Tensile Strength and Toughness via Metal–Ligand Coordination”, *ACS Appl. Polym. Mater.*, Vol. 1, No. 3, pp. 571–583, 2019.

16. Yiping N,, “Polymer Networks Architecture Using Supramolecular Interactions" "Polymer networks architecture using supramolecular interactions,” PhD Thesis, L’Université Jean Monnet, Saint Etienne, 2012.

17. Lin, X., and M. W. Grinstaff, “Ionic Supramolecular Assemblies”, *Isr. J. Chem.*, Vol. 53, No. 8, pp. 498–510, 2013.

18. Krogsgaard, M., M. A. Behrens, J. S. Pedersen, and H. Birkedal, “Self-Healing Mussel-Inspired Multi-pH-Responsive Hydrogels”, *Biomacromolecules*, Vol. 14, No. 2, pp. 297–301, 2013.

19. Beck, J. B., J. M. Ineman, and S. J. Rowan, “Metal/Ligand-Induced Formation of Metallo-Supramolecular Polymers”, *Macromolecules*, vol. 38, no. 12, pp. 5060–5068, 2005.

20. Lei, Y., W. Huang, Q. Huang, and A. Zhang, “A Novel Polysiloxane Elastomer Based on Reversible Aluminum-Carboxylate Coordination”, *New J. Chem.*, Vol. 43, No. 1, pp. 261–268, 2019.

21. Yan, X., F. Wang, B. Zheng, and F. Huang, “Stimuli-Responsive Supramolecular Polymeric Materials” , *Chem. Soc. Rev.*, Vol. 41, No. 18, pp. 6042–6065, 2012.

22. Yang, Y., and M. W. Urban, “Self-Healing of Polymers via Supramolecular Chemistry”, *Adv. Mater. Interfaces*, Vol. 5, No. 17, pp. 1–19, 2018.

23. Burattini, S., *et al.*, “A Supramolecular Polymer Based on Tweezer-Type π - π Stacking Interactions : Molecular Design for Healability and Enhanced Toughness", *Chemistry of Materials Communication*, No. 12, pp. 6–8, 2011.

24. Burattini, S., *et al.*, “A Self-Repairing, Supramolecular Polymer System: Healability as a Consequence of Donor-Acceptor π-π Stacking Interactions”, *Chem. Commun.*,, No. 44, pp. 6717–6719, 2009.

25. Zechel, S., M. D. Hager, and U. S. Schubert, *Self-healing Polymers : From Biological Systems to Highly Functional Polymers*, Springer International Publishing, Germany, 2018, .

26. Hart, L. R., N. A. Nguyen, J. L. Harries, M. E. Mackay, H. M. Colquhoun, and W. Hayes, “Perylene as an Electron-Rich Moiety in Healable, Complementary π-π Stacked, Supramolecular Polymer Systems”, *Polymer (Guildf).*, vol. 69, pp. 293–300, 2015.

27. Mei, J. F., *et al.*, “A Highly Stretchable and Autonomous Self-Healing Polymer Based on Combination of Pt···Pt and π–π Interactions”, *Macromol. Rapid Commun.*, Vol. 37, No. 20, pp. 1667–1675, 2016.

28. Li, J., “Polymer Networks Containing Reversibly Associating Side-Groups”, PhD Thesis, University of Rochester, 2011.

29. Brassinne J. "Self- Organization and Dynamics of Stimuli-Responsive Polymeric Systems”, PhD Thesis, Université catholique de Louvain , 2015.

30. Sijbesma, R. P., *et al.*, "ChemInform Abstract: Reversible Polymers Formed from Self-Complementary Monomers Using Quadruple Hydrogen Bonding", *ChemInform*, Vol. 29, No. 10, p.1604-1604, 2010.

31. Houston, K. R., A. M. S. Jackson, R. W. Yost, H. S. Carman, and V. S. Ashby, "Supramolecular Engineering Polyesters: Endgroup Functionalization of Glycol Modified PET with Ureidopyrimidinone", *Polym. Chem.*, Vol. 7, No. 44, pp. 6744–6751, 2016.

32. Cui, K., *et al.*, "Preparation of Recyclable Polybutadiene Rubber Based on Acid–Base Complexation", *J. Appl. Polym. Sci.*, Vol. 134, No. 36, pp. 6–11, 2017.

33. Hanshaw, R. G., R. V. Stahelin, and B. D. Smith, "Noncovalent Keystone Interactions Controlling Biomembrane Structure", *Chemistry - A European Journal*, Vol. 14, No. 6, pp. 1690–1697, 2008.

34. Aboudzadeh, M. A., *et al.*, "Supramolecular Ionic Networks with Superior Thermal and Transport Properties Based on Novel Delocalized Dianionic Compounds", *J. Mater. Chem. A*, Vol. 3, No. 5, pp. 2338–2343, 2015.

35. Wathier, M., and M. W. Grinstaff, "Synthesis and Creep-rRcovery Behavior of a Neat Viscoelastic Polymeric Network Formed Through Electrostatic Interactions", *Macromolecules*, Vol. 43, No. 22, pp. 9529–9533, 2010.

36. Aboudzadeh, M. A., M. E. Muñoz, A. Santamaría, and D. Mecerreyes, "New Supramolecular Ionic Networks Based on Citric Acid and Geminal Dicationic Ionic Liquids" , *RSC Adv.*, Vol. 3, No. 23, pp. 8677–8682, 2013.

37. Schramm,G., "Creep and Recovery: A Practical Approach to Rheology and Rheometry" , *A Pract. Approach to Rheol. Rheometry*, pp. 101–117, 1994.

38. Goodwin J., Hughes R., *Rheology for Chemists,: An Introduction*, 2nd Edition RSC Publishing, United Kingdom, 2008.

39. Morrison, F. A., *Understandig Rheology*, Vincentz Network, Germany,1998.

40. Mezger T.G., *The Rheology Handbook For Users of Rotational Rheometers, 2nd Edition, 2006.*

41. Dae Han C., "Rheology and Processing of Polymeric Materials", Volume I, Oxford Press, p. 43, 2001.

42. Kempf, M., "*Synthesis and Rheology of Model Comb Polymer Architectures*", PhD Thesis, Karlsruher Institut für Technologie, 2011.

43. Brugger, B. P., "*Nonlinear Behavior In Startup Uniaxial Extension Of Entangled Polymer Melts*," PhD Thesis, The University of Akron, 2014.

44. Habibi, M. H., "*Effects of Out-Time on Cure Kinetics and Rheological Properties of Out-of-Autoclave and Autoclave Prepregs*", MSc Thesis, Wichita State University, 2013.

45. Kısaöz E., "*Rheological Properties Of Calcite Filled Polypropylene Random Copolymer Composites*", M.Sc. Thesis, Istanbul Technical University, 2010

46. Jaishankar A., *Interfacial Rheology of Globular Proteins, MSc Thesis,* Massachusetts Institute of Technology, 2011.

47. Colonna, M., *et al.*, "Poly(1,4-cyclohexylenedimethylene-1, 4-cyclohexanedicarboxylate): Analysis of Parameters Affecting Polymerization and Cis-Trans Isomerization", *Polym. Int.*, Vol. 60, No. 11, pp. 1607–1613, 2011.

48. E. Irish, A. Guzonas, E. Irish, A. Guzonas, and E. Irish, "A Raman and infrared spectroscopic study of triethylenediamine (DABCO) and its protonated forms", Vol 66, No. pp. 1249-1257, 1988.

49. T. P. Lodge, "Polymer", 2nd Edition, Taylor & Francis Group, 2007

50. Spychaj, S *et al.*, "Aminolysis and Aminoglycolysis of Waste Poly(ethylene terephthalate)", *J. Mater. Cycles Waste Manag.*, Vol. 3, No. 1, pp. 24–31, 2001.

APPENDIX A: SPECTROSCOPY DATA

DSC Analysis and rheological data of synthesized polymers. Necessary expansions were made on the data for easy interpretation.

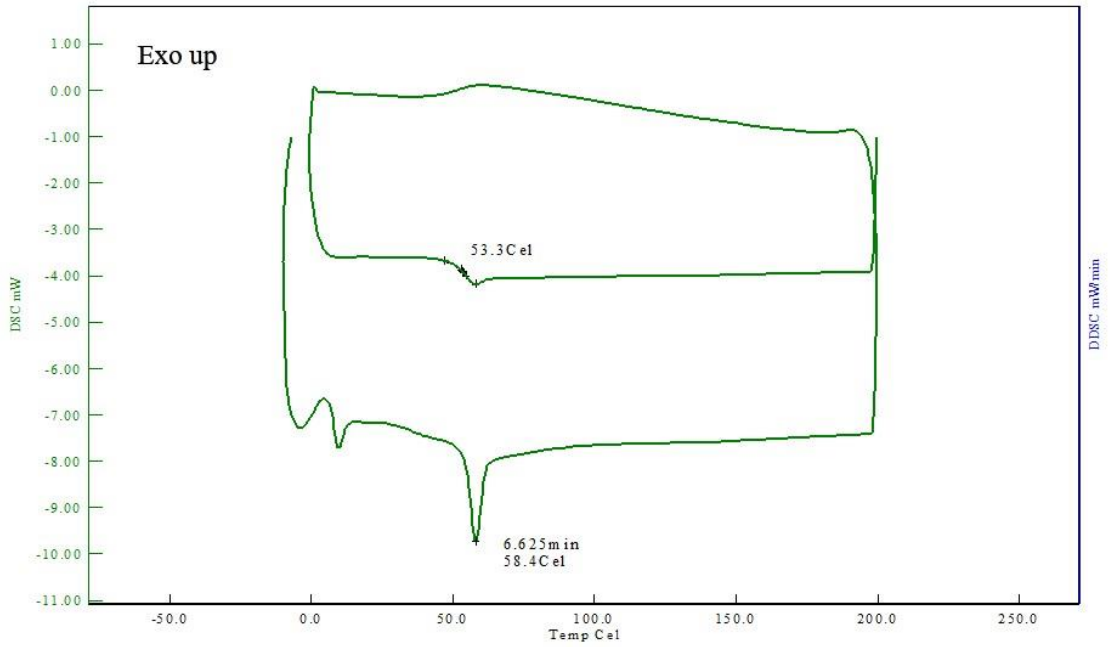

Figure A.1. DSC results of PE-1.

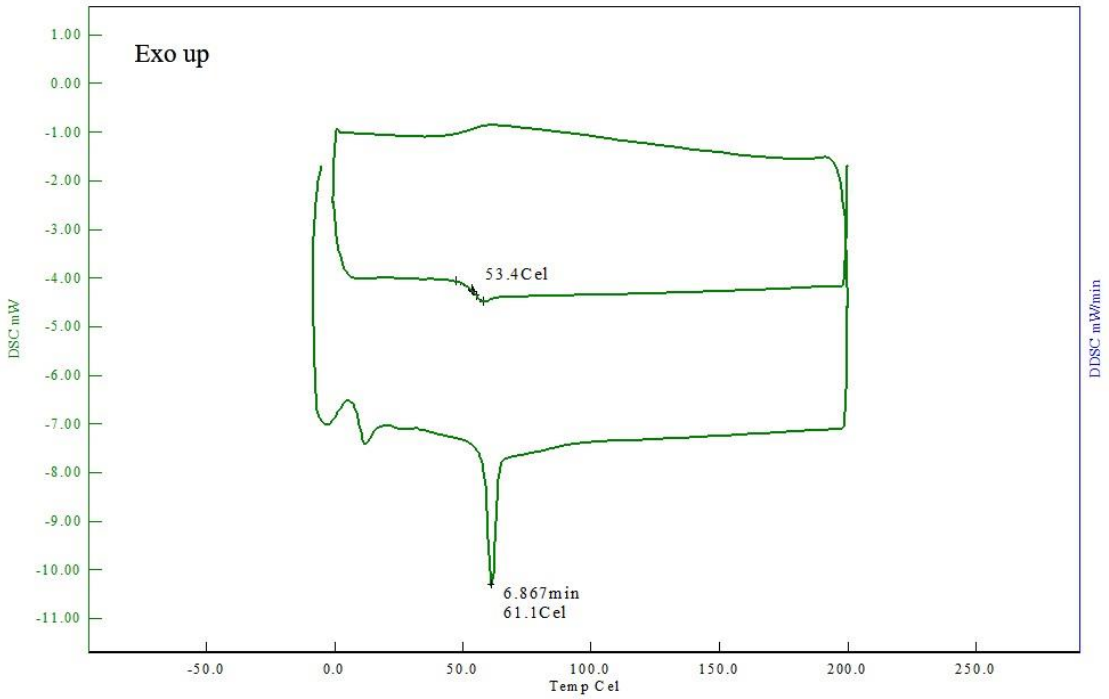

Figure A. 2. DSC results of PE-1control.

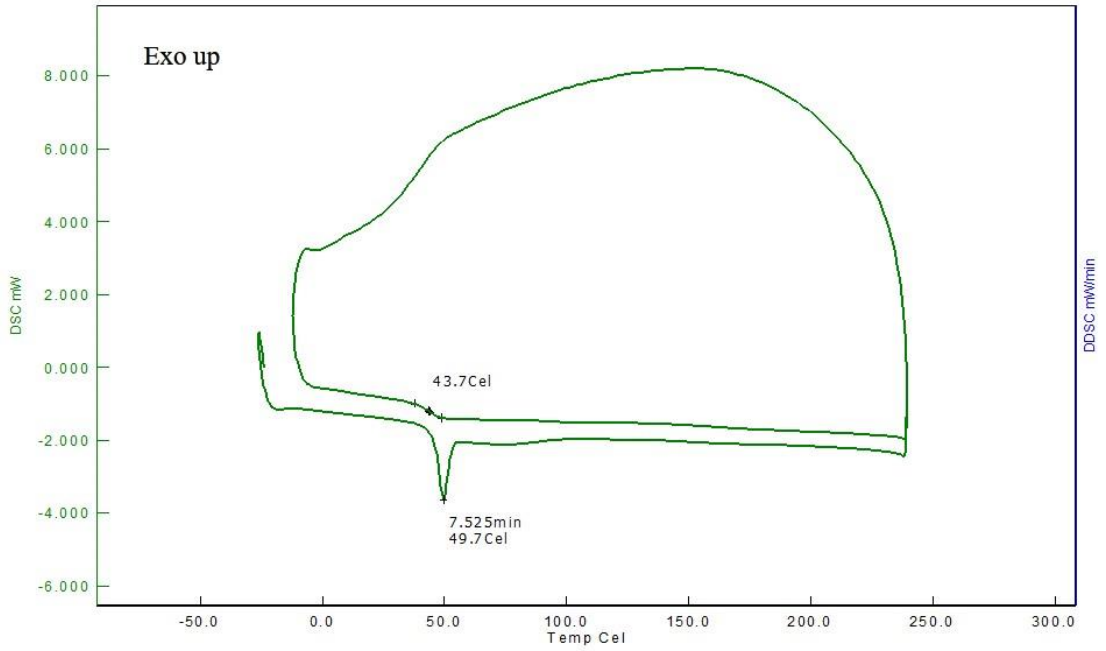

Figure A.3. DSC results of PE-2.

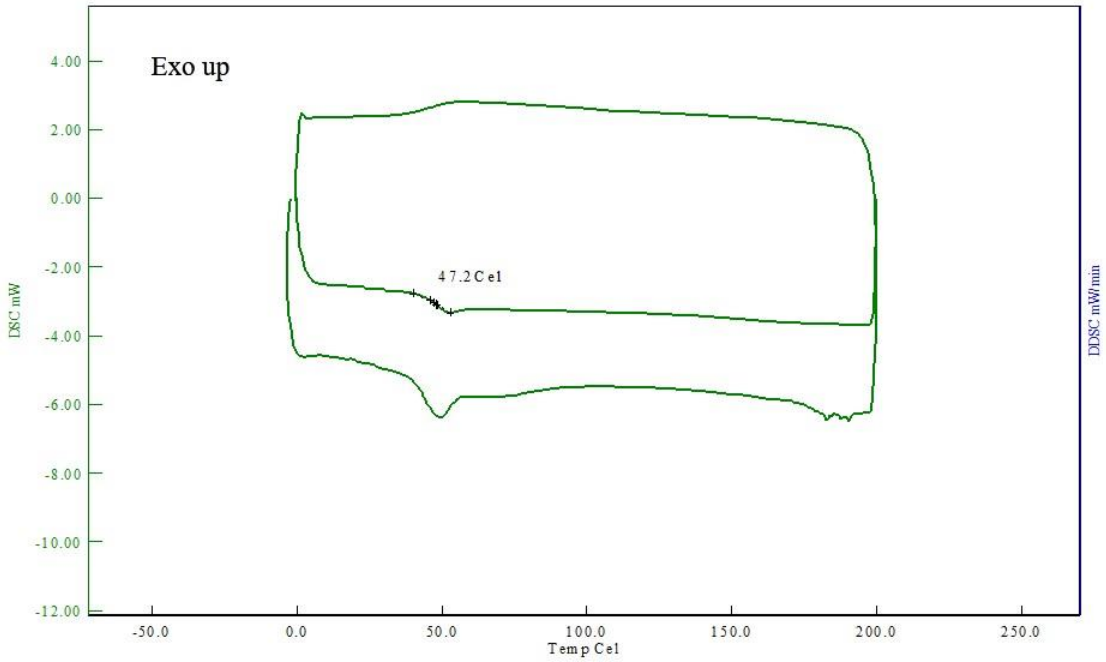

Figure A.4. DSC results of PE-2control.

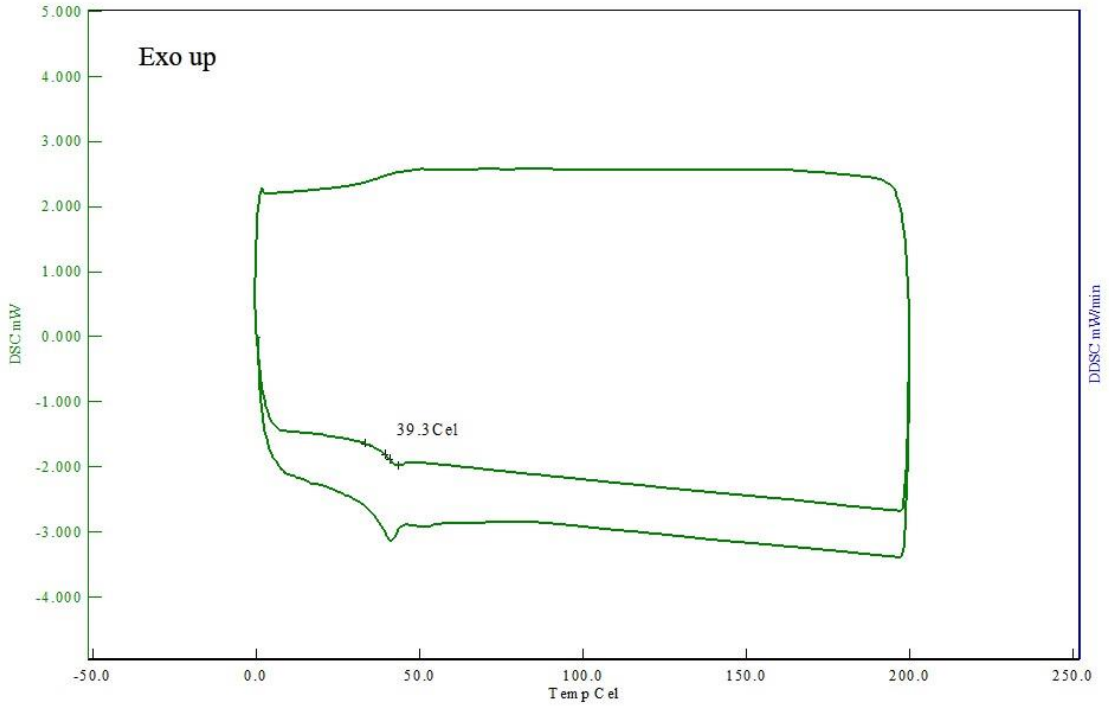

Figure A.5. DSC results of PE-3.

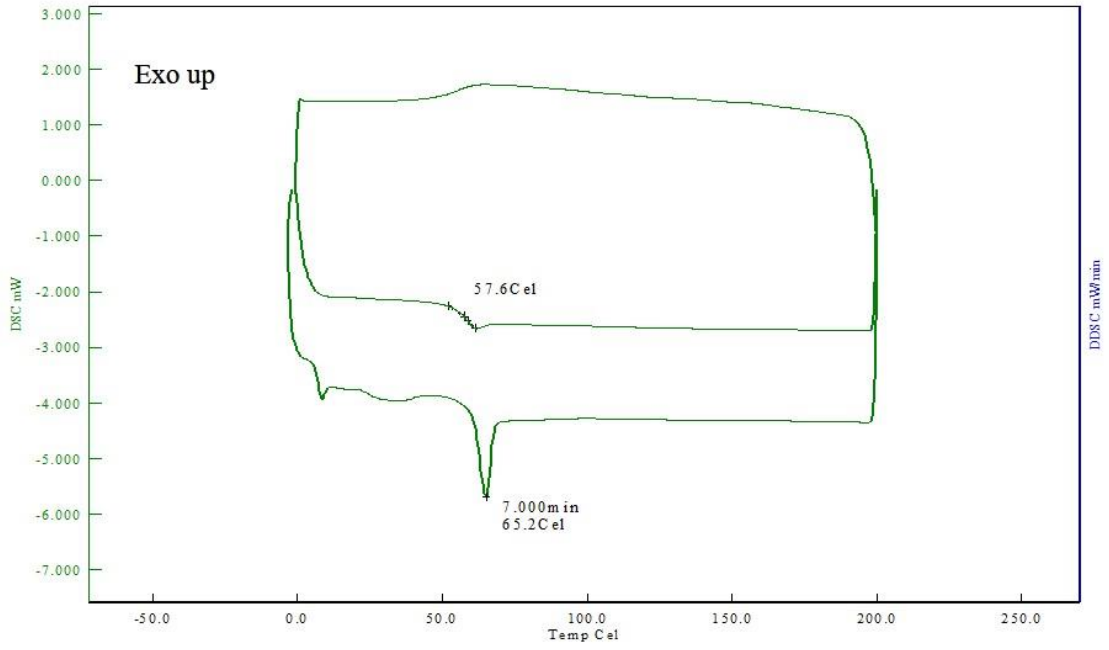

Figure A.6. DSC results of PE-4.

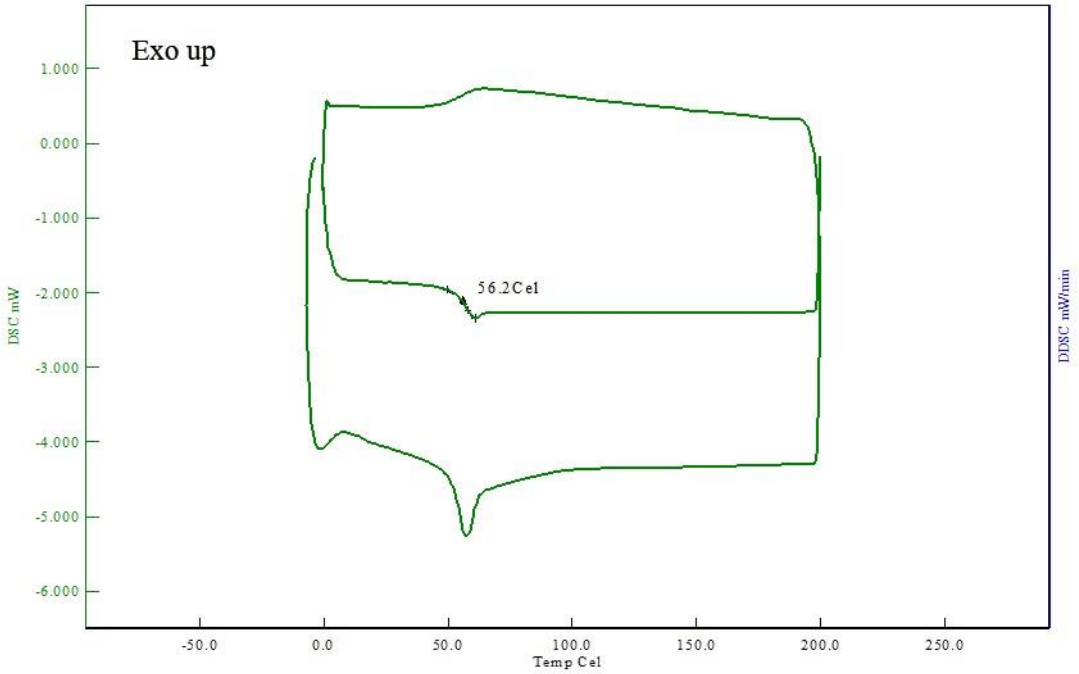

Figure A.7. DSC results of 2MI-1_0.25.

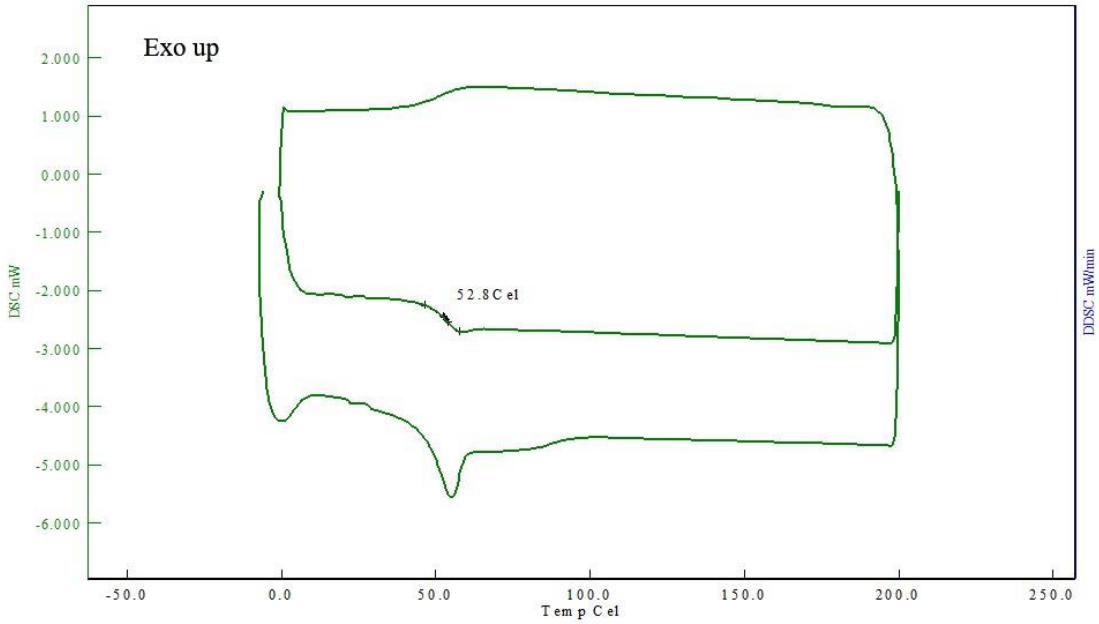

Figure A.8. DSC results of 2MI-1_0.50.

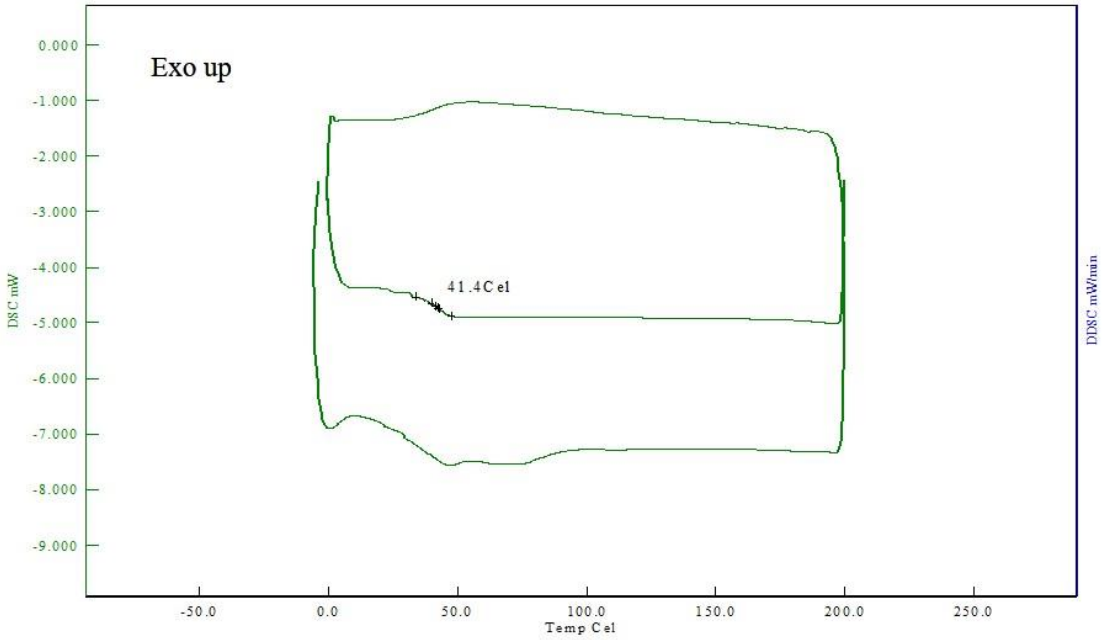

Figure A.9. DSC results of 2MI-1_1.00.

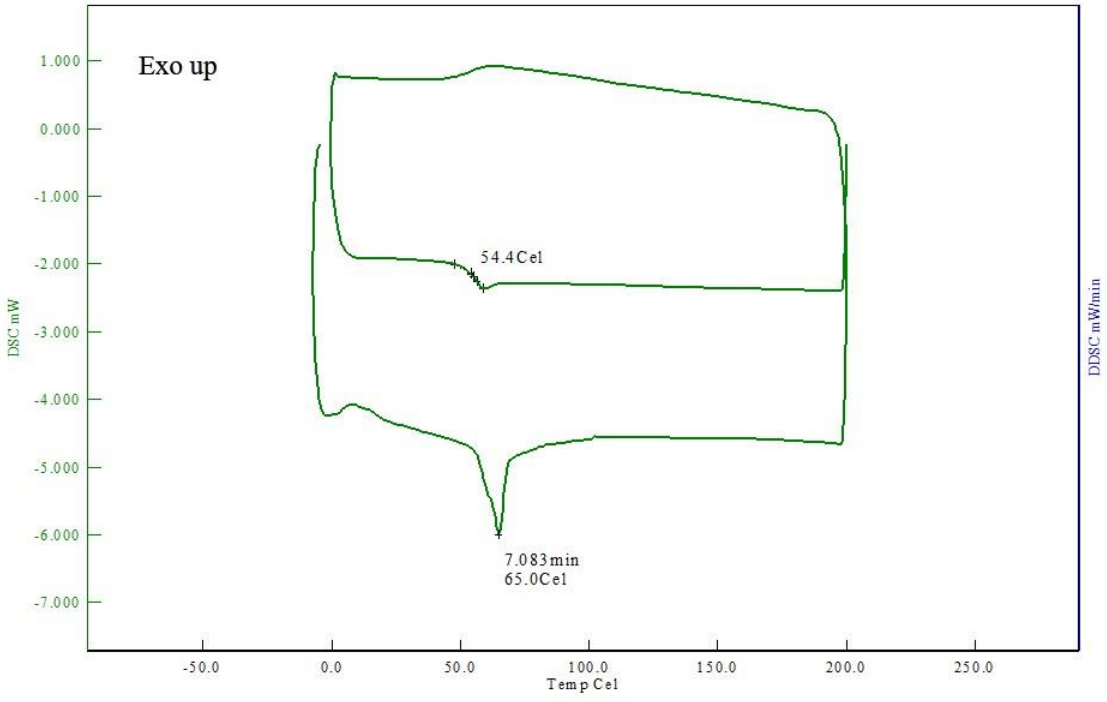

Figure A.10. DSC results of HMDA-1_0.25.

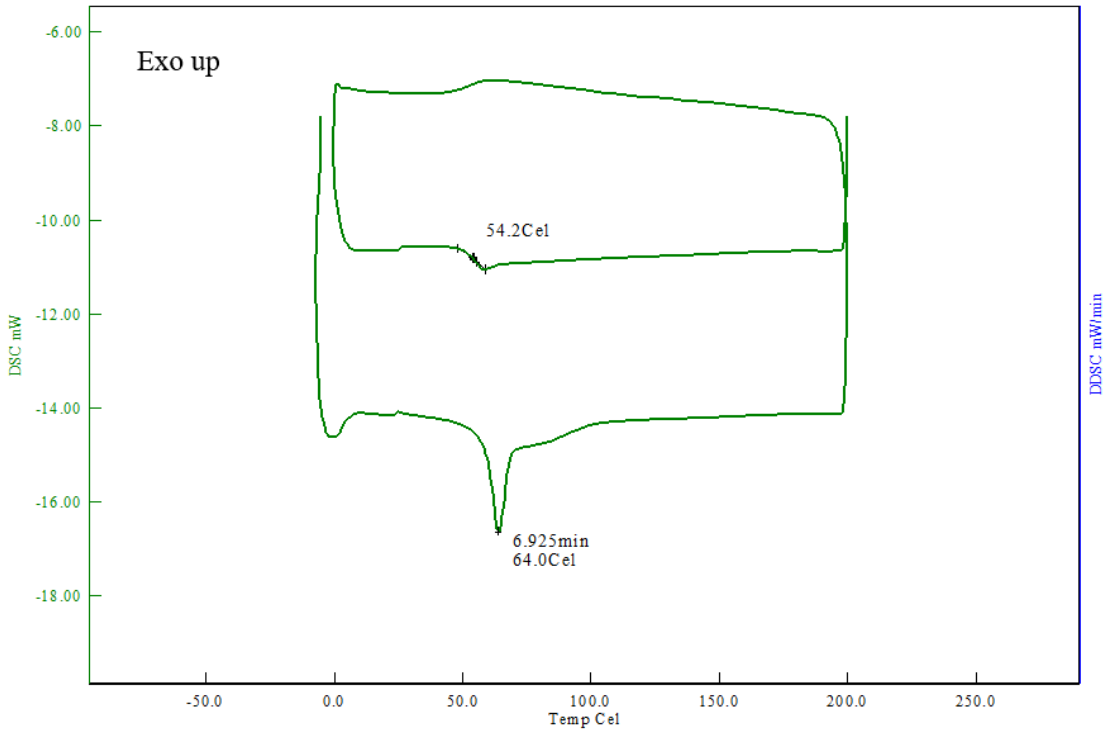

Figure A.11. DSC results of HMDA-1_0.50.

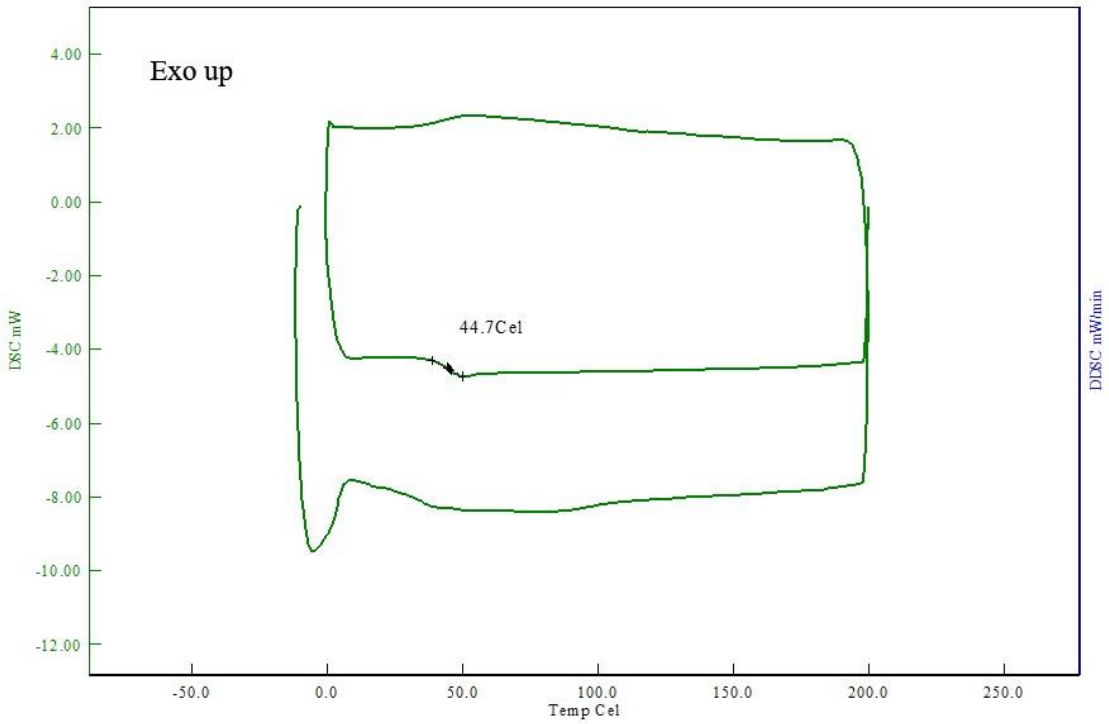

Figure A.12. DSC results of HMDA-1_1.00.

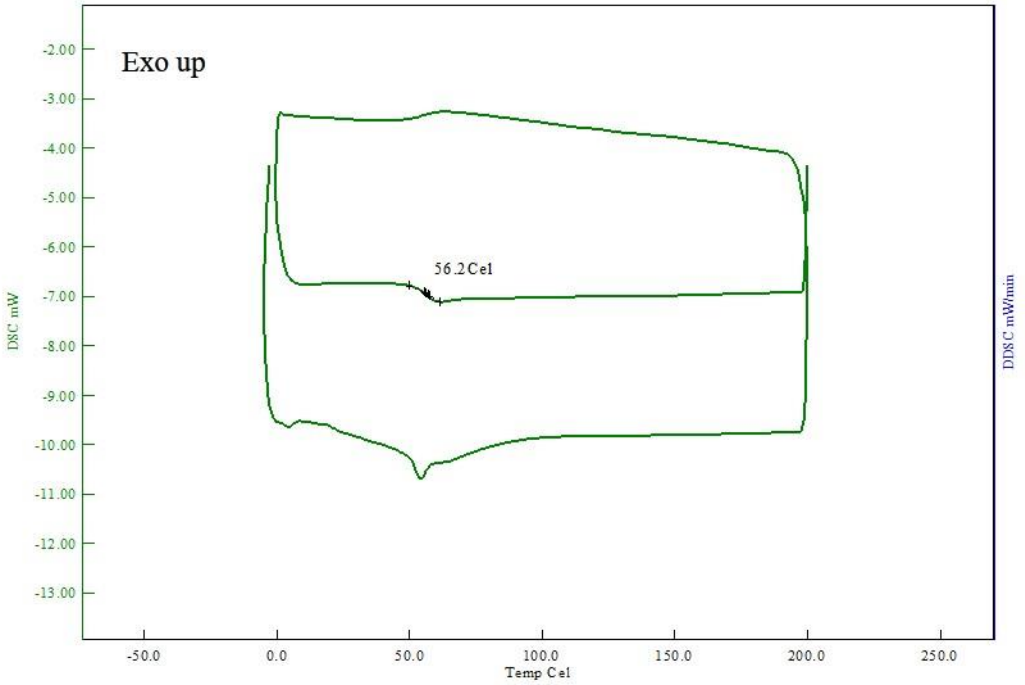

Figure A.13. DSC results of NX3P-1_0.25.

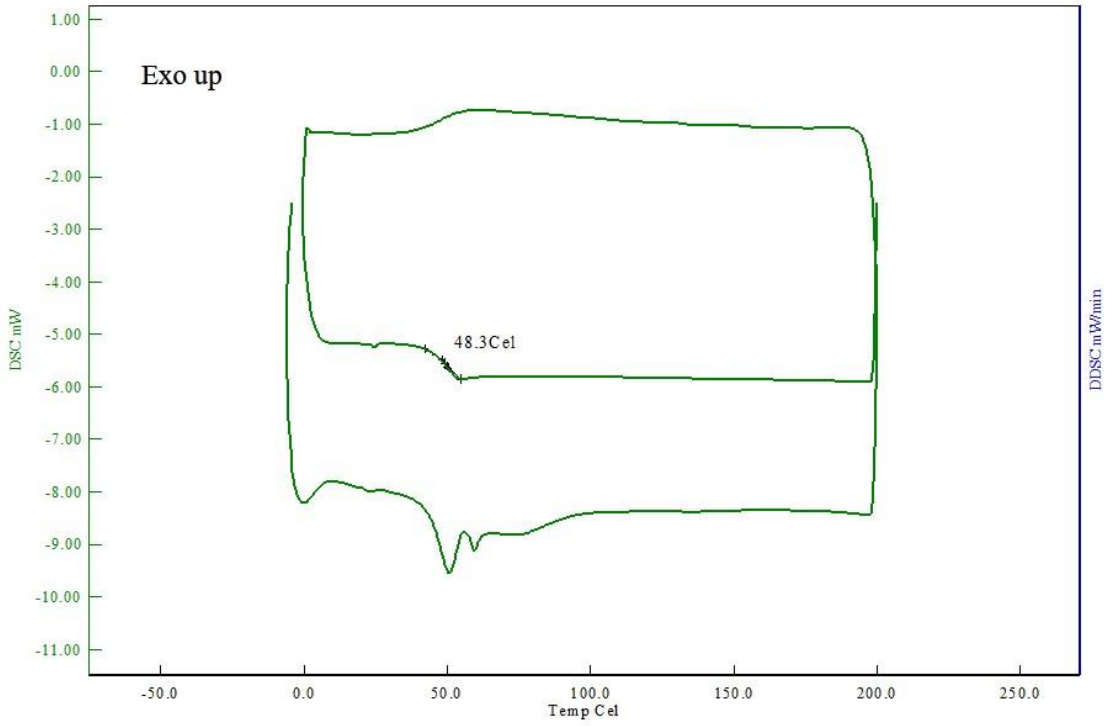

Figure A.14. DSC results of NX3P-1_0.50.

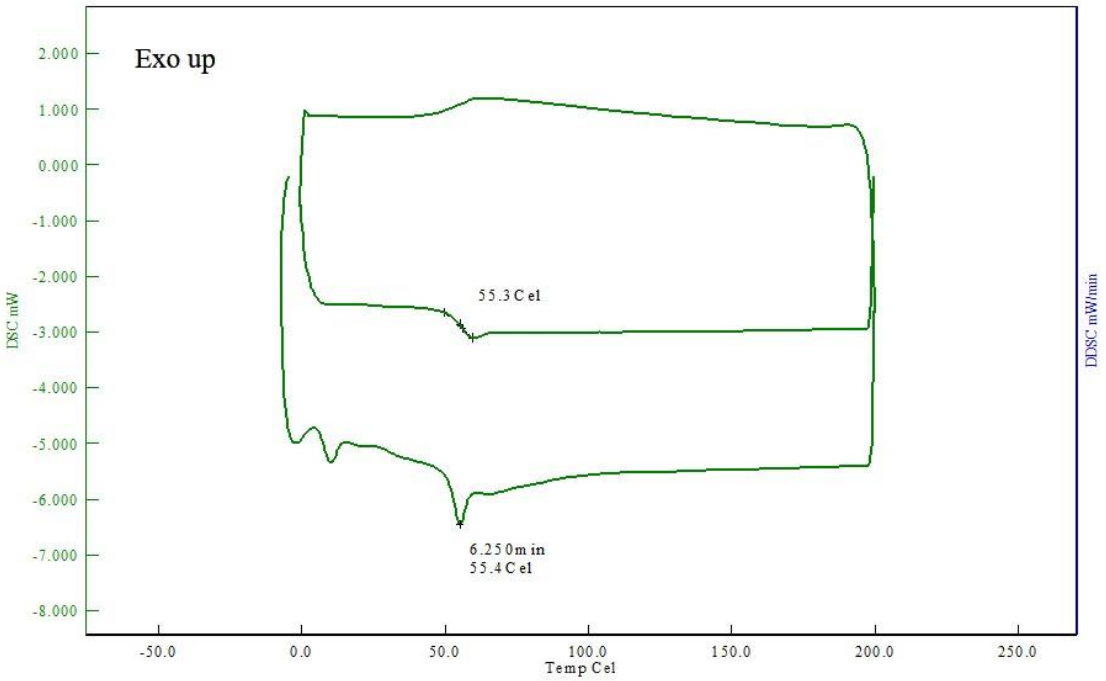

Figure A.15. DSC results of DABCO-1_0.25.

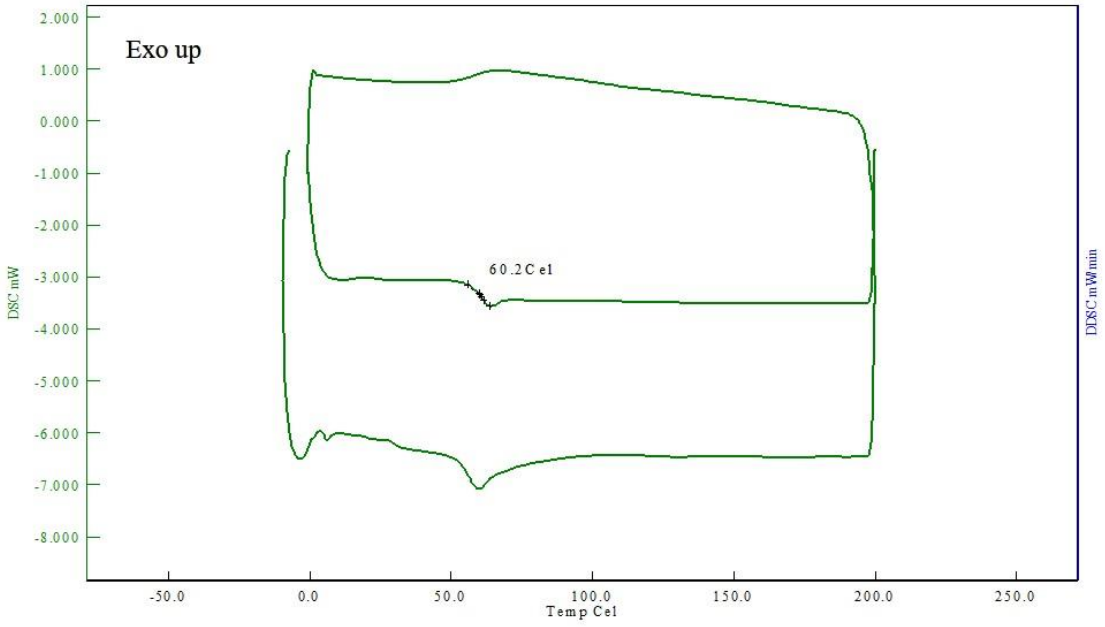

Figure A.16. DSC results of DABCO-1_0.50.

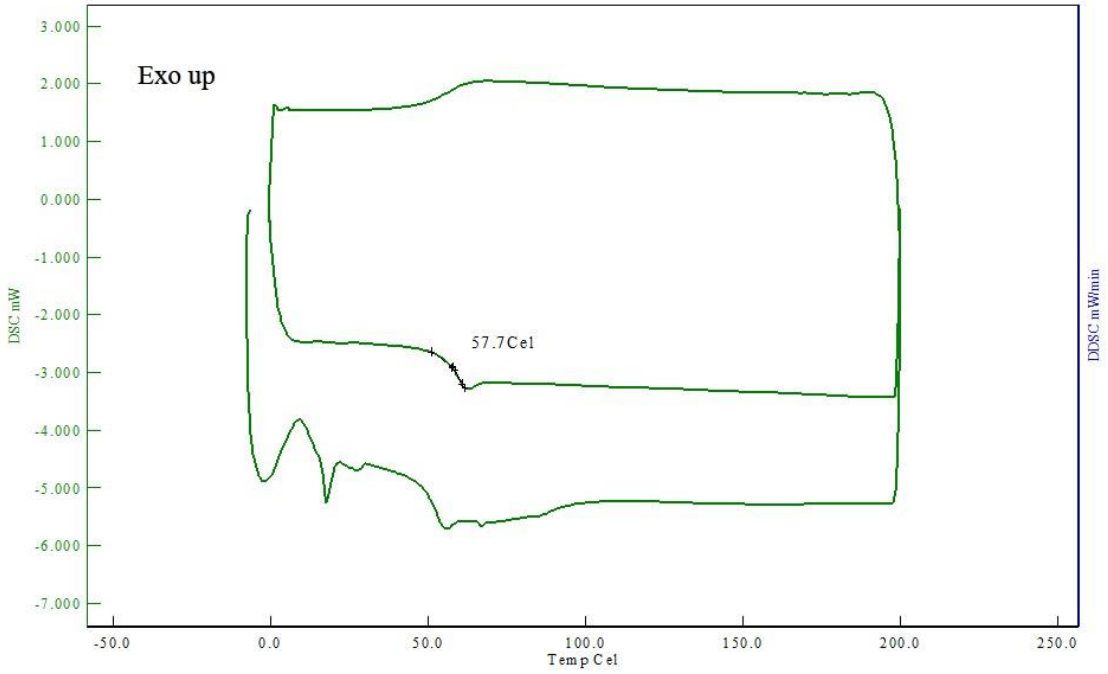

Figure A.17. DSC results of DABCO-1_1.00.

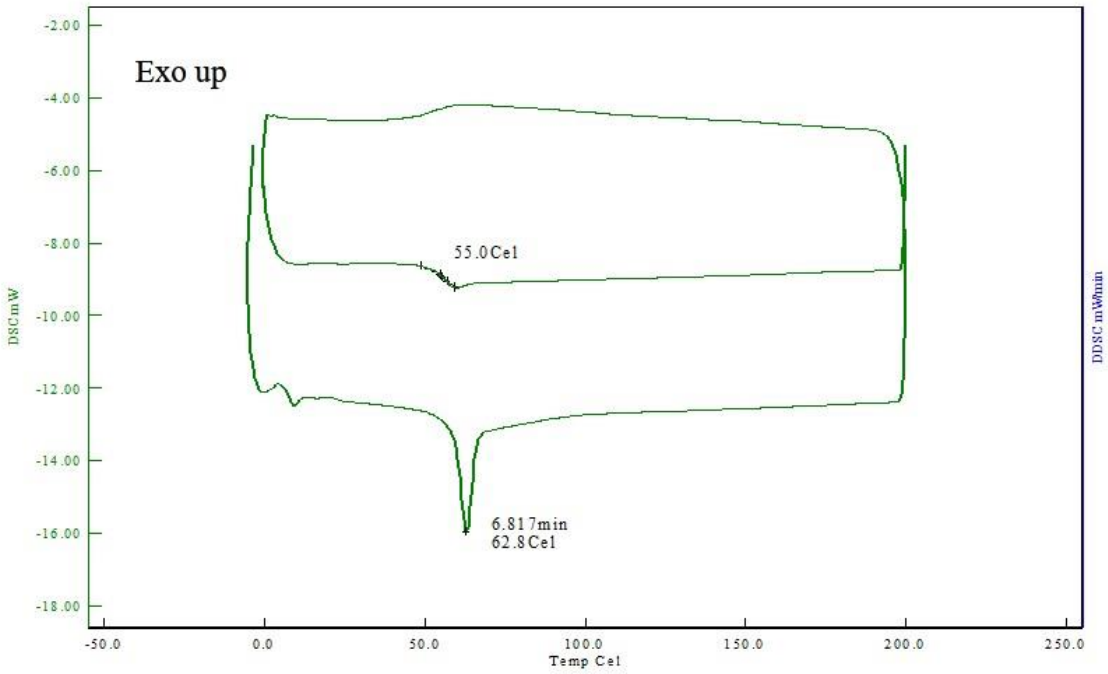

Figure A.18. DSC results of PEI-1_0.25.

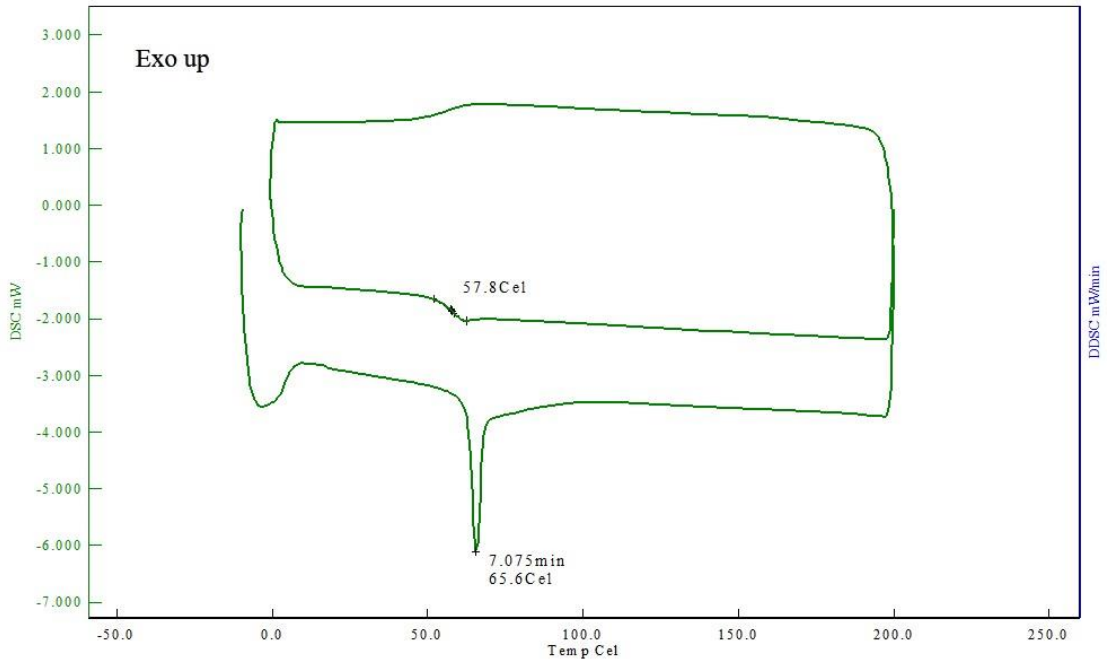

Figure A.19. DSC results of PEI-1_0.50.

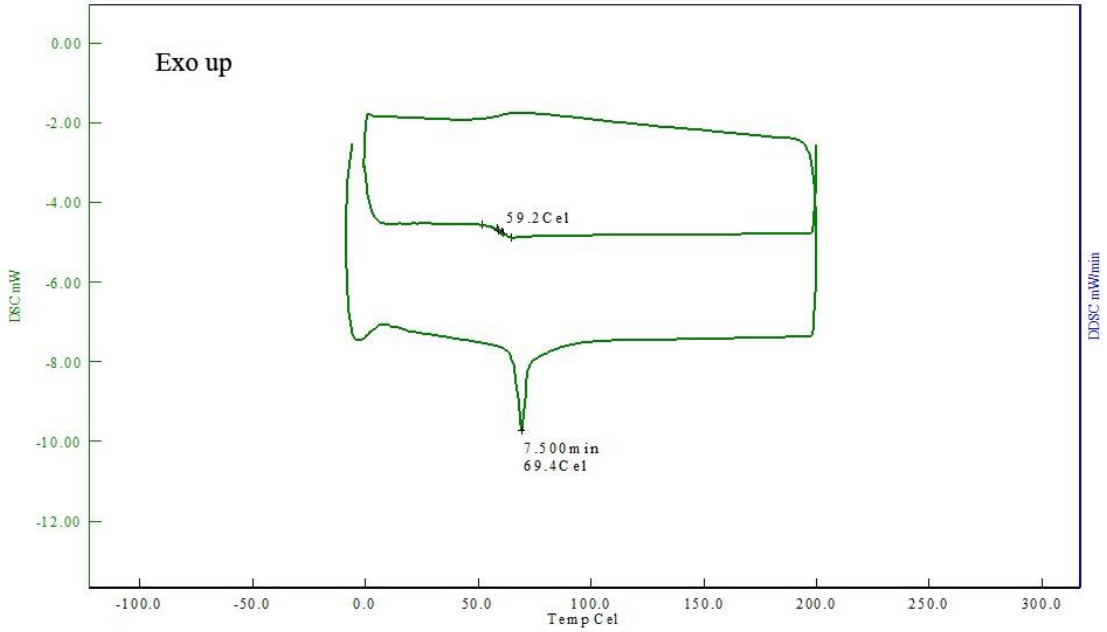

Figure A.20. DSC results of PEI-1_1.00.

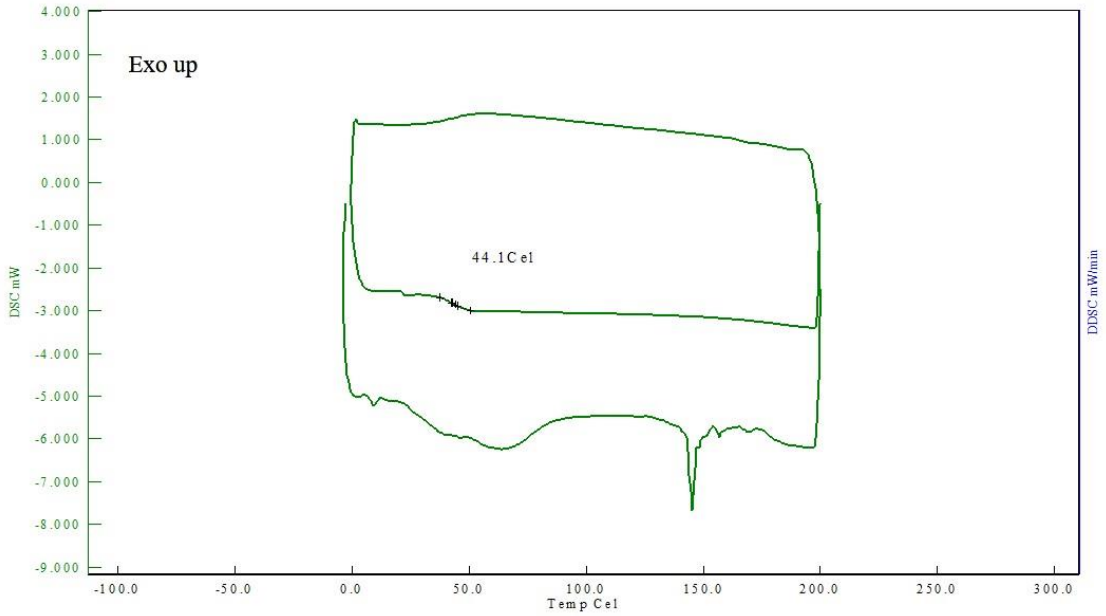

Figure A.21. DSC results of 2MI-2_0.25.

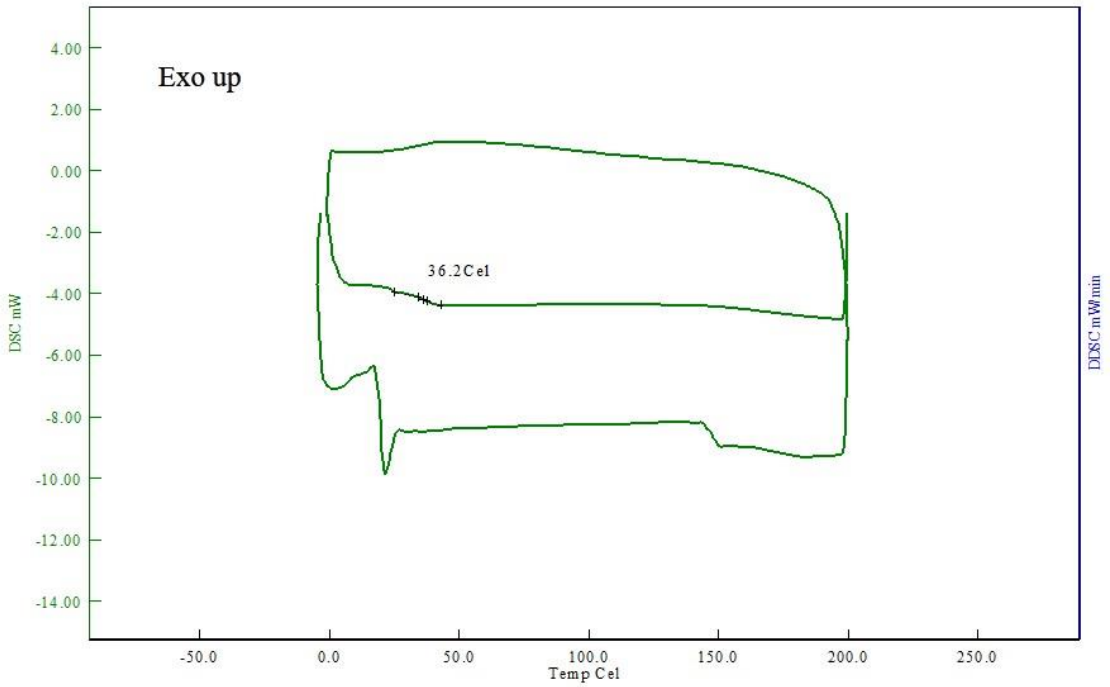

Figure A.22. DSC results of 2MI-2_0.50.

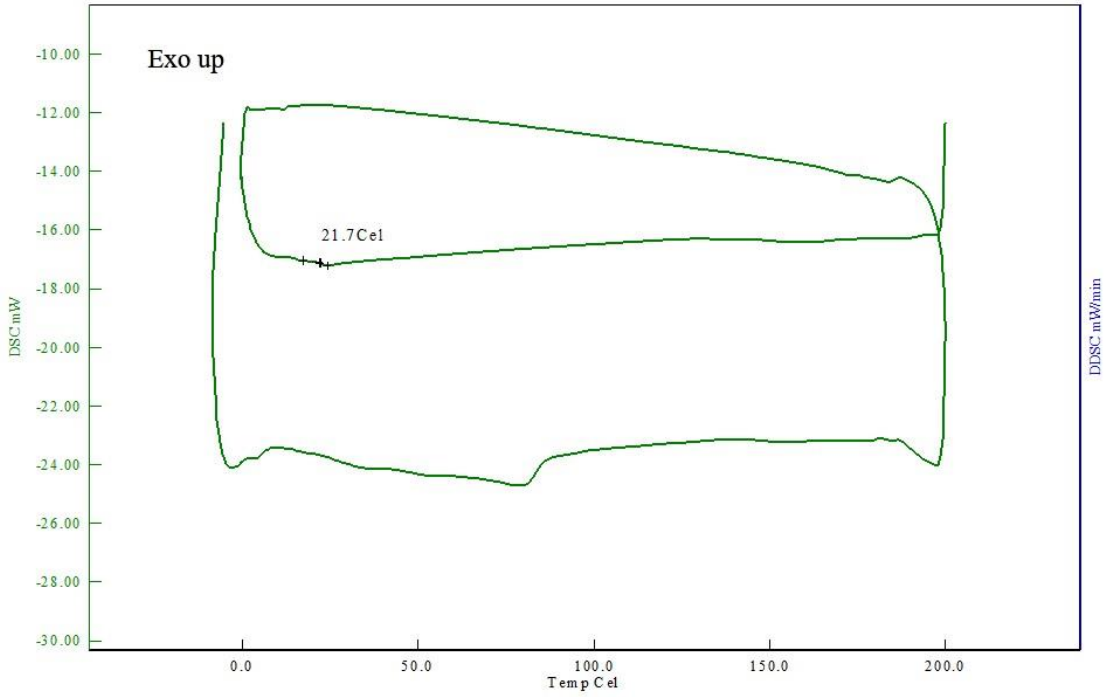

Figure A.23. DSC results of 2MI-2_1.00.

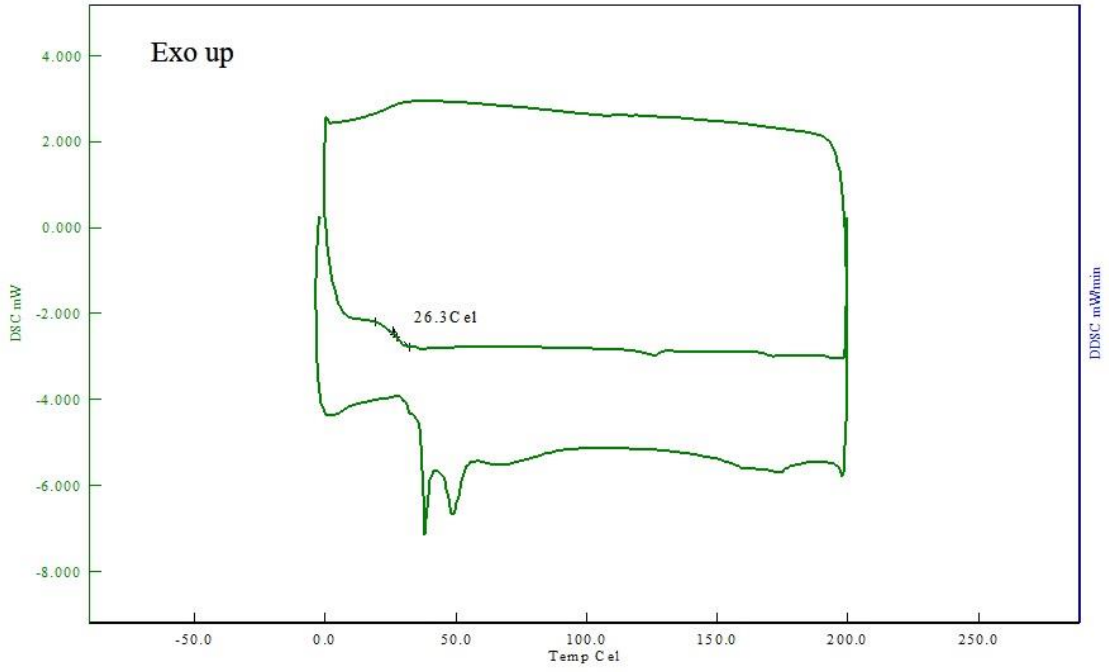

Figure A.24. DSC result of HMDA-2_0.25.

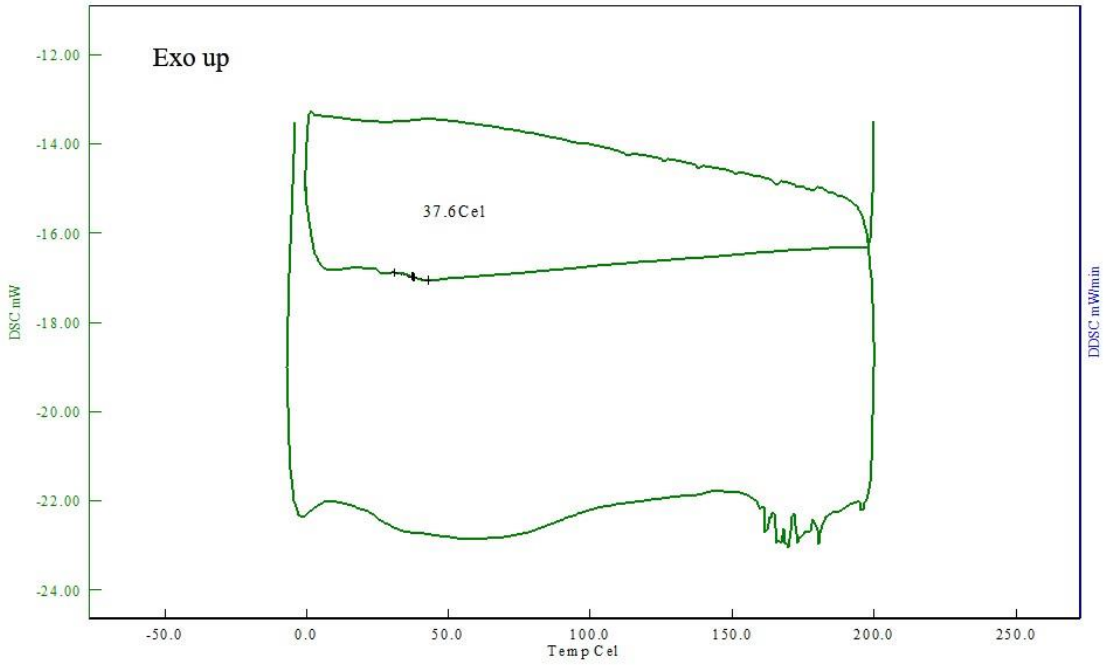

Figure A.25. DSC result of HMDA-2_0.50.

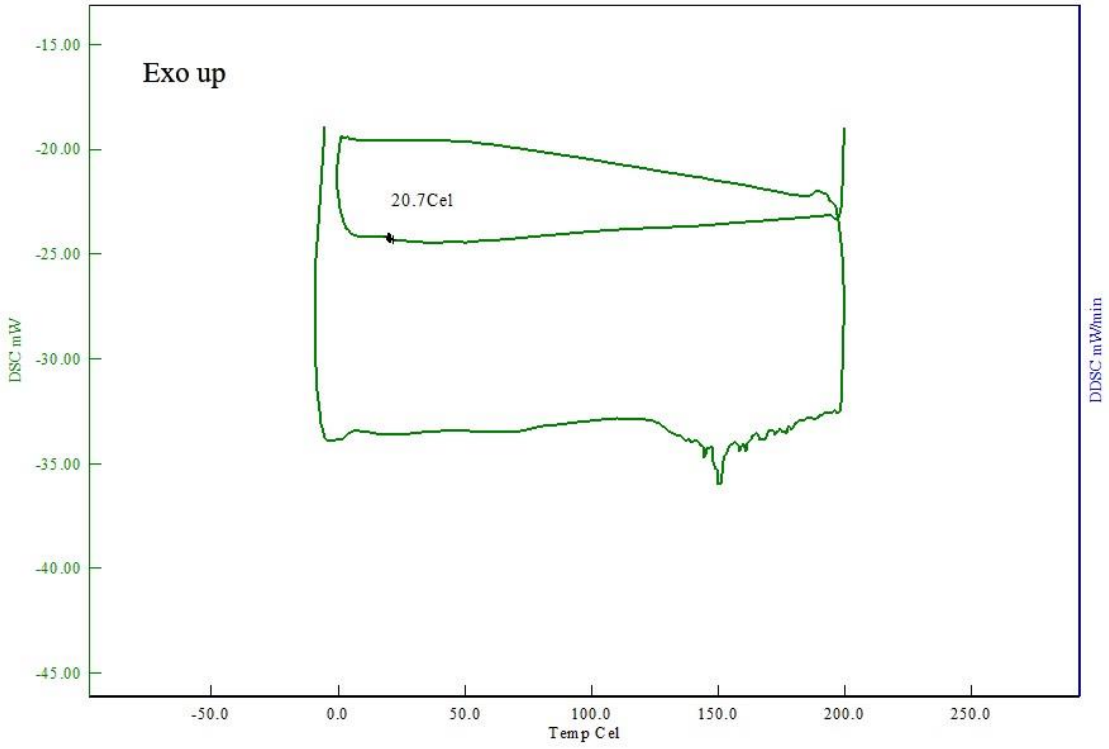

Figure A.26. DSC result of HMDA-2_1.00.

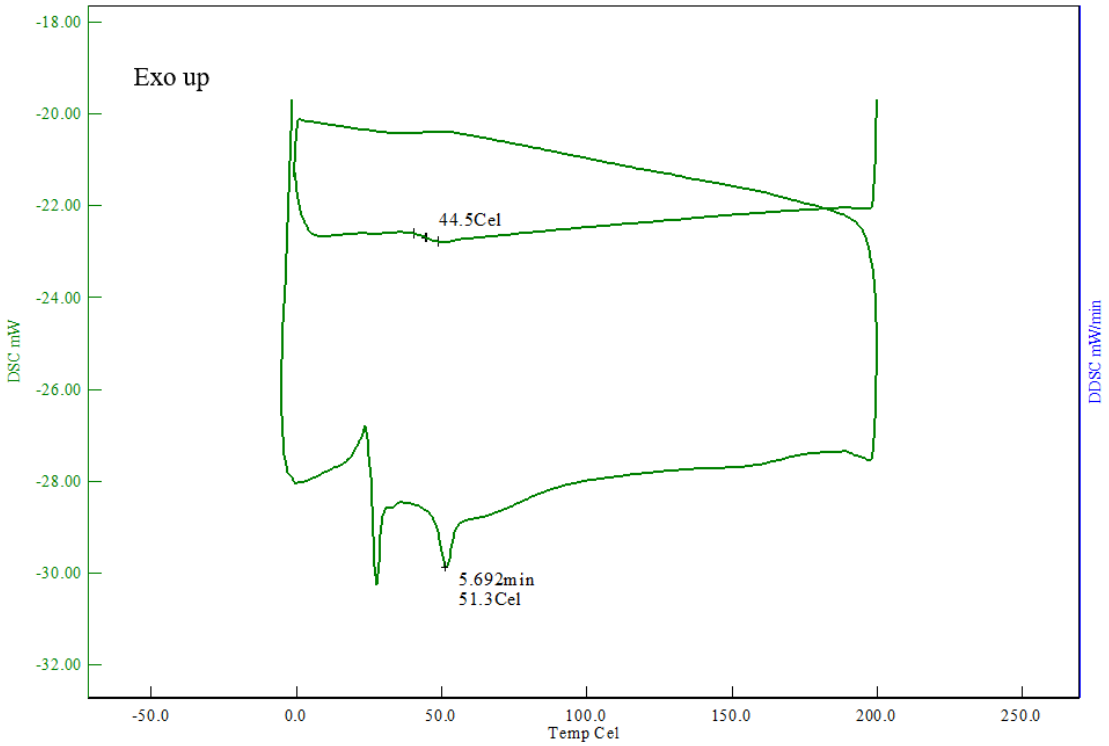

Figure A.27. DSC result of NX3P-2_0.25.

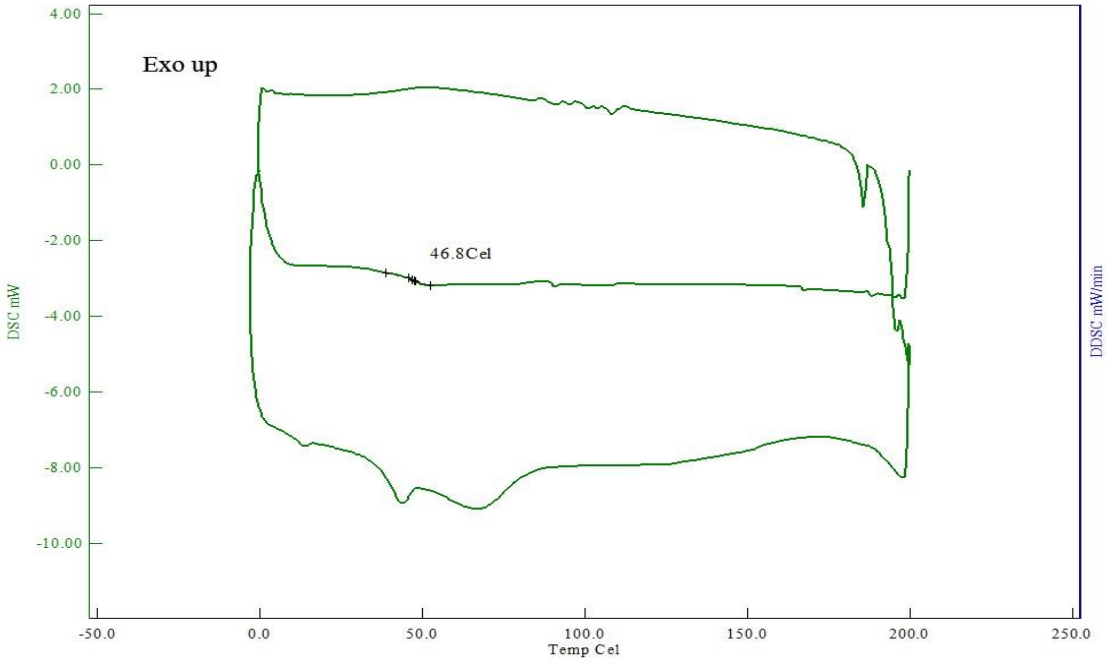

Figure A.28. DSC result of NX3P-2_0.50.

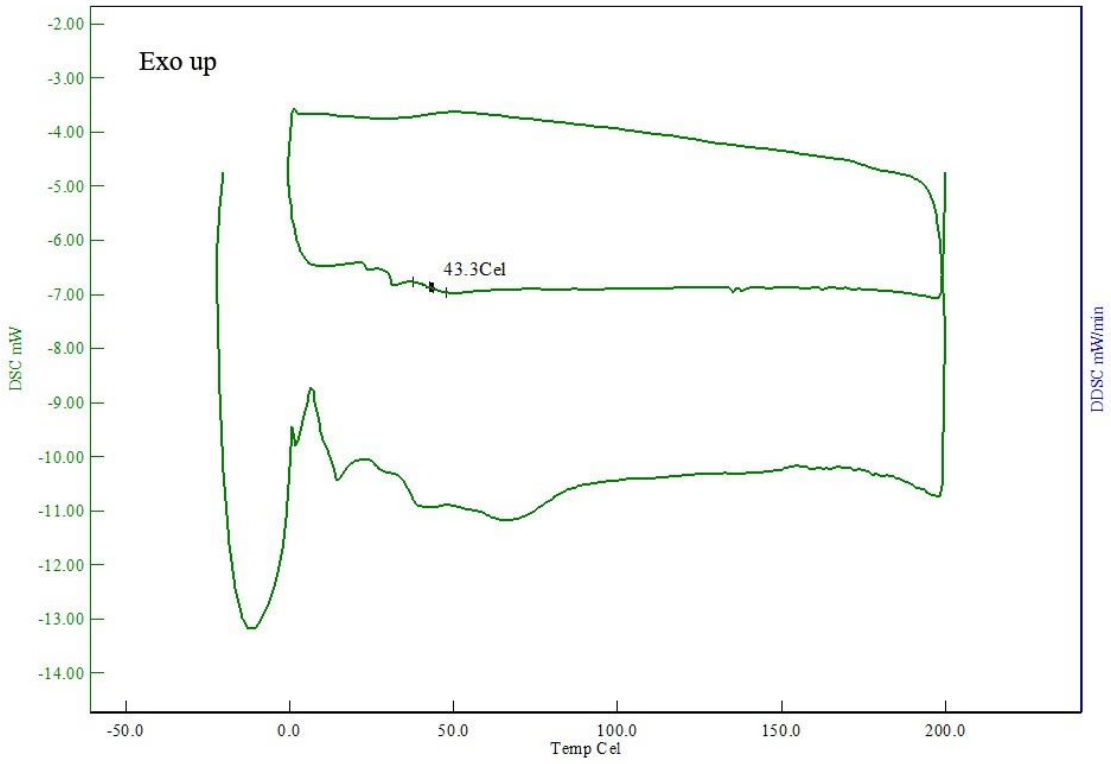

Figure A.29. DSC result of NX3P-2_1.00.

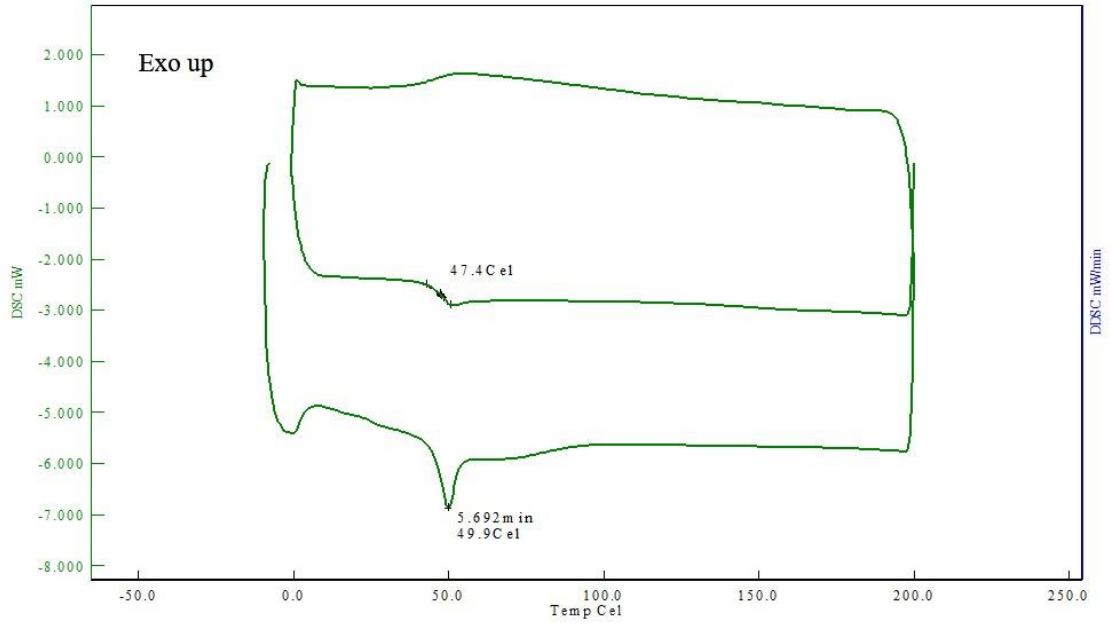

Figure A.30. DSC result of DABCO-2_0.25.

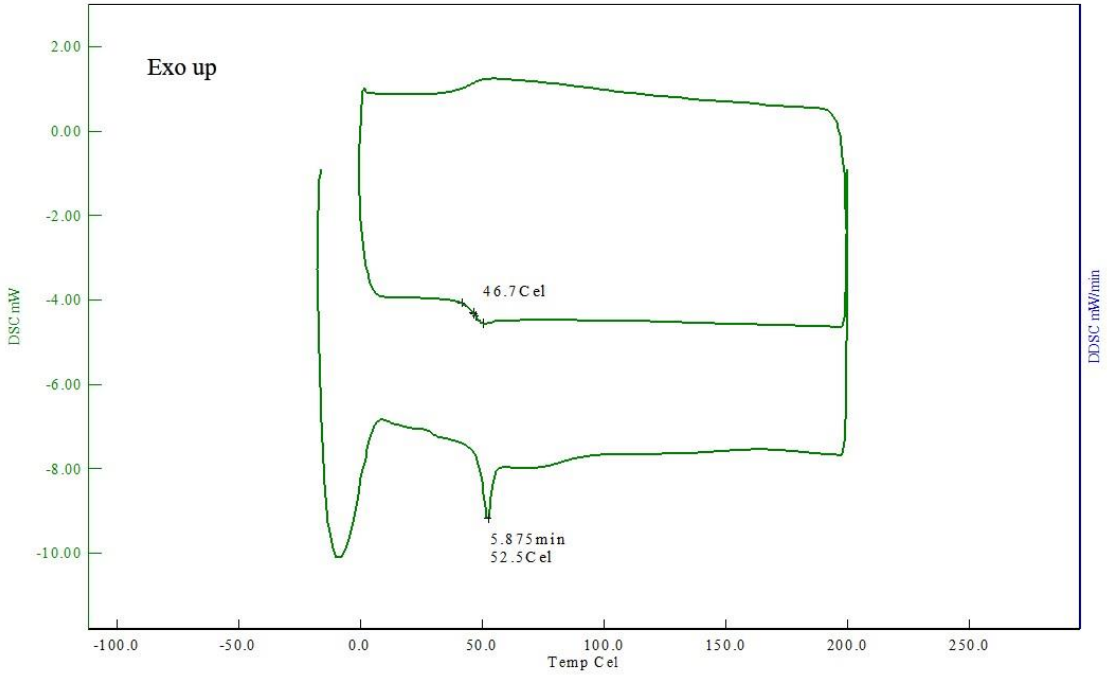

Figure A.31. DSC result of DABCO-2_0.50.

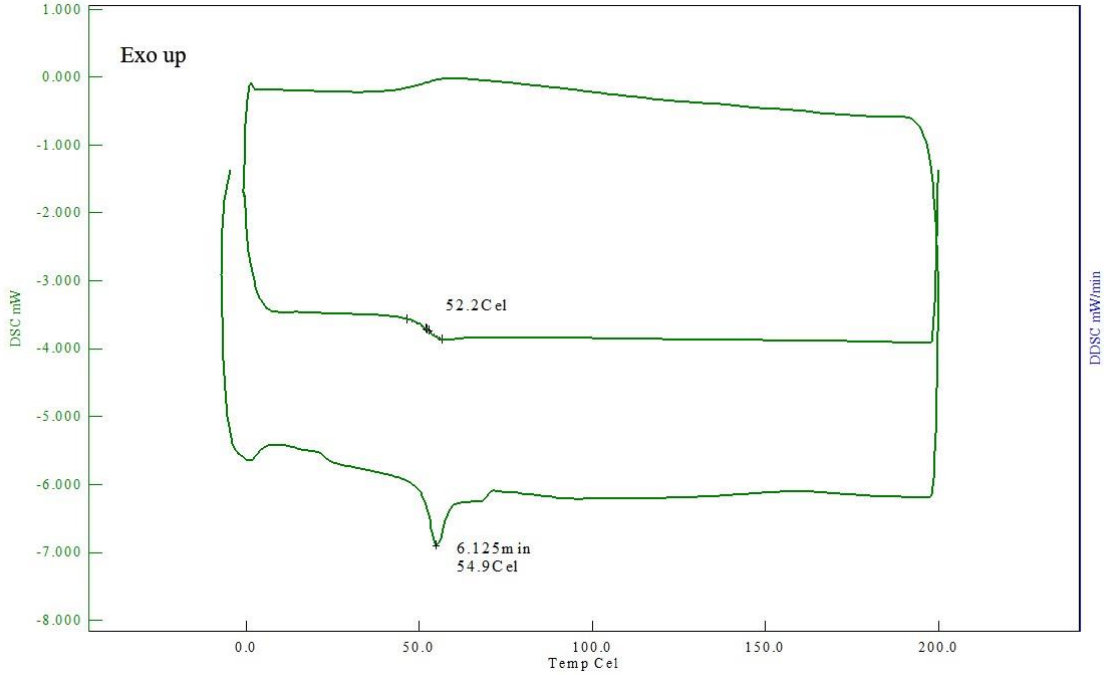

Figure A.32. DSC result of DABCO-2_1.00.

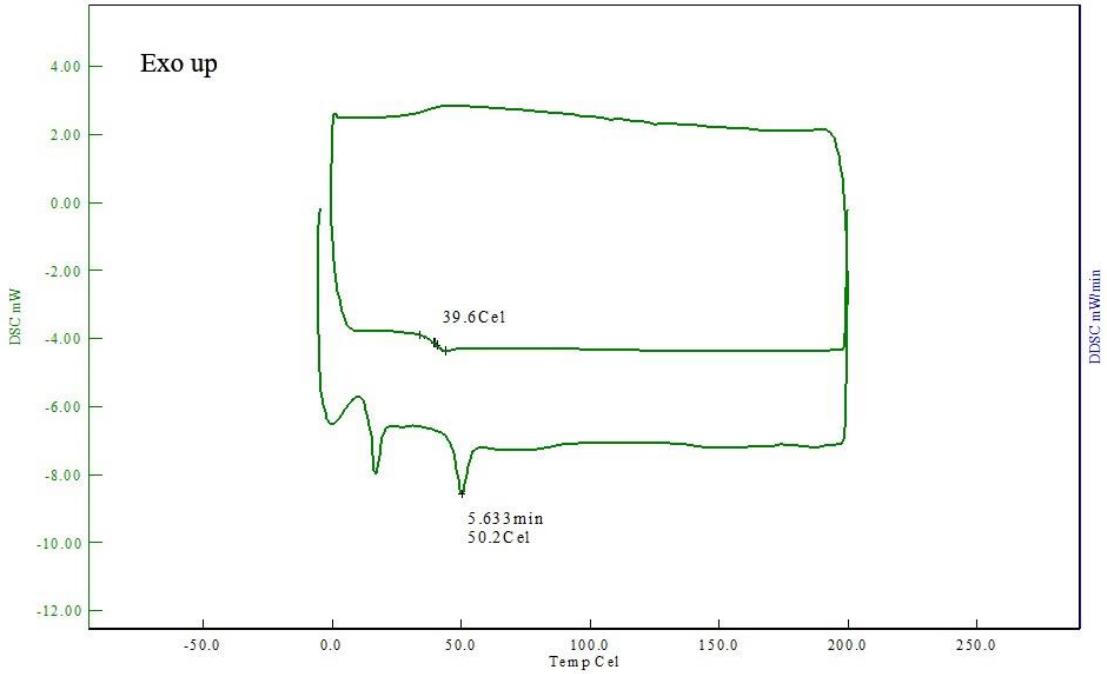

Figure A.33. DSC result of PEI-2_0.25.

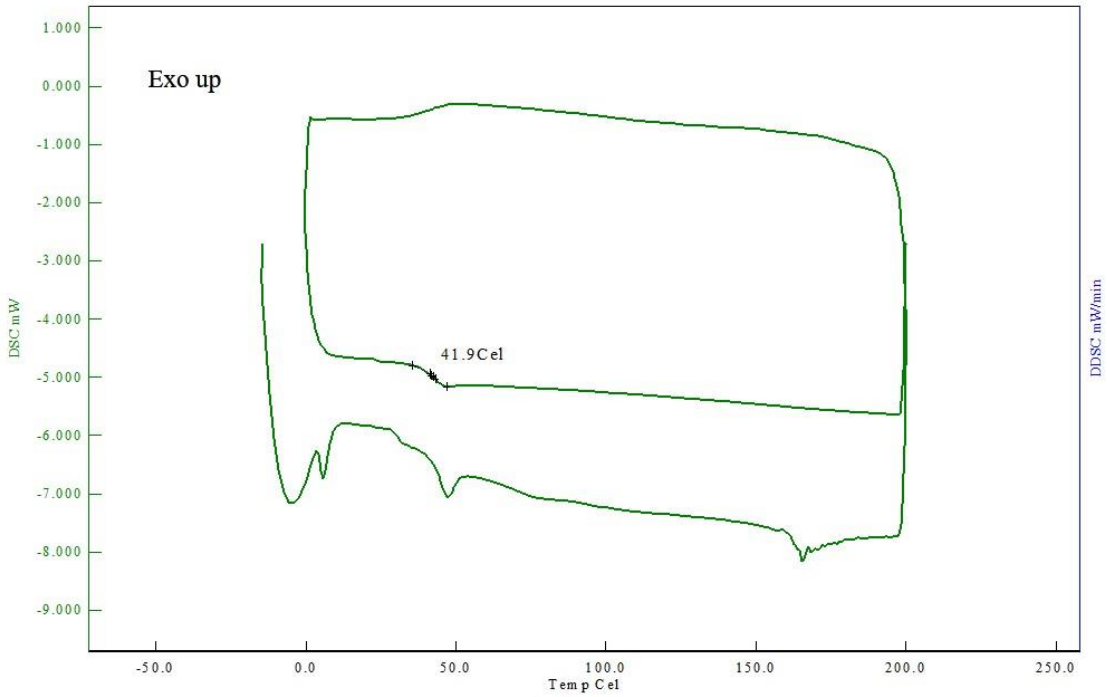

Figure A.34. DSC result of PEI-2_0.50.

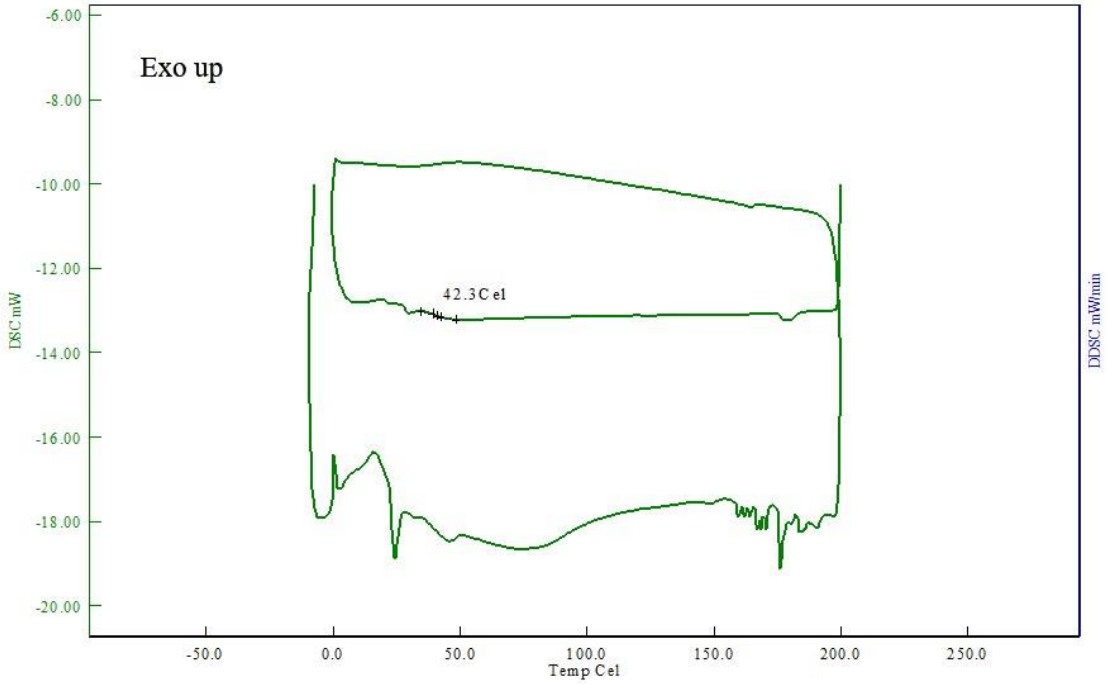

Figure A.35. DSC result of PEI-2_1.00.

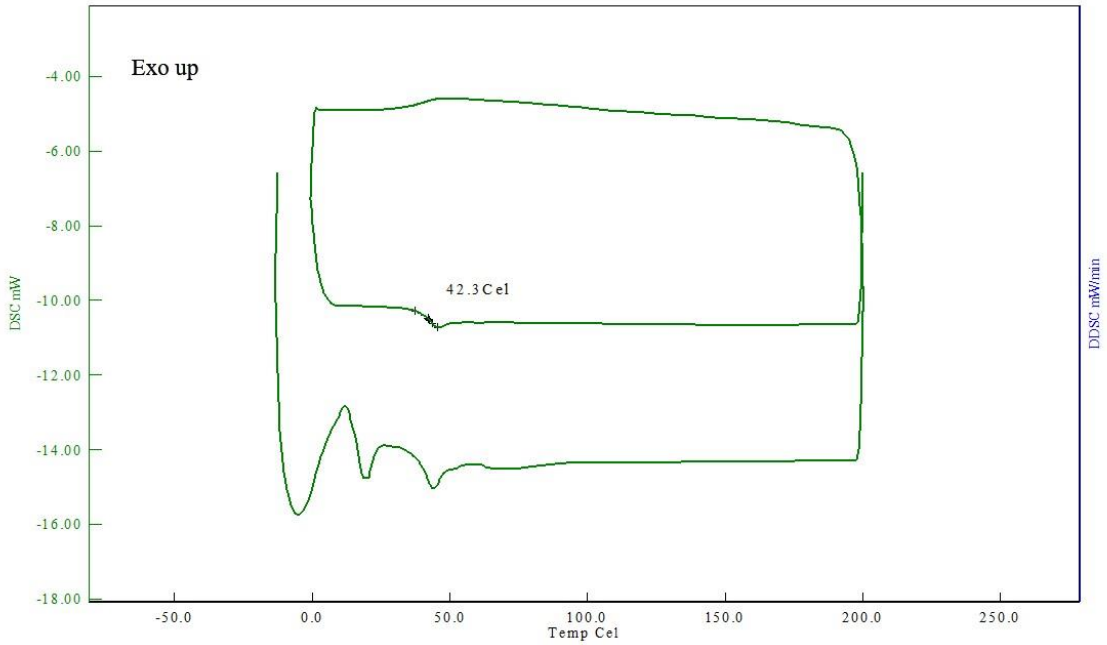

Figure A.36. DSC result of DABCO-3_1.00.

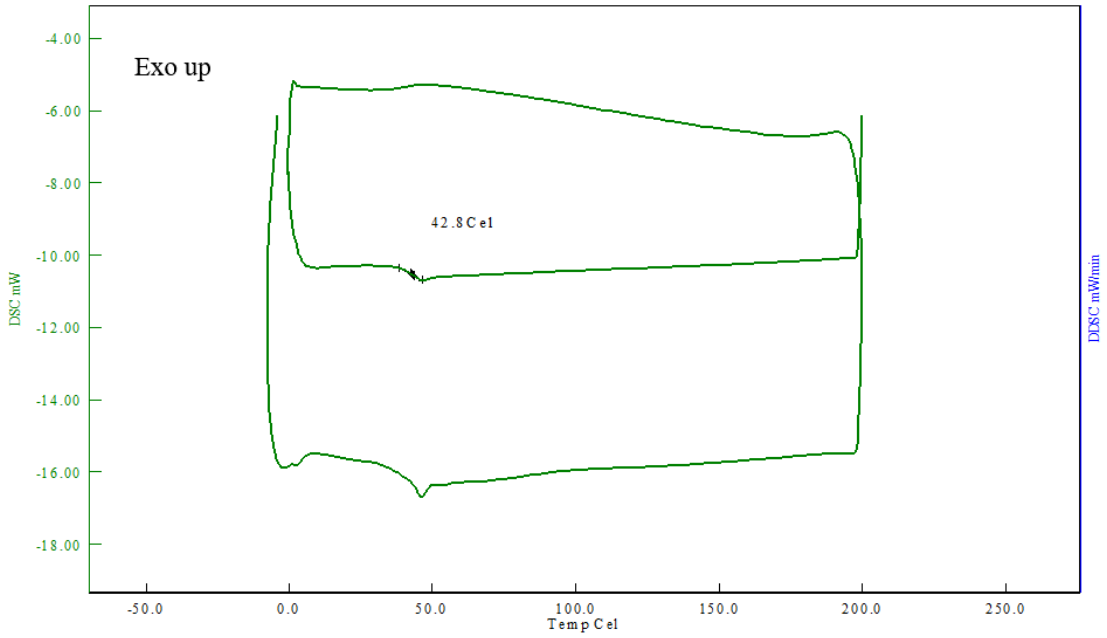

Figure A.37. DSC result of PEI-3_1.00.

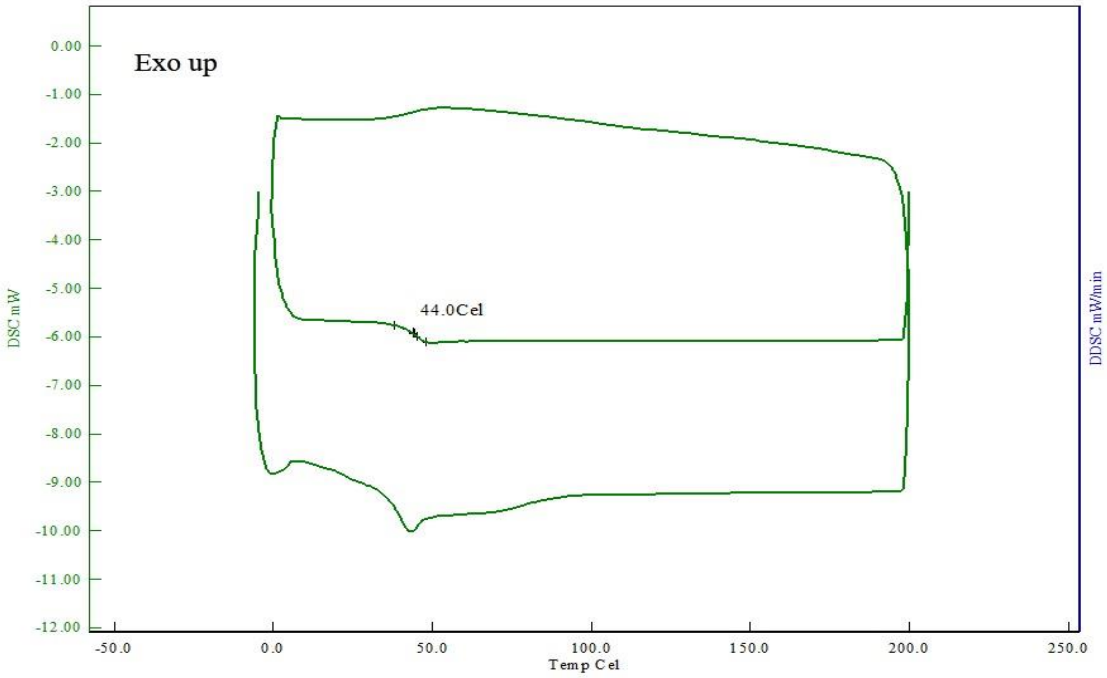

Figure A.38. DSC result of DABCO-4_1.00.

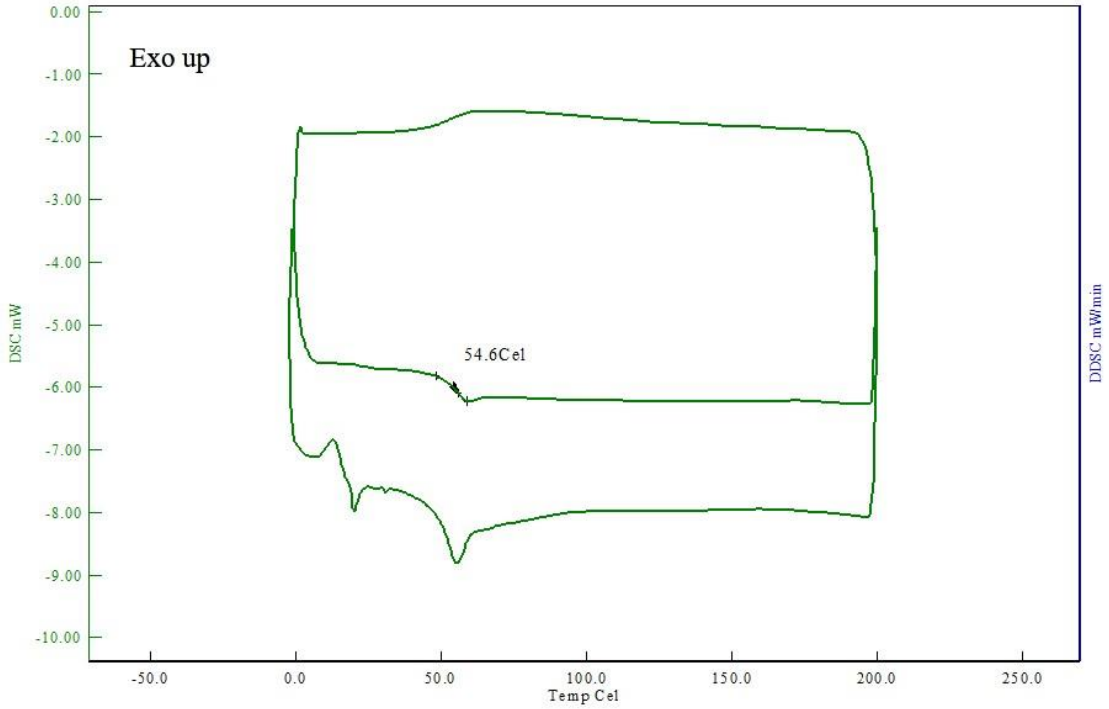

Figure A.39. DSC result of PEI-4_1.00.

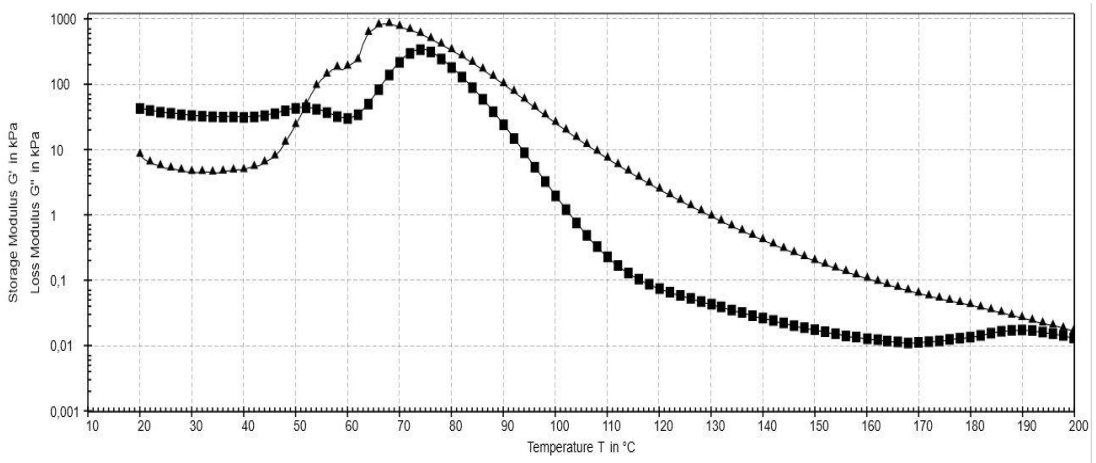

Figure A.40. The temperature sweep graph of PE-2 (storage modulus square line, loss modulus triangle).

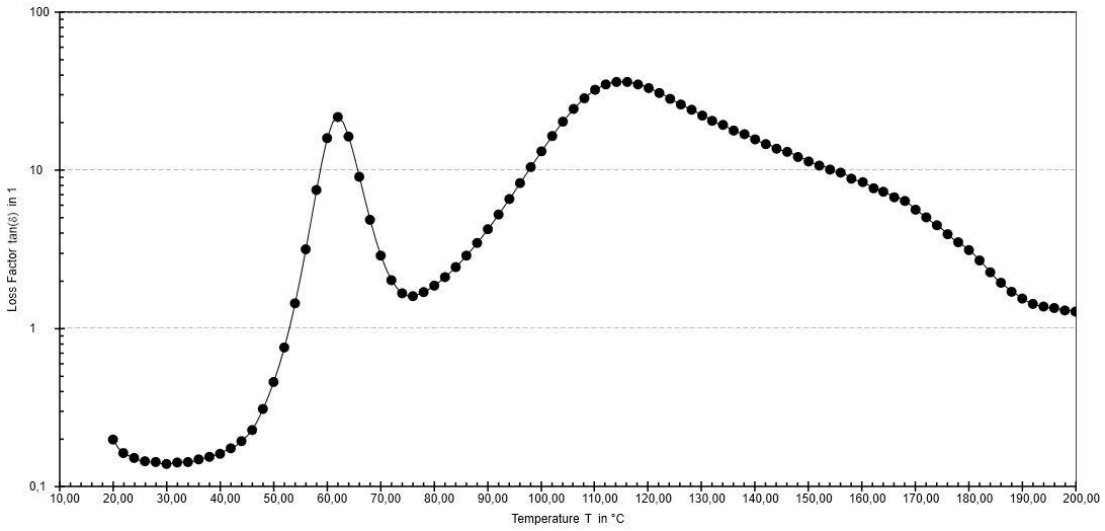

Figure A.41. Loss factor graph of PE-2.

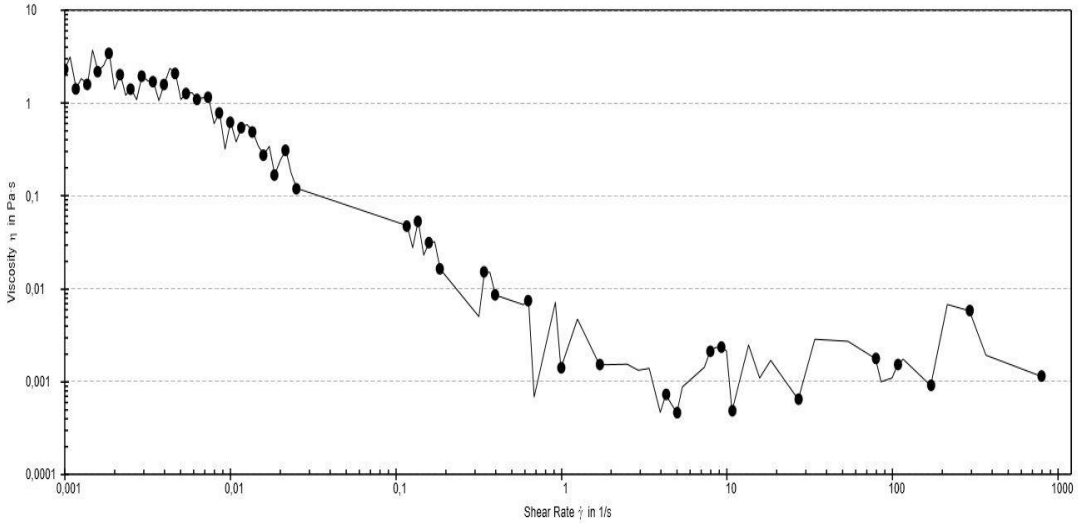

Figure A.42. Flow curve of PE-2.

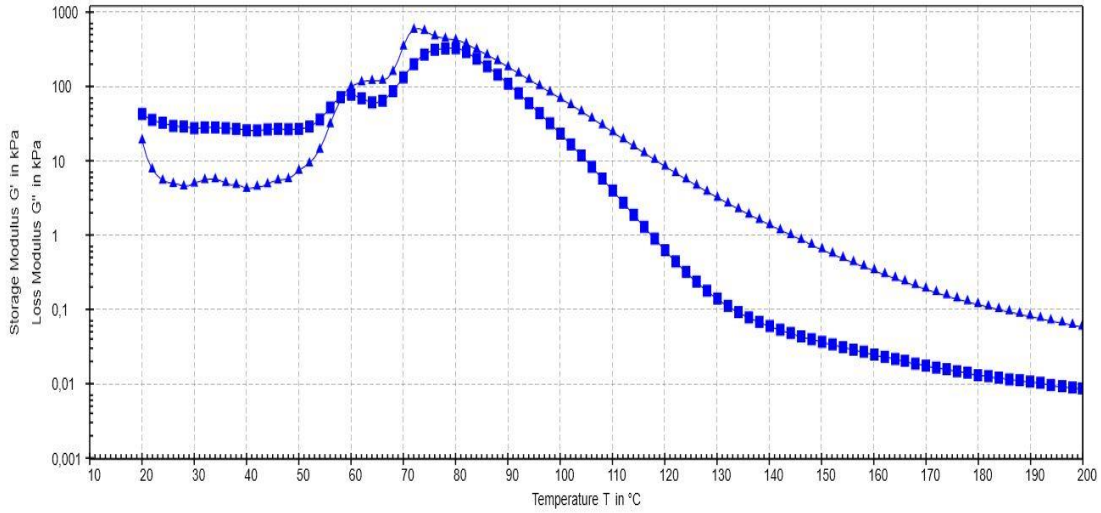

Figure A.43. The temperature sweep graph of PE-1 (storage modulus square line, loss modulus triangle).

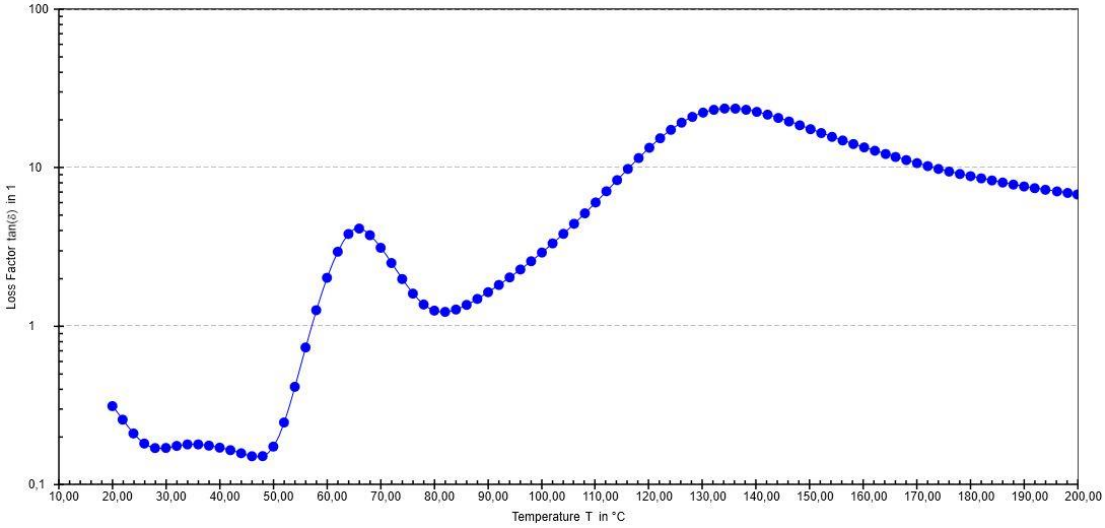

Figure A.44. Loss factor graph of PE-1.

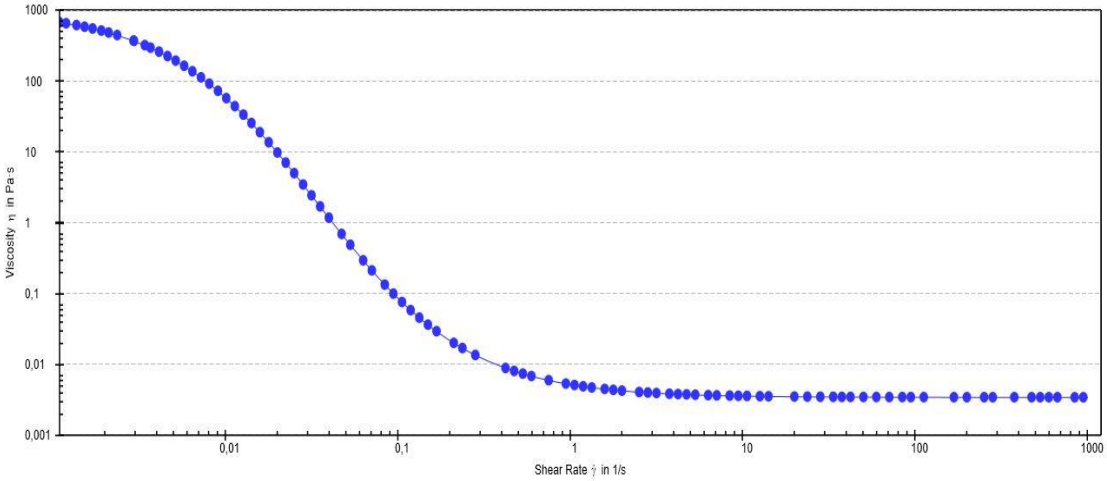

Figure A.45. Flow curve of PE-1.